HOW TO USE EXOSKELETONS TO IMPROVE SELF-SELECTED WALKING SPEED IN OLDER ADULTS

A Dissertation
Presented to
The Academic Faculty

by

Benjamin A. Shafer

In Partial Fulfillment
of the Requirements for the Degree
Robotics in the
George W. Woodruff School of Mechanical Engineering

Georgia Institute of Technology
December 2023

HOW TO USE EXOSKELETONS TO IMPROVE SELF-SELECTED WALKING SPEED IN OLDER ADULTS

Approved by:

Dr. Aaron J. Young, Advisor
George W. Woodruff School of Mechanical Engineering
Georgia Institute of Technology

Dr. Gregory S. Sawicki, Advisor
George W. Woodruff School of Mechanical Engineering
Georgia Institute of Technology

Dr. Lena H. Ting
Coulter Department of Biomedical Engineering
Georgia Institute of Technology and Emory University

Dr. Jason R. Franz
Joint Department of Biomedical Engineering
University of North Carolina Chapel Hill and North Carolina State University

Dr. Fausto A. Panizzolo
Moveo, Padova PD, Italy

Date Approved: August 18, 2023

This work is dedicated to everyone unable to live their fullest life because of physical challenges.

ACKNOWLEDGEMENTS

I would like to thank my mother and father, who gave me the intellectual and emotional tools and support I needed. I would like to thank my lab mates who worked with me on my various projects and inspired me to do more with my work and life. I would like to thank my sisters who supported me and never hesitated to have a good time when I was home or needed to unwind. I would like to thank my friends who made sure I lived a full, happy life while pursuing my education and career goals. I would like to thank my ORISE fellowship advisor who trusted me to conduct independent research, write my first journal articles, which ultimately earned me the opportunity to attend Georgia Tech for my PhD. A final thank you to my advisors who were patient who gave me the opportunity to choose my own projects and taught me how to be thorough, communicate clearly, and be a competent researcher. I am so grateful for my life, connections, and experiences so far and you all have made it possible!

TABLE OF CONTENTS

LIST OF FIGURES

LIST OF SYMBOLS AND ABBREVIATIONS

SSWS	Self-selected walking speed
COT	Cost of transport
HILO	Human-in-the-Loop Optimization
CMAPD	Cumulative muscle activity per distance
Exo	Exoskeleton
4MWT	4-meter walk test
GEN	Generic exoskeleton torque assistance profile
OPT	Optimized exoskeleton torque assistance profile
NoExo	Walking without an exoskeleton on
NoPwr	Walking in an active exoskeleton without assistance/power
Y	Younger adult group (age <65 y/o)
O	Older adult group (age > 65 y/o)
CMAES	Covariance Matrix Adaptation Evolution Strategy

SUMMARY

Older adults are becoming the majority population across the globe and as we age quality of life and ability to live on our own declines. Self-selected walking speed is highly correlated with these declining traits and slows with age. The reason for slowing walking speed with age is unknown. Exoskeletons tested in younger adults have shown success to increase walking speed, decrease energetic consumption, and affect biomechanics across the lower limb, presenting an opportunity to understand more about walking speed. In this work, we (1) apply ankle neuromuscular model-based control to investigate the effects of exoskeleton assistance on user target joint neuromechanics, (2) optimize impedance control at the hip to reduce metabolic cost across walking speeds, (2) optimize hip and ankle assistance profiles independently to increase overground self-selected walking speed, and (4) determine if/how older adults are optimally selecting their walking speed.

This work has contributed to understanding the effects of various exoskeleton control strategies at the hip and ankle on user energetics and neuromechanics during walking. In Chapter 2, we discuss how neuromuscular model-based control at the ankle may not benefit walking metabolic cost but increase total torque production and decrease user moment. In Chapter 3, we demonstrate how impedance torque mimicking a semi-active device applied to the hip can provide metabolic benefits and how these are driven by local muscle activity changes. In Chapters 4 and 5, we apply a novel torque optimization strategy to increase SSWS in younger and older adults to (4) understand the important mechanical characteristics of assistance to increase walking speed and (5) understand the physiological drivers of walking speed selection.

CHAPTER 1. INTRODUCTION

1.1 Older adult health and locomotion

The older population (65+) is rapidly becoming the largest age group in the U.S [1, 2]. As we age, we typically become more sedentary and less able to partake in physical activity [3, 4]. This results in decreased quality of life and independence due to diminished physical health and declined locomotor (walking) ability [1, 5-10]. The biomechanics of walking changes with age. For younger adults, the ankle and hip joints are the primary positive power producers during walking, responsible for propelling the body forward to achieve a desire walking speed [11]. While we chose to walk with decreased kinetic outputs (torque and power) at each of the limb joints with age, evidence suggests that this decrease at the ankle can be explained by significant deficit in muscular power generation [12, 13]. This deficit at the ankle is considered by some to be the primary contributor of slowing walking speed with age [13]. To achieve faster desired speeds, older adults shift the majority of power generation to the hips [14, 15] despite incurring an energetic penalty [16]. In fact, older adults consume more energy to walk at a given speed than younger adults [16].

1.2 Exoskeletons interventions

Exoskeletons (exos) may be able to rapidly enhance mobility to older adults by influencing age related changes in walking, but it is unclear whether returning function to the source of the biomechanical changes with aging (ankle) or assisting at the joint of compensation (hip) would be more effective at increasing mobility. Over the past 10-15 years, exos have focused on reducing the metabolic (energy) cost of walking in lab and overground settings

[17, 18], with hip and ankle assistance providing the highest metabolic benefits to date [19]. To combat age related changes at the ankle, exos need to focus on reducing the user's moment and increasing the total moment. Indeed, ankle exo assistance can not only reduce joint moments and increase total joint moment [20]. In fact, through our previous work applying neuromuscular model-based assistance at the ankle, we found that reducing user moment and increasing total joint moment can occur simultaneously {Shafer, 2021 #313}. Unfortunately, ankle assistance has failed to reduce metabolic cost in older adult applications [21]. This may be due to the high metabolic cost of distal loading while walking [22]. At the hip, the focus would be to reduce the compensatory muscle loading to decrease energetic consumption. In older adults, hip assistance at the has successfully decreased metabolic cost as well [23]. To learn more about the mechanism of metabolic changes, in our previous work, we applied assistance at the hip across walking speeds to reduce metabolic cost {Shafer, 2022 #812}. We found not only did assistance reduce energy consumption across speeds but did so by reducing muscle activation local to the assisted hip joint. These findings inspired the thought that while metabolic reductions are indeed an important goal for exoskeleton assistance, what other locomotion performance measures could be important for older adults?

1.3 Walking speed and older adults

Studies have found that self-selected walking speed (SSWS) is an inexpensive and effect surrogate measure of physical health in older adults and is correlated with quality of life and independence [5-8]. As such, SSWS presents a clear focus for therapeutic and wearable device interventions. To provide the most effective therapeutic interventions, we must know what needs to change about patients physically and tailor exercises accordingly.

Despite the breadth of studies investigating various physical factors correlated with declining SSWS (i.e., increased energy expenditure during walking, decreased muscle strength, and decreased ankle power generation [3, 24-33]), the mechanism for the age-related slowing of SSWS still remains unclear [3, 9, 10, 24, 25, 27-29, 34, 35]. Humans naturally walk at a speed that minimizes their metabolic cost of transport (COT) or energy per unit distance [36]. With aging, the increased proportional loading at the hip significantly affects COT beyond the effects of decreased loading at the ankle [16] resulting in higher COTs across walking speeds but not a shift in the optimal speed [3, 25, 35] (Figure 1). What drives this distal to proximal change in loading and slower SSWS despite the energetic penalty? Occasionally, younger adults use muscle loading to select gait parameters during walking [37] and as power generation at the ankles significantly declines with age compared to the hip [14, 15], it seems this explanation could hold for aging as

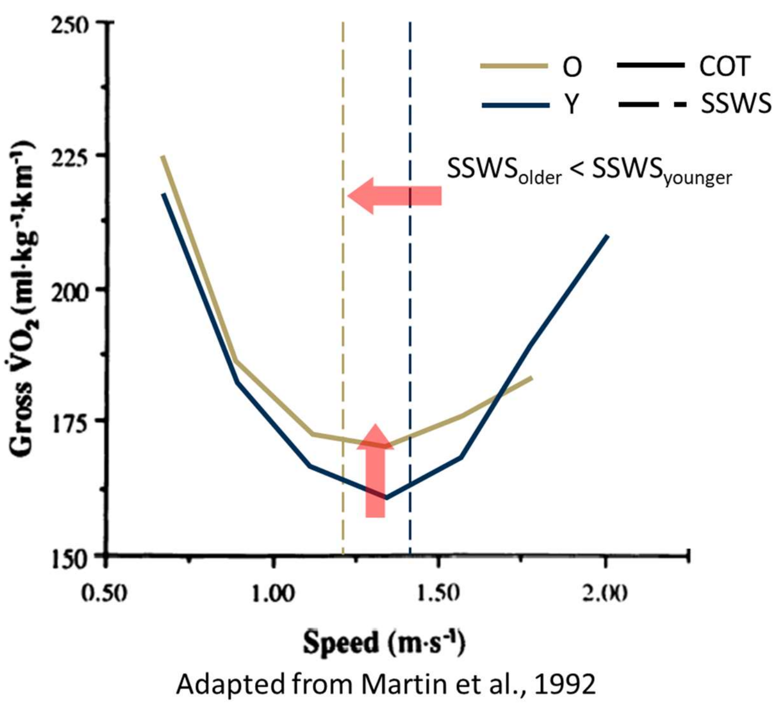

Figure 1 - Age related changes in energetic cost of transport (COT) and self-selected walking speed (SSWS).

well. Simulations implementing age-related changes to the muscles and nerves of a walking model determined that muscle load more accurately predicts SSWS compared to COT in older adults [29]. No studies have analyzed if older adults use COT and/or muscle loading to optimally select walking speed. Wearable robotic interventions could allow us to causally probe for the answer by altering SSWS and allowing us to measure the physiological factors driving this change.

1.4 Exoskeletons and SSWS

Few studies have examined SSWS in younger and older adults. In younger adults, assistance at the ankle has successfully increased SSWS both on a treadmill and overground [18, 38] In older adults, elastic hip assistance has increased walking speed in older adults with neurological disabilities [23], but ankle assistance has not produced any benefits [21]. With only a few studies applying exos to improve SSWS with no direct comparisons, it is unclear if assistance at the hip or the ankle would be more beneficial. Human-in-the-loop optimization (HILO) has the potential to enhance exo performance outcomes in older adults by individualizing exo assistance without mechanistic understanding of SSWS. In younger adults, HILO has been used to maximize metabolic benefits at each lower limb joint [39-41] and SSWS at the ankle [18, 38]. Further, our previous work and other studies have found individually optimized (*i.e.,* individualized, user-dependent) exo torque assistance provides more metabolic benefit than generic (*i.e.,* user-independent) assistance [41-44]. Individualization of assistance may be increasingly important for older adults as muscle activation and gait parameters vary more with age [45, 46]. Unfortunately, the HILO protocols with the highest performance benefits require at least 60-90 minutes of walking in one session. As fatiguability increases with age [47], the ability of older adults to complete strenuous or lengthy HILO protocols is limited. To decrease strain on older adults, we need to carefully select the optimization algorithm and goal. Among the HILO algorithms, Bayesian optimization has reached optimal convergence with the least effort [40, 41, 48]. In terms of optimization goals, optimizing overground SSWS measurements, instead of metabolic cost, would decrease optimization times by ~75% [38, 41, 42]. An additional benefit to using overground SSWS, from our pilot studies, overground walking speed selection when walking with an experimental device has been more comfortable amongst older adults. We think combining a Bayesian optimization with overground SSWS measurement will allow older adults to participate in HILO for ankle and hip assistance and increase assisted walking speeds.

1.5 This work

In the work that follows, we first examined the effects of ankle and hip assistance on walking energetics, biomechanics, and muscle activation and then applied HILO for hip and ankle assistance to maximize overground walking speed for younger and older adults. The optimized assistance would allow us to study the physiological determinants of walking speed by measuring energetics and muscle activity across a range of walking speeds. This work provides: (1) neuromechanical understanding of energy consumption changes with ankle assistance, (2) neurological mechanisms for the energetic benefits of hip assistance across walking speeds, (3) an overground HILO protocol for SSWS that can be used in the clinic to prescribe exoskeleton assistance for healthy younger and older adults, (4) optimal exo assistance profiles to increase overground SSWS at the hip and ankle for both younger and older adults (allowing “out-of-the-box” exoskeleton controllers and comparisons to metabolically and treadmill SSWS optimized profiles), and (5) a causal probe determining if SSWS optimizes energetic and/or muscle activity measures with age. These contributions will increase mechanistic understanding of mobility and help steer exoskeleton and therapeutic interventions to combat age related slowing of SSWS.

CHAPTER 2. NEUROMECHANICS AND ENERGETICS OF WALKING WITH AN ANKLE EXOSKELETON USING NEUROMUSCULAR-MODEL BASED CONTROL: A PARAMETER STUDY

2.1 Introduction

Lower-limb exoskeletons are a promising approach to reduce human effort by providing mechanical assistance to restore, replace, or augment the function of biological musculotendons during walking [17]. Analysis of human gait biomechanics provides a roadmap that can be used to guide the location (*e.g.,* ankle, knee or hip), timing and magnitude of mechanical assistance applied by an exoskeleton system. Indeed, based on the large contribution of ankle musculotendons to the overall mechanical power generated by the lower-limb during walking [49], researchers and engineers have focused heavily on delivering power with ankle exoskeletons as a means for reducing metabolic cost of walking [41, 50-55]. These studies clearly demonstrate that powered ankle exoskeletons are a viable means to decrease metabolic cost of walking, in the best case, by ~10% when compared to walking in normal shoes [53]. Although the number of ankle exoskeletons demonstrating metabolic benefits in a controlled laboratory setting continues to grow [17], to be useful in the real-world, these devices need to be able to automatically adjust to both the user and the environment.

A major factor in determining exoskeleton performance is the control architecture that is used to generate the commands to the motors that apply torques to the lower-limb joints

[56-58]. A wide variety of torque control schemes have been demonstrated in lower-limb wearable robots [59] with a subset employed in powered ankle exoskeletons [60, 61]. Some common examples include applying preset stiffness and damping values set as a function of joint angle [62] or stride percentage (*i.e.,* impedance control); directly driving the exoskeleton actuators with muscle activity of the user (*i.e.,* myoelectric control) [50, 63-67] or specifying a set torque-time trajectory over the stride [41, 51-53]. There are practical benefits and drawbacks to each of these control schemes, but they all share a common pitfall: reliance on *a priori* tuning of parameters. Tuning typically involves a time-consuming, exhaustive sweep of all combinations of the control parameters or, more recently, human-in-the-loop optimization [41] to find the set that is optimal for a given user and a chosen locomotion mode and outcome measure (*e.g.,* the set that minimizes metabolic rate during walking at 1.25 m/s for user A). Even if an optimal parameter set is discovered under those unique conditions, they likely will not transfer to other locomotor modes that reflect normal walking behavior in the 'real-world'[68]. Using an adaptive controller that does not need to be tuned for each mode, optimally once per individual, could increase user acceptance of robotic exoskeletons for everyday use in dynamic environments.

Model-based ankle exoskeleton control is another option that may lead to robust, adaptive behavior in response to changes in the state of the user and/or the environment. In this control approach, a virtual muscle-tendon unit (MTU) is implemented to mimic the biological MTU. Typically, a Hill type MTU model [69] is derived with contractile properties similar to the target biological analogue. Then, the virtual MTU length change is driven by the user's real-time joint kinematics through a virtual moment arm. The virtual muscle is stimulated by a modelled positive force feedback reflex pathway with a preset gain and delay to generate ongoing virtual muscle activation based on the previous force output of the model. In addition, the virtual muscle adheres to force-length and force-velocity relationships that can modify force output. Finally, the virtual MTU force is converted to an exoskeleton torque, again through the virtual moment arm. In essence, if the neuromuscular model were perfect, this approach would generate exoskeleton torque identical to the biological moment of the MTU targeted for assistance. In addition, because the assistance torque manifests from activation, length, and velocity of a virtual muscle with a reflex pathway, the output should be able to spontaneously adapt to changing mechanical demands – similar to the biological system itself. Indeed, previous research has demonstrated that a reflex-driven, neuromuscular model (NMM) [70] of the biological plantarflexors can provide robust torque commands to a powered ankle-foot prosthesis [71] across a range of walking speeds and ground slopes without any need to adjust controller parameters per task. As a result, with NMM-controlled powered ankle-foot prostheses, amputees achieved normalized walking mechanics and energetics across a range of walking speeds [72, 73]. Recently, NMM-based control has been implemented on exoskeleton systems designed to restore movement to people with paralysis due to spinal cord injury or stroke [74-76]. However, to date, it is unclear whether NMM-based control is an effective strategy to provide assistive torques in parallel with neuromechanically intact ankle musculotendons and reduce effort during walking – even at a fixed-speed on level ground.

The purpose of this study was to implement an NMM-based controller designed to emulate the human ankle plantarflexors on a powered ankle exoskeleton and examine how it influences the neuromechanics and energetics of walking at a fixed-speed. Previous studies have demonstrated that both the timing and magnitude of ankle exoskeleton assistance are important for minimizing the metabolic cost of the user [41, 53]. Studies employing NMM-based control on powered ankle-foot prostheses have demonstrated that timing and magnitude of torque can be modulated by adjusting the Gain and Delay of the positive force feedback reflex pathway [71]. Here, we set out to conduct a parameter study to specifically examine how NMM reflex Gain and Delay settings effect (*i*) timing and magnitude of ankle exoskeleton torque and power output and (*ii*) users' physiological response - from whole body metabolic rate to individual muscle activity. To do this we implemented an NMM-based controller on a bilateral, tethered robotic ankle exoskeleton and independently varied the reflex Gain (0.8-2.0) and Delay (10ms-40ms) while recording the exoskeleton mechanics, and users' lower-limb joint neuromechanics, muscle activity and whole-body metabolic rate during walking at a fixed 1.25 m/s. In terms of exoskeleton mechanical performance, we hypothesized that increasing NMM reflex Gain at a set Delay would increase both average exoskeleton torque and net power output. On the other hand, we hypothesized that increasing NMM reflex Delay at a set Gain would not affect average exoskeleton torque but still increase net exoskeleton power due to a shift in peak assistance torques toward the period of peak ankle plantarflexion velocities in late stance. In terms of users' physiological response, we hypothesized that conditions that yielded the most net exoskeleton power would decrease metabolic rate the most (*i.e.,* high Gain=2.0 and long Delay = 40ms).

2.2 Methods

2.2.1 Powered Ankle Exoskeleton

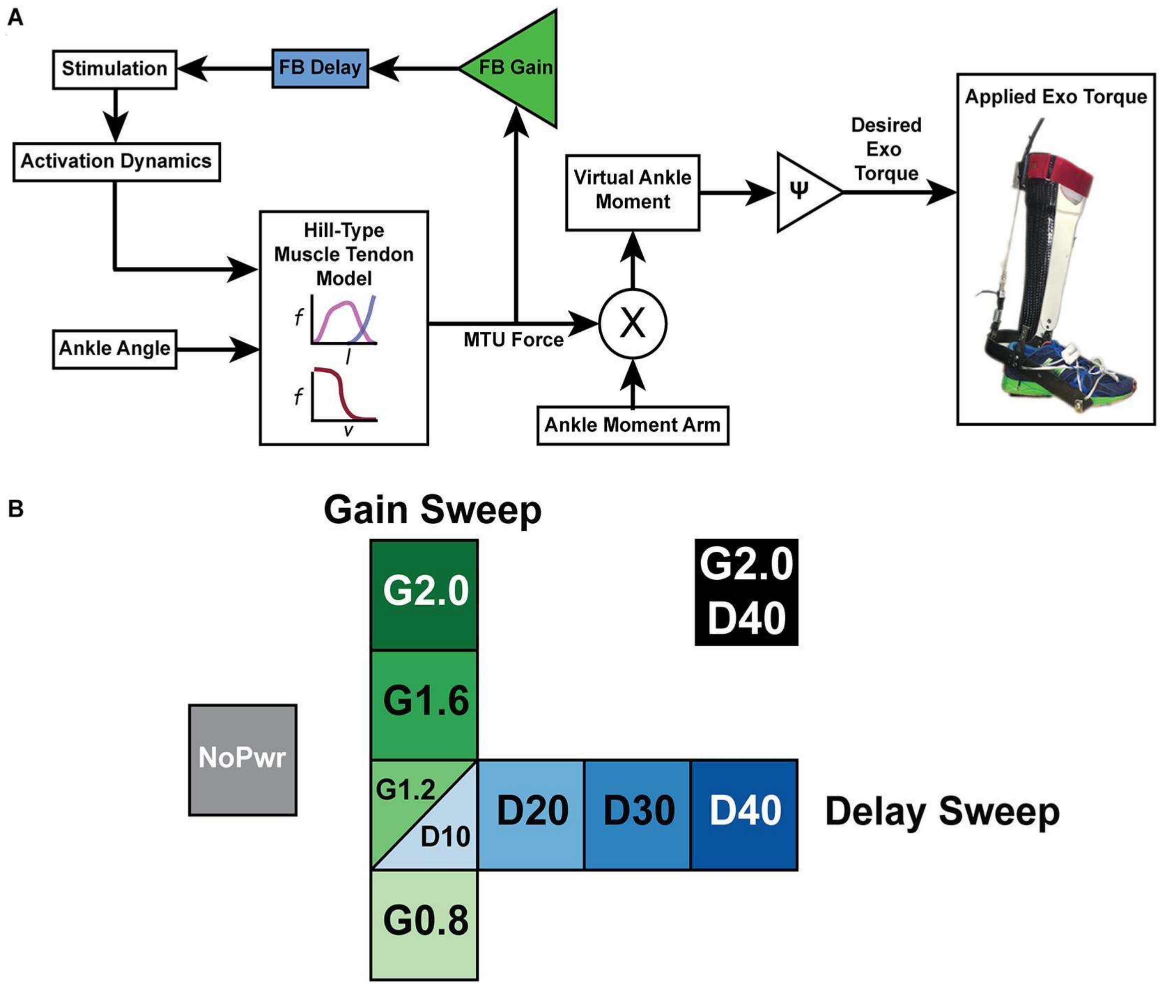

Figure 2 - A powered ankle exoskeleton using neuromuscular model (NMM) based control across a range of virtual reflex settings (A) Block diagram of a neuromuscular model (NMM) based controller to generate torque output of a powered ankle exoskeleton. The user's ankle joint angle drives the length change of a virtual muscle-tendon unit (MTU) that uses a positive force feedback reflex loop to stimulate a virtual Hill-type muscle contractile element with force-length and force velocity properties similar to the human plantarflexors. The virtual muscle produces a force that is transmitted through a virtual tendon and then applied through a virtual moment arm to generate a virtual ankle moment which is scaled to produce a desired exoskeleton torque. (B) Test conditions for NMM reflex Gain and Delay parameter sweeps included an unpowered or zero-torque condition (NoPwr) (gray) along with powered ankle exoskeleton conditions using controllers with increasing virtual reflex Gain = 0.8, 1.2, 1.6, and 2.0 all with a 10 ms Delay (G0.8, G1.2, G1.6, and G2.0, respectively) (green); increasing virtual reflex Delay = 10, 20, 30, and 40 ms all with a 1.2 reflex Gain (D10, D20, D30, D40, respectively) (blue); and a high-Gain-high-Delay condition (G2.0 D40) (black). All tests were conducted during treadmill walking at 1.25 m/s.

A laboratory-based, tethered exoskeleton emulator provided subjects with plantarflexion torque assistance using a combination of powerful off-board motors (Baldor Electric Co., Fort Smith, AR) and lightweight, bilateral carbon fiber ankle foot orthoses. A flexible Bowden-cable transmission system delivered linear motion from the rotational motion of the motors. The 58" long external conduits (5/16", Lexco Cable Mfg., Norridge, IL) housed low stretch Vectran rope (V-12 Vectran Single Braid, 3mm, 1900 lb, West Marine, USA) attached to a moment arm (~10 cm) at the rear of the exoskeleton (Figure 2A, right). Load cells (500 Hz, LCM Systems Ltd, UK) were placed in series with the force transmission cables and series elastic element. Goniometers (500 Hz, Biometrics, UK) were attached to the exoskeleton joint to provide real-time ankle angle information. The control model, designed in Simulink (MathWorks, USA), was embedded on a real-time computer (dSPACE, Germany) that handled analog sensor data sampled at 5 kHz and generated motor commands at 500 Hz. Motor commands were implemented via motor driver (ABB, Cary, NC) operating in velocity control mode.

2.2.1.2 Exoskeleton Neuromuscular Model (NMM) Controller

We implemented a neuromuscular model (NMM) based feedback controller with features similar to a previous implementation on a powered ankle-foot prosthesis [70, 71], and recently demonstrated on a tethered ankle exoskeleton [60, 61, 77] (Figure 2A) . The emulated plantarflexor muscle tendon unit (MTU) was based off a Hill-type muscle model that consisted of a contractile element (CE), possessing both active and passive properties, and a series elastic element (SEE) modeling the tendon [69]. The internal states of the muscle-tendon model were calculated in a given time-step i (Figure 2B), such that the length of the MTU was a function of modeled musculoskeletal geometry and ankle angle

(Equation 1). SEE length was calculated by subtracting CE length from MTU length (Equation 2).

$$L_{MTU,i} = f(\theta_{ank}, r_{ank}) \tag{1}$$

$$L_{SEE,i} = L_{MTU,i} - L_{CE,i} \tag{2}$$

The force developed in the MTU (F_{MTU}) was a function of the modeled nonlinear stiffness of the SEE and the calculated strain in the SEE (Equation 3).

$$F_{MTU,i} = f(k_{SEE,i}, L_{SEE,i}) \tag{3}$$

CE velocity was calculated from muscle force-length, force-velocity, and activation relationships derived from the Hill model (Equation 4). The parameters of the lumped-plantarflexors (*e.g.,* F_{max} = 6000N, L_o = 0.04m, V_{max} = 0.326 m/s, k_{SEE} = 315.4 N/mm) were all taken from our previous modelling and simulation work [78]. The CE velocity was then integrated to calculate the length of the CE in the next time step (*i+1*) (Equation 5).

$$\dot{L}_{CE,i} = f\left(F - L, F - V, a_{,i}\right) \tag{4}$$

$$L_{CE,i+1} = \int \dot{L}_{CE}\, dt \tag{5}$$

In the reflex pathway, F_{MTU} (Figure 2A) was normalized by a F_{max}, multiplied by a feedback Gain, and then subjected to a Delay to emulate a positive force feedback neural input signal (Stimulation) (Figure 2 - A powered ankle exoskeleton using neuromuscular model (NMM) based control across a range of virtual reflex settings (A) Block diagram of a neuromuscular model (NMM) based controller to generate torque output of a powered ankle exoskeleton. The user's ankle joint angle drives the length change of a virtual muscle-tendon unit (MTU) that uses a positive force feedback reflex loop to stimulate a virtual Hill-type muscle contractile element with force-length and force velocity properties similar to the human plantarflexors. The virtual muscle produces a force that is transmitted through a virtual tendon and then applied through a virtual moment arm to generate a virtual ankle moment which is scaled to produce a desired exoskeleton torque. (B) Test conditions for NMM reflex Gain and Delay parameter sweeps included an unpowered or zero-torque condition (NoPwr) (gray) along with powered ankle exoskeleton conditions using controllers with increasing virtual reflex Gain = 0.8, 1.2, 1.6, and 2.0 all with a 10 ms Delay (G0.8, G1.2, G1.6, and G2.0, respectively) (green); increasing virtual reflex Delay = 10, 20, 30, and 40 ms all with a 1.2 reflex Gain (D10, D20, D30, D40, respectively) (blue); and a high-Gain-high-Delay condition (G2.0 D40) (black). All tests were conducted during treadmill walking at 1.25 m/s.A). The feedback loop was closed by modeling the activation dynamics (a) of the CE and integrating to find a new activation level at time $i+1$ (Equation 6).

$$a_{i+1} = \int \dot{a}_i \, dt \tag{6}$$

Finally, the desired exoskeleton torque assistance was set using a gain ψ to set the fraction of the estimated biological torque coming from the NMM (Equation 7) (Figure 2B).

$$\tau_{exo} = F_{MTU} \times r_{ankle} \times \psi \qquad (7)$$

Based on our own pilot experiments to qualitatively examine user preference/comfort and others' work indicating that ankle exoskeleton torques that are optimal for reducing metabolic energy cost of walking rarely, if ever, exceed 50% of the biological ankle moment [41, 53, 67], we fixed the value ψ =0.5 in this study.

2.2.2 Experimental protocol

2.2.2.1 Participants

Nine able-bodied participants (age = 24 ± 3 years; mass = 71.3 ± 7.1 kg; height = 1.76 ± 0.05 m; mean ± s.d.) signed a consent form to participate in this study. All consent forms and testing procedures were approved by the University of North Carolina, Chapel Hill and North Carolina State University institutional review board and followed the procedures outlined by the Declaration of Helsinki.

2.2.2.2 Testing Procedure

All trials were completed on an instrumented treadmill (Bertec Inc., Columbus, OH, USA) at a fixed walking speed of 1.25 m/s. First, subjects walked for 25 minutes with bilateral ankle exoskeletons powered in a baseline condition (Gain=1.2; Delay=10ms) to get comfortable using the device. Baseline values for the parameter sweeps (Gain=1.2 and Delay = 10ms) were based on the optimal values of a NMM controller that generated biological plantarflexor torque outputs in previous work using in powered ankle foot prosthesis [70, 71, 73]. We chose a 25 minute acclimation period based on previous research indicating that subjects need ~20-30 mins of walking to reach steady state metabolic effort in powered ankle exoskeletons [79]. Subjects were encouraged to experiment with different gaits during this time, but no further instructions were given. Next, each participant walked during nine different experimental conditions lasting seven minutes each while wearing the exoskeletons. The nine exoskeleton conditions consisted of one unpowered (NoPwr) where we applied zero-torque; four powered conditions with different NMM reflex Gain (0.8-2.0 = G0.8, G1.2, G1.6 and G2.0) at a set delay (10ms); four powered conditions with different NMM reflex Delay (10-40ms = D10, D20, D30, D40) at a set gain (1.2), and a final condition with the highest gain and delay (2.0 gain/40ms delay = (G2.0/D40) (Figure 2B). The conditions were applied in a pseudo-randomized order. Participants wore a safety harness to decrease the risk of falling or sustaining an injury. The harness did not provide any body weight support. Subjects were instructed to only use the handrails for small balance corrections throughout the trials.

2.2.3 Measured Outcomes

2.2.3.1 Lower-limb Joint and Exoskeleton Mechanics

We collected anthropometric data for each subject before testing started. Reflective markers were placed on the left and right anterior superior iliac spine, greater trochanters, medial and lateral epicondyles of the knee, medial and lateral malleoli of the ankle, third metatarsophalangeal joint of the toe, and posterior calcaneus of the heel. Four marker clusters were placed on rigid plates and attached to the pelvis, thighs, shanks, and feet. An eight-camera motion analysis system (Vicon Inc., Oxford, UK) captured the position of 44 reflective markers at 120 Hz.

To assess lower limb joint kinematics/kinetics, we used a seven-segment rigid body model composed of two thighs, two shanks, two feet, and one pelvis. Raw marker positions were filtered using a second-order low pass Butterworth filter with a cut-off frequency of 10 Hz. Ankle, knee, and hip joint angles were computed as the orientation of the distal segment with reference to the proximal segment. The results reported in this study are of the right leg only. Lower-limb joint moments were computed using standard inverse dynamics analyses (Visual 3D, C-Motion Inc., Germantown, MD). Ankle exoskeleton torque was calculated by multiplying the recorded tension in the exoskeleton Bowden cable (Omegadyne Inc., Norwalk, CT) by the moment arm length to the user's ankle joint center. Lower-limb joint moments and ankle exoskeleton torque were multiplied by corresponding joint angular velocities to calculate lower-limb joint and exoskeleton mechanical power output. Next, moments/torques/powers were normalized to each subject's body mass. The biological contribution to total ankle joint moment/power was found by subtracting the measured exoskeleton torque/power from the inverse-dynamics derived, total ankle joint moment/power. Then, stride average, normalized lower-limb joint and exoskeleton moments/torques/powers were obtained by averaging ~10 representative strides for each subject in each condition. For each subject in each condition, average normalized ankle joint moment/exoskeleton torque was calculated as the integral of the joint moment/exoskeleton torque time-series over the gait cycle divided by the stride time. Net mechanical power outputs at each joint and for the exoskeleton were calculated as the integral of the joint mechanical power time-series over the gait cycle divided by the stride time.

2.2.3.2 Ankle Muscle Activity

Ankle joint muscle activity was measured using surface electromyography (EMG). Wired surface electrodes (SX230, Biometrics Ltd., Newport, UK), sampled at a frequency of 960 Hz, were placed on the lateral aspect of the soleus (SOL), the medial and lateral gastrocnemius (MG and LG, respectively) and the tibialis anterior (TA) of the right leg. The EMG signals were high-pass filtered with a cutoff frequency 20Hz, rectified, and low-pass filtered with a cutoff frequency of 6 Hz to get EMG envelopes over the gait cycle. Next, for each muscle, envelopes were normalized to the peak activity observed during walking with zero exoskeleton torque (NoPwr condition). Then, stride average normalized EMG envelopes were obtained by averaging ~10 representative strides for each subject in each condition. Finally, for each subject in each condition, average normalized EMG activity for each muscle was calculated as the integral of the normalized EMG envelope time-series over the gait cycle divided by the stride time. The EMG data for Subject 2 was determined to be a statistical outlier and was omitted from reported EMG data and associated statistical analyses.

2.2.3.3 Whole-body Metabolic Rate

Users' whole-body metabolic rate was estimated using indirect calorimetry. A portable metabolic system (Oxycon Mobile, Viasys Healthcare Inc., Yorba Lina, CA, USA) was used to record the flow rates for oxygen inspired and carbon dioxide expelled. These flow rates were converted to a metabolic rate (Watts) using the Brockway equation [80] and then normalized to the subject's body mass (Watts/kg). The metabolic rate from the last two minutes of each seven-minute trial were averaged to calculate the steady-state metabolic rate for each condition. The metabolic rate data for Subject 4 was determined to be a statistical outlier and was omitted from reported metabolic rate data and associated statistical analyses.

2.2.4 Statistical Analyses

Formal comparisons between powered ankle exoskeleton NMM control parameter conditions were made by comparing subject averages for exoskeleton mechanics, ankle joint mechanics, ankle joint muscle activity and metabolic rate across the test conditions (see above for details). Standard error of the mean was used to represent variability between subjects. Two separate, single-factor, repeated-measures ANOVA analyses were performed to test the significance of trends in each measured outcome across NMM controllers; one to test for an effect of NMM reflex Gain (G0.8, G1.2, G1.6, and G2.0) and one to test for an effect of NMM reflex Delay (D10, D20, D30, D40) on exoskeleton mechanics and user's physiological response. For physiological variables, the NoPwr condition was included for both Gain and Delay tests. Metrics that had a significant main effect (ANOVA; $p<0.05$) were followed by post-hoc pairwise comparisons between individual conditions. A Bonferroni correction was applied to account for multiple comparisons. Finally, several post-hoc least-squares linear regression (LSLR) analyses were performed to quantify the relationship between changes in users' metabolic rate and changes in users' neuromechanics with respect to the unpowered exoskeleton condition. R^2 values are reported only when regressions were deemed statistically significant ($p<0.05$).

2.3 Results

2.3.1 Ankle kinematics

Users assumed a more plantarflexed posture while walking with powered versus unpowered ankle exoskeletons (Figure 3A, B; Figure 33 - Users' total (bio + exo) ankle kinematics and kinetics over a stride cycle. Measurements of users' ankle angle (A and B), total ankle moment (C and D), and total ankle power (E and F) over a stride from heel strike (0%) to heel strike (100%) of the same leg are shown. Ankle plantarflexion is depicted as positive and dorsiflexion as negative for the angle and moment plots. All data were first averaged across many strides per participant and then across all participants (N=9) per condition. Time-series data across Gain conditions can be seen on the left (A, C, and E) and across Delay conditions on the right (B, D, and F). Conditions are abbreviated and color coded as follows: unpowered (NoPwr)(gray), NMM reflex Gains of 0.8, 1.2, 1.6, and 2.0 all with reflex Delay=10ms (G0.8, G1.2, G1.6, and G2.0, respectively) (green), NMM reflex Delays of 10, 20, 30, and 40ms all with a reflex Gain=1.2 (D10, D20, D30, D40, respectively) (blue), and a high-Gain-high-Delay condition (G2.0 D40) (black).). Qualitatively, plantarflexion bias tended to increase when increasing either neuromuscular model (NMM) controller reflex Gain (Figure 2A) or reflex Delay (Figure 2B) and was apparent throughout the entire gait cycle, including times of peak plantarflexion and even during swing phase (Figure 2A). Peak ankle angular velocities (both plantar- and dorsiflexion) decreased from the unpowered to the powered conditions, with increasing Gain (Figure 2C) having a larger effect, qualitatively, than increasing Delay (Figure 2D).

2.3.2 Exoskeleton mechanics

Powered ankle exoskeleton torque and net mechanical power output were both modulated by changes in neuromuscular model (NMM) controller reflex Gain and reflex Delay parameters (Figure 3E-H, Figure 4). Increasing Gain increased both exoskeleton average torque (ANOVA, $p < 0.001$) (Figure 3A) and net power output (ANOVA, $p < 0.001$)

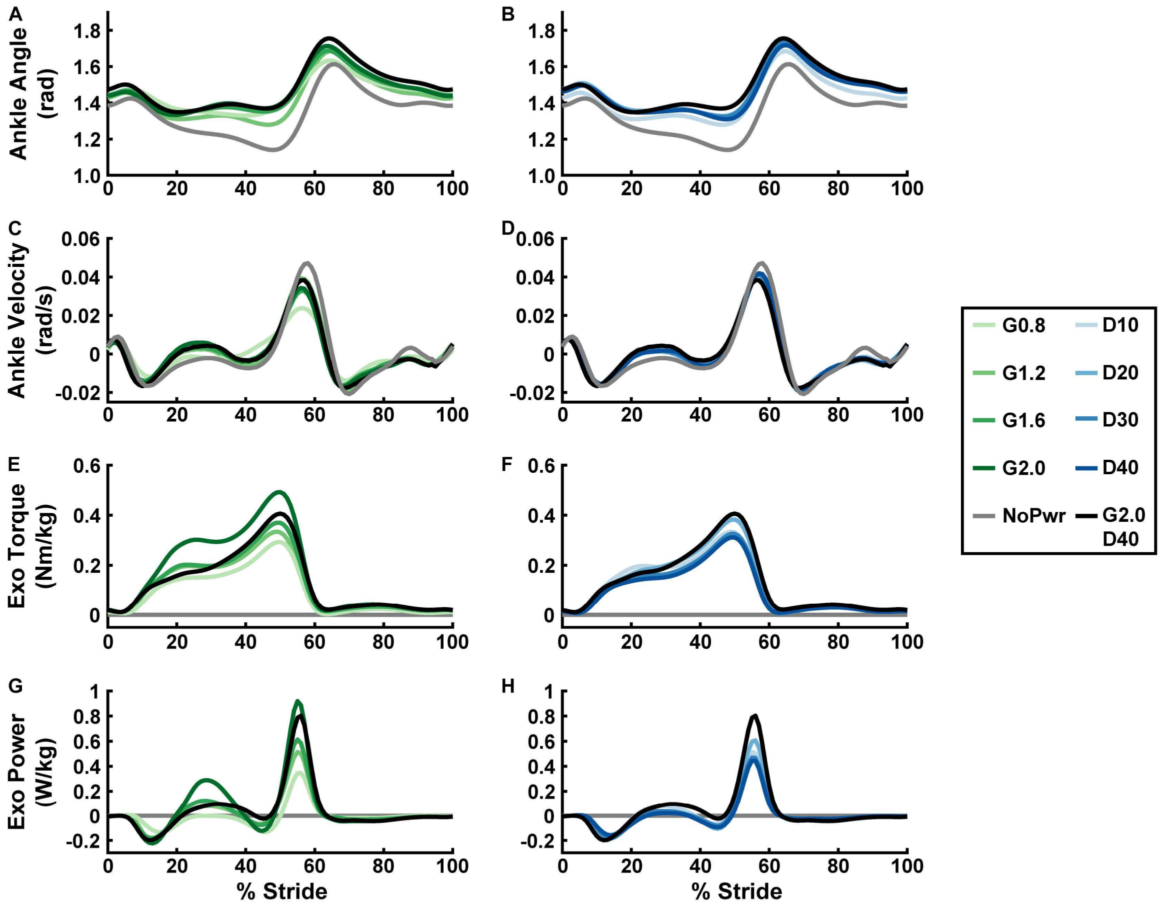

Figure 3 - Users' ankle joint kinematics, and exoskeleton mechanics over a stride cycle. Measurements of users' ankle angle (A,B), ankle angular velocity (C,D), ankle exoskeleton torque (E,F), and ankle exoskeleton mechanical power (G,H) over a stride from heel strike (0%) to heel strike (100%) of the same leg are shown. Ankle plantarflexion is depicted as positive and dorsiflexion as negative for the angle, angular velocity, and torque plots. Positive/negative power indicates net energy transfer from exoskeleton to user and vice versa. All measurements are averages across the study participants (N = 9) in each condition with varying neuromuscular model (NMM) controller reflex Gain (green) in left panel (A,C,E,G) and Delay (blue) in the right panel (B,D,F,H). Conditions are abbreviated and color coded as follows: unpowered (NoPwr) (gray), NMM reflex Gains of 0.8, 1.2, 1.6, and 2.0 all with reflex Delay = 10 ms (G0.8, G1.2, G1.6, and G2.0, respectively) (green), NMM reflex Delays of 10, 20, 30, and 40 ms all with a reflex Gain = 1.2 (D10, D20, D30, D40, respectively) (blue), and a high-Gain-high-Delay condition (G2.0 D40) (black).

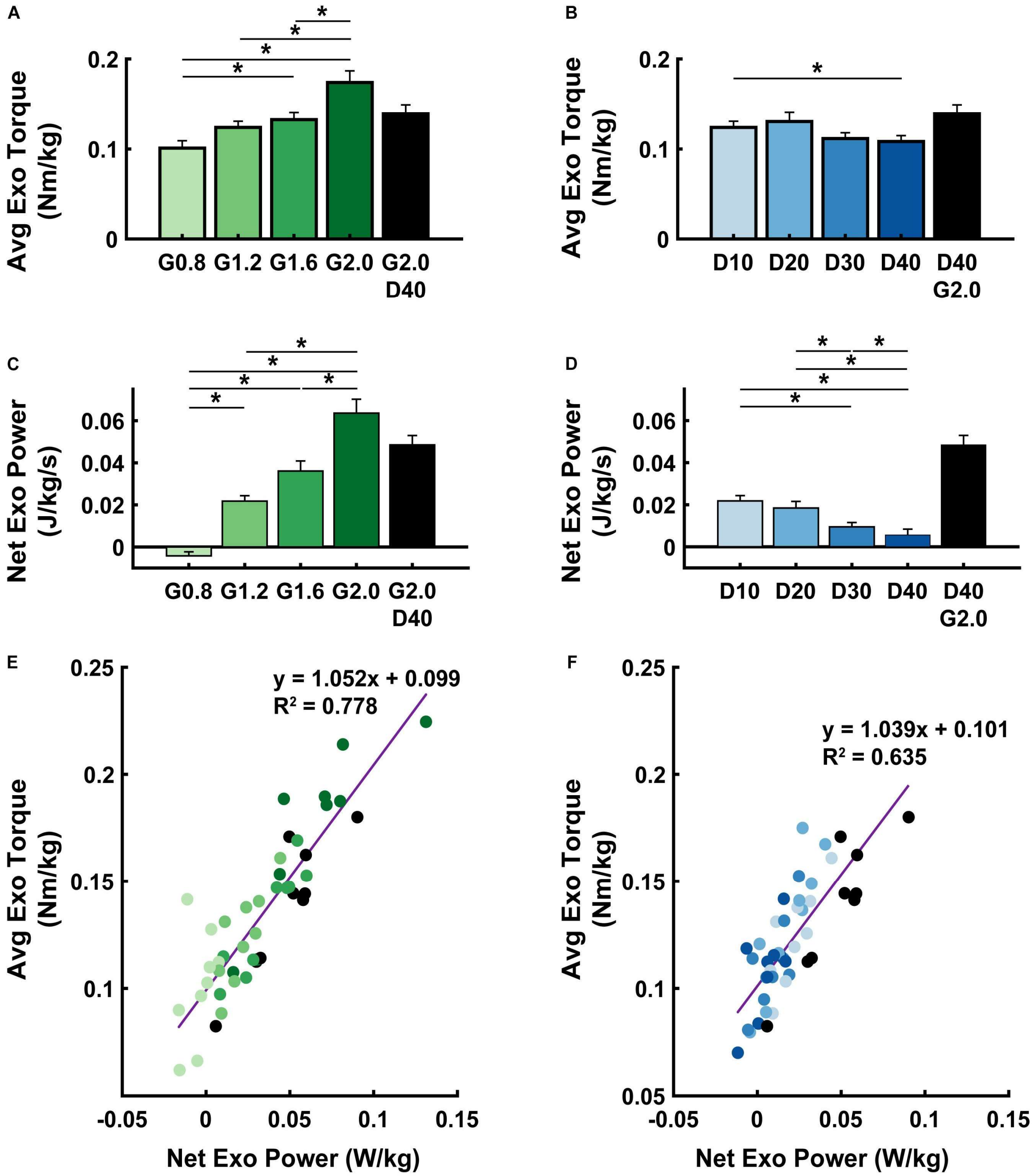

Figure 4 - Exoskeleton mechanics. Average (± S.E.M., N = 9 participants) exoskeleton torque (A,B), net exoskeleton power (C,D), and a linear regression between the two (E,F) across NMM controller reflex Gain (green) (A,C,E) and Delay (blue) (B,D,F) conditions. * denotes pairwise significant difference with $p < 0.05$. R2 values are denoted with a "~" if the linear regression was not statistically significant. Conditions are abbreviated and color coded as follows: NMM reflex Gains of 0.8, 1.2, 1.6, and 2.0 all with reflex Delay = 10 ms (G0.8, G1.2, G1.6, and G2.0, respectively) (green), NMM reflex Delays of 10, 20, 30, and 40 ms all with a reflex Gain = 1.2 (D10, D20, D30, D40, respectively) (blue), and a high-Gain-high-Delay condition (G2.0 D40) (black).

(Figure 3C). All Gain conditions produced significantly different average torques except

G1.2 compared to G0.8 and G1.6 (paired t-test, $p = 0.187$ and $p = 1.000$, respectively) (Figure 3A). Similarly, all net power outputs were significantly different except G1.2 and G1.6 (paired t-test, $p = 0.073$). In addition, G0.8 provided net negative power (-0.01 ± 0.00 W/kg) while all others produced net positive power (Figure 3C).

Increasing Delay decreased exoskeleton average torque (ANOVA, $p = 0.004$) (Figure 3B), and net power output (ANOVA, $p < 0.001$) (Figure 3D). Increasing Delay from 10ms to 40ms significantly reduced average exoskeleton torque by ~12.6% (paired t-test, $p = 0.030$) (Figure 3B). Increasing Delay produced significantly different net exoskeleton power between all conditions except D10 to D20 (paired t-test, $p = 1.000$) (Figure 3D).

When viewing the interaction between exoskeleton torque and power for both the Gain (Figure 3E) and Delay (Figure 3F) parameter sweeps, there was a near 1:1 positive relationship between net exoskeleton power (W/kg) and average exoskeleton torque (Nm/kg). Each relationship was statistically significant (Gain: LLSR, $p < 0.0001$; $R^2 = 0.7784$ and Delay: LLSR, $p < 0.0001$; $R^2 = 0.6351$). The internal states of the neuromuscular model (NMM) that generated exoskeleton torque output through time across conditions are summarized in Figure 32.

2.3.3 Metabolic rate

Users' metabolic rate was unchanged when walking with powered ankle exoskeletons using neuromuscular model (NMM) based control across a range of parameter settings (Figure 5). Neither increasing NMM reflex Gain (ANOVA, $p = 0.1535$) (Figure 5A) or reflex Delay (ANOVA, $p=0.0558$) (Figure 5B) had a significant effect on users' metabolic rate. Metabolic rate varied slightly across NMM reflex parameter space compared to the

NoPwr condition. The D20 condition yielded the lowest average metabolic rate at 5.1 ± 0.2

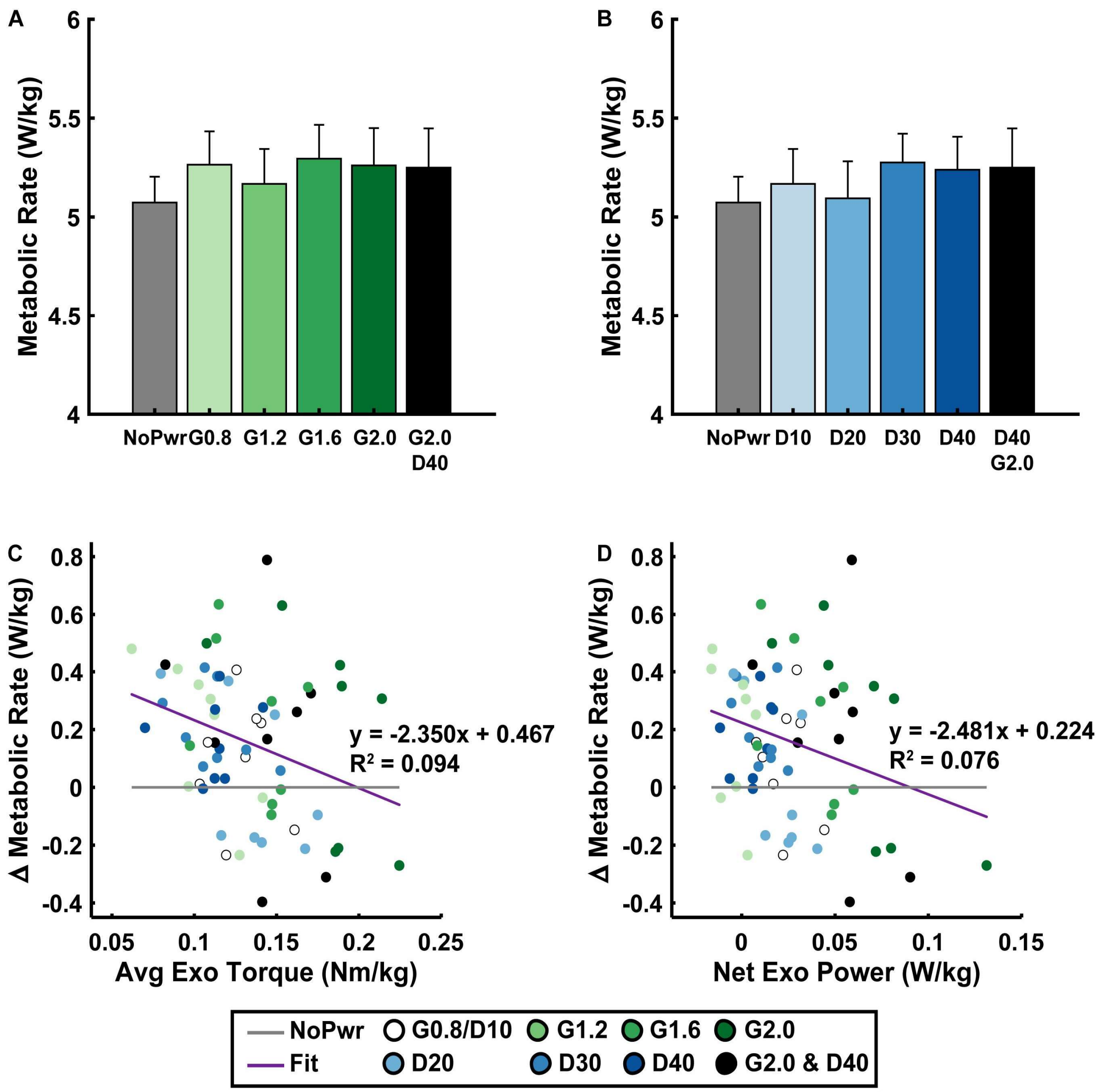

Figure 5 - Users' metabolic rate. Average (± S.E.M., N = 9 participants) metabolic rate across NMM reflex Gain (green) (A) and Delay (blue) (B) conditions. Linear regressions between the change in metabolic rate versus the change in average exoskeleton torque with respect to the unpowered (NoPwr) condition (C) and the change in metabolic rate versus the change in net exoskeleton power with respect to the unpowered (NoPwr) condition (D). * denotes pairwise significant difference with $p < 0.05$. R2 values are denoted with a "~" if the linear regression was not statistically significant. Conditions are abbreviated and color coded as follows: unpowered (NoPwr) (gray), NMM reflex Gains of 0.8, 1.2, 1.6, and 2.0 all with reflex Delay = 10 ms (G0.8, G1.2, G1.6, and G2.0, respectively) (green), NMM reflex Delays of 10, 20, 30, and 40 ms all with a reflex Gain = 1.2 (D10, D20, D30, D40, respectively) (blue), and a high-Gain-high-Delay condition (G2.0 D40) (black).

(a <1.0% increase from NoPwr) and the G1.6 condition yielded the highest metabolic rate at 5.3 ± 0.2 (a 4.4% increase from NoPwr) (Figure 5 A, B).

Changes in users' metabolic rate (*i.e.,* Δ with respect to NoPwr) were not well correlated with standard measures of exoskeleton mechanical assistance across Gain and Delay parameter space. For example, changes in users' metabolic rate were negatively correlated with both average exoskeleton torque (LLSR, $p = 0.0136$; $y = -2.350x + 0.467$) (Figure 5C), and net exoskeleton power (LLSR, $p = 0.0275$; $y = -2.482x + 0.224$,) (Figure 5D), but these significant relationships explained only a small amount of the variability in metabolic rate ($R^2 = 0.094$ and $R^2 = 0.076$, for average torque and net power respectively).

2.3.4 Biological ankle mechanics

Users' biological ankle moment and mechanical power were both modulated by changes in powered ankle exoskeleton NMM controller reflex Gain and Delay parameters (Figure 6, Figure 33). In general, during powered conditions, biological ankle moment (Figure 6 A-D) increased during the first half of stance (0-30% stride) and decreased during the second half of stance (30-60% stride), but the timing of peak biological ankle moment was unchanged (Figure 6A, B). Increasing either Gain (ANOVA, $p<0.001$) (Figure 6C) or Delay (ANOVA, $p=0.020$) (Figure 6D) caused a decrease in average biological ankle moment. The largest Gain condition (G2.0) was the only powered condition significantly different from the NoPwr condition (paired t-test, $p = 0.005$) (Figure 6C), decreasing biological moment by 17.6%. Overall, changes in average biological ankle moment were not significantly correlated with changes in metabolic rate (LLSR, $p = 0.855$) (Figure 6I).

For biological ankle power output (Figure 6 E-H), when the exoskeletons were powered

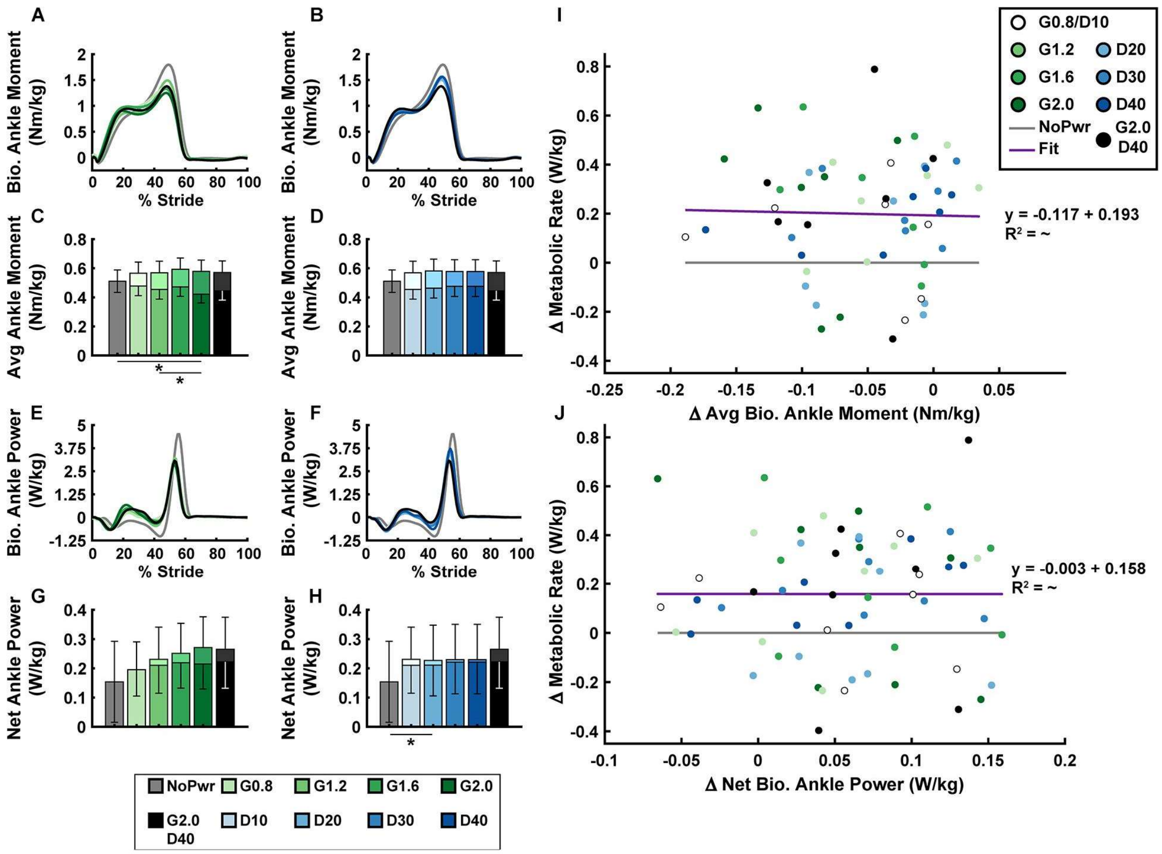

Figure 6 - Users' biological ankle mechanics versus metabolic rate. Measurements of users' average biological ankle moment (A,B) and power (E,F) over a stride from heel strike (0%) to heel strike (100%) of the same leg are shown. Ankle plantarflexor torque is depicted as positive. Positive/negative power indicates net energy generation/absorption by the biological structures acting about the ankle. Bar graphs are average biological (darker bars in front) and total = bio + exo (lighter bars in back) ankle moment (C,D) and net ankle power (G,H). All measurements are averages across the study participants (N = 9) in each condition with varying neuromuscular model (NMM) controller reflex Gain (green) in left panel (A,C,E,G) and Delay (blue) in the right panel (B,D,F,H). Linear regressions between the change in metabolic rate versus the change in average biological ankle moment with respect to the unpowered (NoPwr) condition (I) and the change in metabolic rate versus the change in net biological ankle power with respect to the unpowered (NoPwr) condition (J). * denotes pairwise significant difference of $p < 0.05$. R2 value is denoted with a "~" if the linear regression was not statistically significant. Conditions are abbreviated and color coded as follows: unpowered (NoPwr) (gray), NMM reflex Gains of 0.8, 1.2, 1.6, and 2.0 all with reflex Delay = 10 ms (G0.8, G1.2, G1.6, and G2.0, respectively) (green), NMM reflex Delays of 10, 20, 30, and 40 ms all with a reflex Gain = 1.2 (D10, D20, D30, D40, respectively) (blue), and a high-Gain-high-Delay condition (G2.0 D40) (black).

on, users exhibited attenuated negative biological ankle power during the early to mid-stance energy storage phase (15-50% stride) and attenuated positive biological ankle power during late-stance push-off phase (50-60% stride). Increasing either the Gain (ANOVA, p=0.009) (Figure 6G) or Delay (ANOVA, p=0.007) (Figure 6H) caused an increase in net biological ankle power. This trend toward net positive biological ankle power was accompanied by a shift in the timing of peak power generation earlier in the stride during powered conditions (Figs. 5E, F). Similar to average biological ankle moment, changes in net biological ankle power were not significantly correlated with changes in metabolic rate (LLSR, p = 0.996) (Figure 6J).

Knee and hip joint mechanics are summarized in Figure 34 and Figure 35. Qualitatively, with exoskeletons powered on, users assumed a more extended knee posture throughout the walking stride and exhibited larger knee flexion moments during stance compared to the unpowered condition. The knee joint absorbed more energy between 15-40% of the stride and generated more energy between 40-60% of the stride. At the hip, users assumed a more extended posture at peak flexion and extension. Although not statistically analyzed, there is slight evidence of higher extension moments generated at the hip during early and mid-stance (~5-40% stride) causing an increase in positive power, especially with Delay conditions. Mechanical power, generated at the hip near the end of swing to pre-emptively extend the limb before heel strike (85-100% stride), was amplified in powered conditions. These trends were not examined statistically.

2.3.5 Ankle muscle activity

Powered ankle exoskeletons significantly altered users' ankle muscle activity and changes were qualitatively similar across NMM controller Gain and Delay parameters (Figure 7, Figure 36, Figure 37, Figure 38, Figure 39). In general, with exoskeletons powered-on, the plantarflexors (*i.e.,* soleus (SOL), medial gastrocnemius (MG), and lateral gastrocnemius

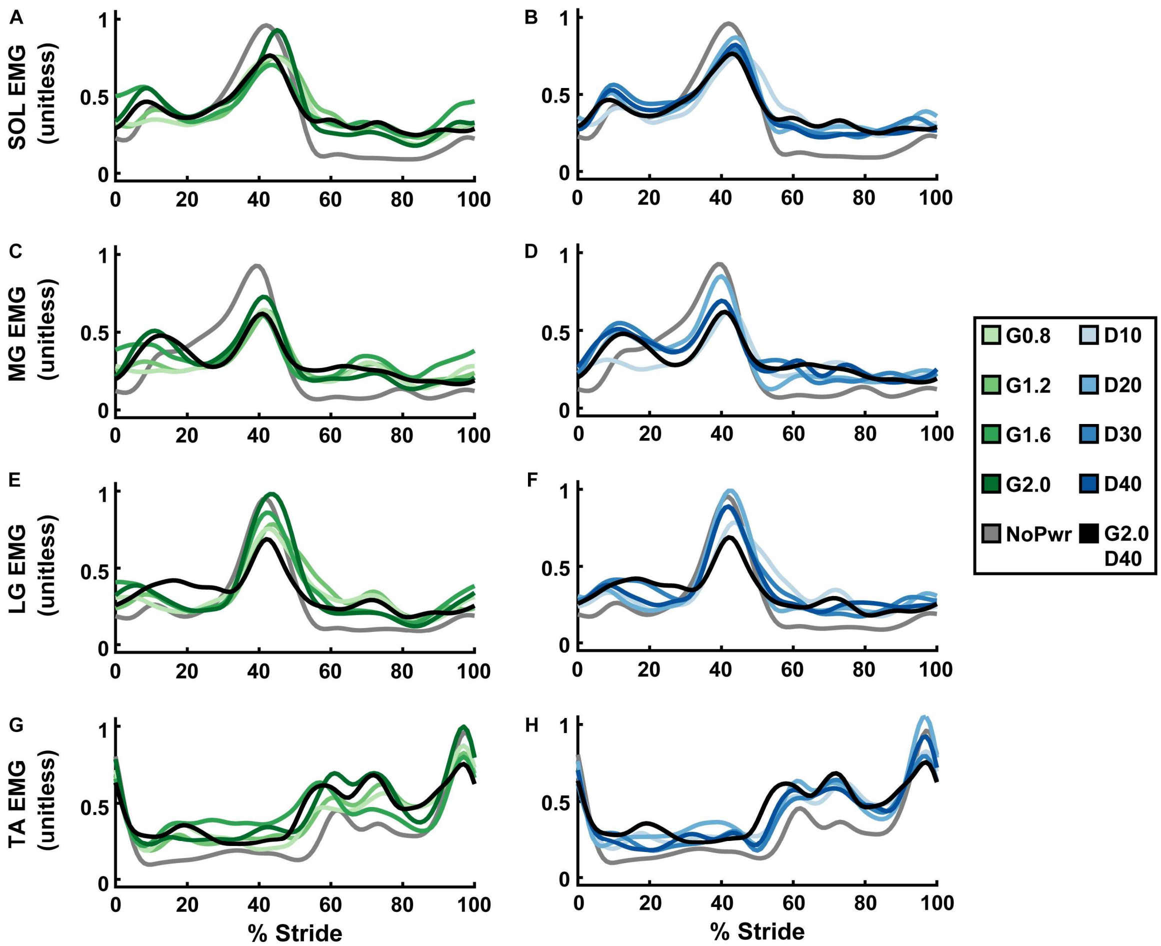

Figure 7 - Users' ankle muscle activity over a stride cycle. Measurements of users' normalized electromyography (EMG) signals recorded from soleus (SOL; A,B), medial gastrocnemius (MG; C,D), lateral gastrocnemius (LG; E,F), and tibialis anterior (TA; G,H) over a stride from heel strike (0%) to heel strike (100%) of the same leg are shown. All measurements are averages across the study participants (N = 9) in each condition with varying neuromuscular model (NMM) controller reflex Gain (green) in left panel (A,C,E,G) and Delay (blue) in the right panel (B,D,F,H). Conditions are abbreviated and color coded as follows: unpowered (NoPwr) (gray), NMM reflex Gains of 0.8, 1.2, 1.6, and 2.0 all with reflex Delay = 10 ms (G0.8, G1.2, G1.6, and G2.0, respectively) (green), NMM reflex Delays of 10, 20, 30, and 40 ms all with a reflex Gain = 1.2 (D10, D20, D30, D40, respectively) (blue), and a high-Gain-high-Delay condition (G2.0 D40) (black).

(LG)) showed reduced activity during mid- to late stance phase (15-60% stride) and markedly increased activity during swing phase through early stance (60-15% stride) (Figure 7 A-F). Summed ankle muscle activity (Figure 8 A&B) increased during early stance (0-30% stride) and swing (60-100% stride) with powered assistance. However, during late stance/push-off, summed EMG decreased compared to the unpowered condition. On average (Figure 8 C&D), summed ankle muscle activity increased across all powered condition from unpowered. Specifically, G1.6, G20, and D20 significantly increased summed EMG compared to the unpowered condition (paired t-test; $p = 0.003$, 0.007, and 0.043, respectively). Average summed ankle EMG was significantly correlated with changes in metabolic cost (LLSR, $p < 0.001$) (Figure 8 E).

When viewing average muscle activity of plantarflexor muscles individually; peak SOL (Figure 36) and MG activity (Figure 37 C&D, Figure 37 - Measurements of users' normalized medial gastrocnemius (MG) electromyography (EMG) over a stride from heel strike (0%) to heel strike (100%) of the same leg are shown (A, B). Bar graphs are averages of the normalized MG EMG signal over the stride (C and D). All measurements are averages across the study participants (N=9) in each condition with varying neuromuscular model (NMM) controller reflex Gain (green) in left panel (A, C) and Delay (blue) in the right panel (B, D). Linear regression between the change in metabolic rate versus the change in average SOL EMG with respect to the unpowered (NoPwr) condition (E). * denotes pairwise significant difference of $p < .05$. R2 value is denoted with a "~" if the linear regression was not statistically significant. Conditions are abbreviated and color coded as follows: unpowered (NoPwr) (gray), NMM reflex Gains of 0.8, 1.2, 1.6, and 2.0

all with reflex Delay=10 ms (G0.8, G1.2, G1.6, and G2.0, respectively) (green), NMM reflex Delays of 10, 20, 30, and 40 ms all with a reflex Gain=1.2 (D10, D20, D30, D40, respectively) (blue), and a high-Gain-high-Delay condition (G2.0 D40) (black).) decreased and occurred later in the gait cycle with powered conditions; peak LG activity (Figure 38 E&F, Figure 38) increased with increasing Gain. Average LG activity was significantly correlated with metabolic cost (LLSR, p<0.001) (Figure 38E).

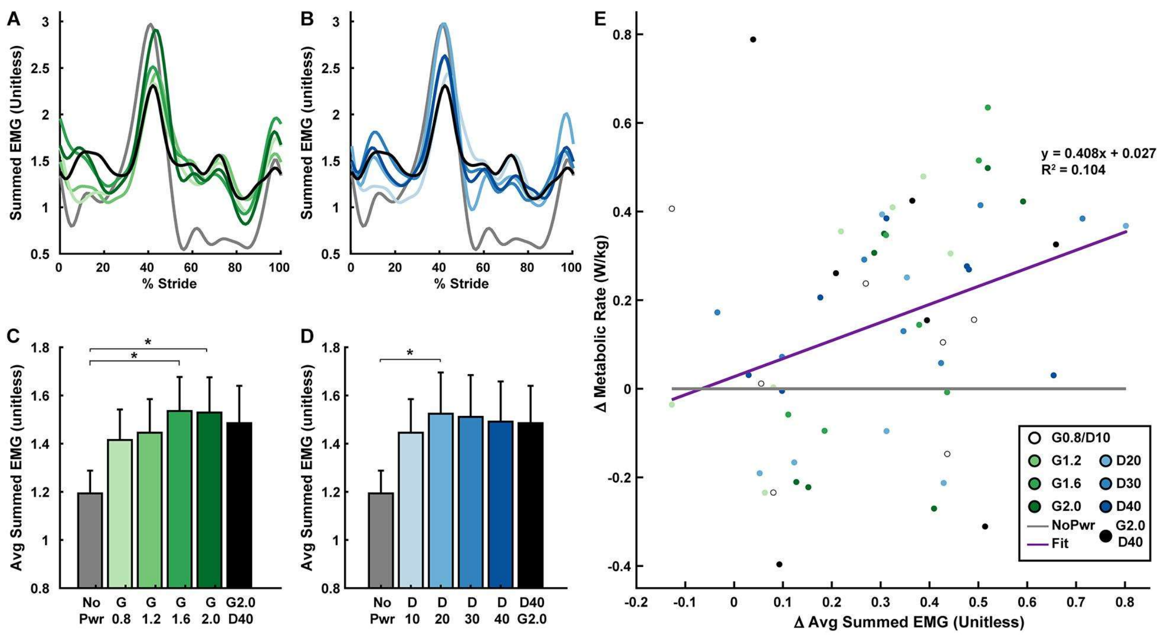

Figure 8 - User's summed ankle muscle activity versus metabolic rate. Measurements of users' summed normalized electromyography (EMG) signals recorded from soleus + medial gastrocnemius + lateral gastrocnemius + tibialis anterior (SOL+MG+LG+TA) over a stride from heel strike (0%) to heel strike (100%) of the same leg are shown (A,B). Bar graphs are averages of the summed EMG signals over the stride (C,D). All measurements are averages across the study participants (N = 9) in each condition with varying neuromuscular model (NMM) controller reflex Gain (green) in left panel (A,C) and Delay (blue) in the right panel (B,D). Linear regression between the change in metabolic rate versus the change in average summed EMG with respect to the unpowered (NoPwr) condition (E). * denotes pairwise significant difference of p < 0.05. R2 value is denoted with a "~" if the linear regression was not statistically significant. Conditions are abbreviated and color coded as follows: unpowered (NoPwr) (gray), NMM reflex Gains of 0.8, 1.2, 1.6, and 2.0 all with reflex Delay = 10 ms (G0.8, G1.2, G1.6, and G2.0, respectively) (green), NMM reflex Delays of 10, 20, 30, and 40 ms all with a reflex Gain = 1.2 (D10, D20, D30, D40, respectively) (blue), and a high-Gain-high-Delay condition (G2.0 D40) (black).

Dorsiflexor (*e.g.,* tibialis anterior (TA)) activity increased throughout the stride in powered conditions, except at terminal swing (90-100% stride) where it was reduced (**Error! Reference source not found.** G&H). On average, TA EMG increased with Gain (ANOVA, p<0.001) compared to NoPwr. Substantial increases in TA activity are seen during early swing phase (60-80% stride). TA EMG was not significantly correlated with metabolic cost (LLSR, p = 0.258) (**Error! Reference source not found.**E).

2.4 Discussion

The purpose of this study was to apply a neuromuscular model (NMM) of the human plantarflexors to control torque output of a powered ankle exoskeleton during walking. As a first step, we developed an NMM comprised of a Hill-type musculotendon driven by a simple positive force feedback reflex loop and examined the effects of the NMM reflex Gain and Delay settings on (*i*) ankle exoskeleton mechanical performance and *(ii*) users' physiological response. First, we hypothesized increasing Gain would consequently increase average exoskeleton torque and net power output while increasing Delay would have no effect on torque but increase net exoskeleton power. Indeed, increasing Gain increased both average torque and net power outputs (Figure 4A&C). Surprisingly, increasing Delay decreased both average torque and net power (Figure 4B&D). We assumed that powered exoskeleton assistance would not affect ankle kinematics when predicting the effects of each control parameter on exoskeleton torque and power. Contrary to our expectation, users assumed a more plantarflexed posture and decreased peak angular velocities when walking with powered assistance (Figure 3A&B). This altered the virtual muscle dynamics within the NMM and ultimately decreased torque and power outputs with increasing delays (Figure 32). Apparently, there is a more complex relationship between the NMM-based exoskeleton control and the user than we initially expected. Second, we hypothesized conditions with higher net exoskeleton power would result in higher metabolic benefit. Even though we successfully modulated net exoskeleton power output, we found no NMM controller parameter set that reduced metabolic rate (Figure 5 A&B).

Maximizing metabolic benefit is not as simple as increasing exoskeleton torque and power delivery. Tuning the timing of assistance is essential. In our study, increasing exoskeleton torque and power output was weakly correlated with reductions in metabolic rate (Figure 5 C&D), lending some support for the idea that more positive net exoskeleton power yields higher metabolic benefits [54, 66]. Extrapolating this trend suggests: if our device had generated higher net power, we may have achieved a significant metabolic benefit. Our device achieved average torque magnitude per leg (0.1-0.2 Nm/kg) consistent with Jackson and Collins [66], resulted in ~15% reduction with respect to zero torque, ruling out hardware limitations as a source of poor performance. In contrast, torque onset in our study was much earlier (~10% of stride versus ~40%) and generated negative power in early stance that acted to counter the impulsive positive power delivered late in stance (Figure 3E-H). Overall, the data suggest that our relatively small net power outputs did not result from lack of torque magnitudes but poor timing. Indeed, there are infinite ways to deliver a given amount of net positive power over a stride. While the difference between pos/neg power is the driving factor, evidence is mounting that the timing of power delivery may be even more critical.

Previous studies have directly examined the relationship between timing of ankle exoskeleton assistance and metabolic cost [52, 53] and found that assistance torque onsets between 35-45% of the gait cycle are most beneficial. Similarly, using human-in-the-loop optimization to tune timing-based ankle torque assistance on an individual basis, Zhang et al. [41] reported the highest metabolic benefits to date (~24% below unpowered), with torque onsets between 20-40% of the walking stride. Furthermore, examining the exoskeleton power vs. time patterns from these aforementioned studies reveals peak positive power delivery to the user's ankle occurred between 50-60% of the gait cycle (*i.e.,* in the 'push-off 'stage) [51, 53, 81]. Our device also delivered peak positive power focused near push-off (Figure 3G&H). However, our torque onset was much too early, with plantarflexion assistance beginning at ~5-10% of the gait cycle for all powered conditions (Figure 3E&F). This poor timing resulted in a jerky, oscillatory power delivery as evidenced by a rapid sequence of energy absorption and return to/from the exoskeleton in early stance (Figure 3G&H). Concurrently, a lack of normal ankle dorsiflexion resulting from "too early" exoskeleton plantarflexor torque may have disrupted the normal storage and return of energy in the Achilles tendon. One possibility, while our device hardware was powerful enough, the NMM control scheme yielded "too-much" torque "too-early", even when the Gain and Delay were set to maximize net power delivery (*i.e.,* G2.0 D40) and this may explain our lack of metabolic benefits. However, a recent study using heuristic coadaptive control [66] demonstrated metabolic benefits similar to the human in the loop optimized pattern with bimodal peaks similar to ours. That study highlights the fact that the relationship between user response is complicated, depend on other physiological factors like muscle activity and joint posture.

Analyses that focus only on exoskeleton mechanical performance when evaluating physiological response of the human user may be short sighted. Ultimately, a user's metabolic cost depends on how a device influences underlying metabolic demand on muscles spanning the lower-limb joints [82]. Along these lines, perhaps examining changes in users' limb-joint mechanics (Figure 6) would better reflect changes in metabolic demand than exoskeleton mechanics alone (Figs. 3, 4). Numerous studies, focusing on a single locomotion task (*e.g.,* walking on level ground at fixed speed) have shown that the metabolic benefit from exoskeleton assistance is proportional to reductions in biological power output of the target joint [50, 54, 83]. Surprisingly, when we examined study-wide powered exoskeletons conditions (*i.e.,* all NMM controller settings), we did not find significant correlations between changes in users' metabolic rate and changes in *either* average biological ankle moment (Figure 6I) *or* net power (Figure 6J). It is important to note, that our formal statistical analyses focused on changes in user's ankle kinetics, but changes in kinetics at proximal joints could also impact metabolic demand [84]. For example, a qualitative glance at knee (Figure 34) and hip (Figure 35) moments and powers reveals changes in early-mid stance knee kinetics in response to NMM-based ankle assistance. It is important to note, that changes in limb-joint mechanical demand driven by exoskeleton-assistance need not be a good predictor for changes in metabolic demand of the user. This is especially true for assistance applied at the ankle, where limb-joint power may be a poor indicator of muscle contractile dynamics due to presence of the highly elastic Achilles tendon in series [62]. Focusing directly on muscles may be a more tractable way to gain insight into how exoskeletons alter metabolic demand [82].

Muscle activity measurements may be the best way to estimate how exoskeleton assistance impacts muscle-level mechanical and metabolic demand during walking. Various studies have found positive correlations between measures of muscle activity and metabolic rate [51, 60, 62, 81, 85]. In this study, we calculated peak summed electromyography (EMG) for the major muscles spanning the ankle joint: soleus (SOL), medial & lateral gastrocnemius (MG & LG), and tibialis anterior (TA). Stride averaged summed EMG increased for all powered conditions, especially during swing phase and into early stance (Figure 32 A, B). We found significant least-squares linear regression between changes in summed EMG and changes in metabolic rate due to exoskeleton assistance (Figure 32E). Though summed EMG could only explain 10.4% of the variability in metabolic response to the exoskeletons, this was still higher than the variability explained by either the exoskeleton (Figure 5 C, D) or biological ankle joint mechanics (Figure 6 I, J). Interestingly, when this same analysis was done for each muscle individually, changes in LG and SOL muscle activity (Fig S4 and Fig S5), had higher correlation with changes in metabolic rate (R^2 = 0.393 and 0.208, respectively) than the summed activity across *all* of the muscles (R^2 = .104). According to Beck et al. [82], scaling each muscle's activity by its physiological volume (*i.e.,* physiological cross sectional area (PSCA) x rest length) may yield better estimates of metabolic rate because larger muscles would consume more energy per activation than smaller muscles. Indeed, when we performed a post-hoc analysis that scaled EMG by relative muscle volumes, and then calculated the correlation between changes in summed muscle activity and changes in metabolic rate our R^2 improved from 0.104 to 0.133. These correlations are still low compared to other reported values (*e.g.,* R^2 ~0.4 in [50, 51, 62, 81]). By incorporating muscles beyond those than span the ankle joint, and including muscle volume scaling, we would expect correlations to continue to improve. Finally, it is important to acknowledge that other studies have stated the duration of the contraction, *i.e.,* accounting for the *rate* of muscle activation [86, 87], may also be a key factor that can help relate EMG and metabolic cost of muscle contraction. Recently, Nuckols et al [62], employed this technique when analyzing the effects of ankle exoskeleton assistance across speeds and reported R^2 up to 0.69. While these results seem promising, there is still considerable debate on whether cycle averaged [82] or step duration averaged [62] more accurately depicts muscular energy consumption. Nevertheless, our study and many others are building strong support for using users' muscle activity rather limb-joint mechanics to explain changes in metabolic cost.

Habituation, or the ability of user to adapt a motor coordination strategy that leverages robotic assistance, is another factor that influences whether an exoskeleton control strategy yields metabolic benefit. A hallmark observation during motor adaptation to exoskeleton assistance is an initial onset of high levels of muscle co-activation both local to the exoskeleton assistance (*e.g.,* tibialis anterior (TA)) and more globally across the limb (*e.g.,* biceps femoris). Over time, users typically exhibit attenuated co-activation and thus avoid the metabolic penalty associated with the additional muscle activity of antagonist muscles [50, 56, 66, 67, 79, 88]. In this study, across powered conditions, we observed substantial co-activation of plantar- and dorsiflexor muscles over most of the stride (Figure 7). Even after 25 minutes of training in the device, we observed increased TA (dorsiflexor) activation over ~90% of the stride duration, including during stance (Figure 7 G, H; **Error! Reference source not found.**). In addition, we observed heightened activity of MG, LG, and SOL (plantarflexor) during swing phase (60-100% of stride) (Figure 7A-F, Figure 36, Figure 37, Figure 38). Two possibilities for persistent co-activation are: we did not give users a long enough time to learn to walk with the NMM controller or NMM-based control is impossible to learn at all.

Though we did not formally examine the time-course of habituation to our device, it is possible that users needed more time to reach the full metabolic benefit of NMM-based control. It is well known that it takes users a significant amount of training time to learn to use robotic exoskeletons. For ankle exoskeletons, the time to reach a walking pattern with new steady state neuromechanics and energetics is on the order of 15 minutes to 1.5 hours, depending on the observed state variable [50, 56, 57, 62, 67, 79, 88]. In this study we gave users 25 minutes of training time based on benchmarks indicating that >20 minutes of exposure is sufficient to ensure full metabolic benefit in an ankle exoskeleton [79]. However, even after training, we found no NMM control parameters that could significantly reduce users' metabolic rate (Figure 5). One possibility for poor user performance is that NMM-based control is harder to learn than time-based [79] or EMG-driven [50, 67, 88] controllers. Indeed, there is some evidence that adaptation rate may be specific to the exoskeleton control architecture. For example, data comparing adaptation rate between myoelectric and bang-bang foot-switch control strategies on an ankle exoskeleton indicate that although users reached steady state human-exoskeleton behavior within 30 minutes with both controllers, it occurred 15 minutes faster with the bang-bang control [56]. Even amongst adaptive myoelectric control schemes, heuristics-based control [66] converged faster than traditional strategies [67]. Thus, it is possible that despite its strong grounding in human sensorimotor physiology, our NMM-based controller is less intuitive, making it harder for users to find an efficient movement strategy. Follow up studies could examine the extent to which people can learn NMM-control if given more time and a larger parameter space, perhaps with some guidance to proactively encourage users to broadly explore motor coordination strategies [89-91]. It is important to note, it is entirely possible that the structure of NMM-based control is impossible to learn at all. Perhaps, the NMM-control architecture is identified by the human nervous system as a persistent source of uncertainty (*i.e.,* an unidentifiable disturbance), and thus stiffening the joints via co-activation of antagonist muscles is the optimal feed-forward strategy to deal with consequences of inherent sensorimotor delays in the nervous system that would otherwise undermine stable movement [92], a strategy that may also be the most economical manner to deal with uncertainty.

Based on our results it is tempting to dismiss NMM-based ankle exoskeleton control as an effective strategy for minimizing users' metabolic cost of walking. However, it is important to note that our study only examines a small subset of possible NMM control architectures in a limited set of locomotion tasks (*i.e.,* fixed speed at 1.25 m/s). For example, in the reflex-based NMM control architecture, torque assistance is predominantly dependent on ankle kinematics which are only indirectly influenced by the user, creating a complex human-machine interaction. More direct control could simplify the human-machine interaction allowing for quicker adaptation to the device and improved metabolic benefit. Along these lines, researchers have recently begun to explore hybrid versions of NMM-based control that directly feed the user's muscle activity to drive the activation of the muscle-tendon model instead of implementing a positive force feedback reflex pathway [58]. In this case, preliminary results using human in the loop optimization (HiLO) to tune parameters in the controller's virtual MTU model yield up to 10% reduction in metabolic rate for medium and fast walking speeds. Notably, in that study NMM-based control was still outperformed by pure EMG and time-based controllers implemented on the same subjects and hardware. These results highlight the possibility that the torques that are generated by the NMM architecture may be constrained in such a way that prevents the exoskeleton from delivering the energetically optimal time-based torque profile [41]. Indeed, despite the intuition that applying the physiological torque pattern observed in human gait (*a la* NMM) should provide a sound template for exoskeleton assistance, evidence is growing that physiologically-based controllers are not optimal for reducing users' metabolic cost in unchanging walking environments (*e.g.,* fixed speeds on level ground with even terrain), at least at the ankle joint.

Exoskeletons have utility beyond the context of reducing energy cost of locomotion. Locomotion in natural environments is dynamic and unsteady. A key point often overlooked is that time-based, human-in-the-loop optimized controllers are successful at reducing metabolic cost in steady, unchanging tasks because they provide identical assistance for each step. This provides a consistent platform for quick-and-easy user adaptation to an efficient motor strategy, but inherently lacks the versatility to adapt to even slight changes in either the user or the environment. In natural locomotion, gait speed, ground slope, and smoothness of the terrain change from step to step and control strategies must progress to be versatile in dynamic environments. Despite its potential drawbacks in steady conditions, NMM-based control may be ideal for more dynamic tasks. For example, NMM-based control on robotic prostheses can robustly restore lost function in people with amputation by automatically adapting assistance over changing speeds without explicit changes in the control parameters [71, 73]. It is possible that NMM-based control of exoskeletons is equally adaptive, and future studies are needed to examine the extent to which NMM controllers can respond directly to rapid changes in a user's state (*e.g.,* kinematics or muscle activity). In short, exploring a broader lens of applications that include a diverse, dynamically changing locomotion task-environment space will truly define the capability of NMM-based exoskeleton control to augment movement outside of the laboratory.

CHAPTER 3. EMULATOR-BASED OPTIMIZATION OF A SEMI-ACTIVE HIP EXOSKELETON CONCEPT: SWEEPING IMPEDANCE ACROSS WALKING SPEEDS

3.1 Introduction

Exoskeletons have been increasingly successful at providing enhanced walking performance by reducing the metabolic rate of the user [17]. Exoskeletons (exos) showing the largest metabolic benefits typically use control systems optimized to generate assistive torques at a target joint (*e.g.*, ankle or hip) with timing and magnitude set specifically for a fixed gait (*e.g.*, walk or run) and locomotor demand (*e.g.*, speed or grade) on a treadmill [53, 93-97]. These studies have provided a valuable foundation upon which the field is poised to expand. Indeed, a grand challenge remains to develop exos that can provide assistance outside the laboratory across the full functional range of locomotion modes (*i.e.*, gaits, speeds, grades, stairs, unstructured terrain, etc.) used in everyday life. Toward this end, more research is needed to uncover strategies that are versatile enough to provide useful assistance across a broad range of locomotion behaviors in a form-factor that is streamlined and easy to use and maintain. Our goal here was to build on recent studies that have started to examine how exo assistance should change with gait [96], across speed [62], and according to the target joint for assistance [98]. Comprehensively examining users' physiological response to single-joint exo assistance strategies across walking speed is an important first step.

Taking clues from basic neuromechanics and energetics studies that address the joint-level mechanisms humans use to adapt locomotion behavior in response to changing demands could help guide versatile exoskeleton assistance strategies [11, 99]. For example, above self-selected walking speeds (>~1.3 m/s), there are stereotypical changes in lower-limb joint mechanics that accompany higher metabolic rate and metabolic cost of transport [11, 100]. As walking speed increases, both positive and negative mechanical work done on the center of mass increase in proportion to net metabolic rate [101]. To effectively handle the increased demand for mechanical work, humans increase muscle power output at all lower-limb joints, with hip (>40%) outpacing ankle (<40%) at the fastest speeds [11, 100, 102]. Observing which joints inject positive work into the gait cycle could provide guidance regarding where to place exo motors and when to activate them. Joint-level biomechanics can also be characterized by the relationship between the net muscle-tendon moment and the joint angle during steady-state movement, the quasi-stiffness. In fact, the quasi-stiffness of the lower-limb joints is modulated with speed. Throughout stance phase, quasi-stiffness increases with speed at all joints with the exception of the knee during weight acceptance [103-105]. The quasi-stiffness could provide guidance regarding stiffness and engagement timing of exo springs to provide unpowered elastic torque assistance. More studies are needed to understand whether and how exo assistance strategies should change in accordance with changing mechanical properties of the lower-limb joints across walking speed.

Given the goal to provide metabolic benefit across walking speeds, the hip joint emerges as a desirable target for exo assistance. Indeed, as previously mentioned, the hip muscle-tendons are major positive power generators during walking and become increasingly important at the fastest speeds [102]. It is also worth noting that the hip emerges as an even clearer power source uphill [99] and during accelerations [106, 107]. Further, simulation studies have predicted hip musculature may consume more energy during walking than muscles at the ankle [108]. This could be in part, due to morphological differences in ankle vs. hip muscle-tendons that make efficiency of positive work lower at the hip [109]. Focusing exo assistance on the least efficient lower-limb joint could yield more 'bang-for-buck' in terms of metabolic energy savings of the user. In addition to the physiological basis for focusing on the hip, it is also important to consider that the metabolic penalty due to added load of an exo placed at the hip would be small compared to other joints. Carrying added mass close to the body center or mass is relatively cheap compared to carrying it distally on the legs [22].

Despite the inability to generate positive mechanical power, passive devices have successfully enhanced walking performance at the hip, with modest metabolic benefits around 3% [110-112]. Success is mainly due to the lightweight nature of passive exos and tuning the elastic properties of the system (*i.e.*, stiffness and equilibrium point) to generate useful assistance torque patterns that help the hip flex the leg into swing. A downside of the passive approach is that static mechanical properties of springs and dampers are static and may not be appropriate for all locomotion modes. To increase passive assistance adaptability, electromechanical clutches have been implemented in knee exoskeletons to modulate passive element properties and engagement but did not allow positive power generation. [113, 114]. Powered devices are bulky, require an energy source and may be harder to maintain, but can modulate torque assistance patterns on-line. In addition, powered exo assistance at the hip shows clear (and much larger) benefit, especially when timed to deliver torque during the early stance extension phase of walking [94, 115-117].

Hybrid designs that combine elements of both passive and active systems could allow adaptive torque assistance with lower actuator mass. For example, semi-active systems containing both motors and elastic elements could inject mechanical power in one gait phase and provide torque to support bodyweight in another, switching modes through a clutch-able transmission. Or perhaps low-power output motors could be used to merely switch the mechanical properties of elastic elements rather than directly drive motion of the user. We contend that semi-active solutions could enable high performance of active systems with simplicity of passive systems.

A semi-active approach that combines passive and active elements has been applied to wearable devices, but mostly in prostheses. In one type of semi-active system, the passive components directly assist the user while the active components are used to alter the mechanical properties or state of the passive components. Indeed, semi-active foot-ankle prostheses can modulate stiffness step by step to emulate physiological torques across modes like speeds, inclines, and stairs [118-121]. To our knowledge, semi-active lower-limb exo applications have not yet been realized, although there are creative actuator designs [122-125] and exciting theoretical concepts for how they might function [99, 126]. To explore these concepts, impedance control (torque based on virtual passive mechanical elements) can be implemented to mimic passive and semi-active devices to maximize performance, as seen with an ankle-foot prosthesis emulator [127]. Nevertheless, research addressing if/how the optimal passive properties (*i.e.*, torque profile) of semi-active exo systems should change across modes and/or where active elements can best contribute is missing. Before spending time and effort building semi-active systems, lab-based emulator systems could be a useful tool to explore the utility and lay groundwork for semi-active exoskeletons.

Here, we employ a tethered exo emulator to apply hip torque to human users and examine whether the metabolic benefit of a virtual hip spring (*i.e.*, a simple impedance) depends on its passive mechanical properties across walking speed. In short, we examined changes in users' metabolic rate across a wide range of stiffness and equilibrium angle of a virtual hip torsion spring [30 sets = 5 stiffness values (k) by 6 equilibrium angles (θ_0) at each of three walking speeds (1.0, 1.3, and 1.6 m/s). We hypothesized that: (i) optimal 'semi-active' assistance would provide a metabolic benefit at each speed; but (ii) the optimal assistance parameters would mirror changes in physiological moment-angle behavior (*i.e.*, quasi-stiffness [103]) with increasing speed. That is, with increasing walking speed we expected an increase in optimal hip exo spring stiffness (k) and a decrease in optimal hip exo spring equilibrium angle (θ_0) (*i.e.*, biased closer to peak hip extension).

3.2 Methods

3.2.1 Impedance Controller

To evaluate human locomotion performance with a semi-active hip exoskeleton (exo), we emulated the function of motor-spring-clutch system using a tethered, cable-driven bilateral hip exoskeleton [128] (Human Motion Technologies, Pittsburgh, PA) while participants walked on an instrumented split-belt treadmill (Bertec, Inc.) (Figure 9A) with assistive torque generated by a simple impedance controller (*i.e.,* virtual torsional spring) (Figure 9B, top schematic). During assistance to the user (STATE 1, light gray), virtual Clutch 1 engaged the spring to the user and exo torques emulated a passive spring as a function of hip angle, θ_{hip}, according to a preset passive spring stiffness, k, and equilibrium angle, θ_0 according to Equation 2 below (Figure 9B, bottom timeseries graphs).

$$\tau = -\boldsymbol{k}(\theta_{hip} - \boldsymbol{\theta}_0) \tag{2}$$

During STATE 1, torque assistance was applied independently to each leg for both hip flexion (pos.) and extension (neg.). As a key feature of the semi-active concept, we also implemented a zero-impedance (ZI) output period, a control strategy where no torque or resistance applied to the user (STATE 2 – dark gray in Fig 1B). STATE 2 was implemented during swing phase starting when the hip angle reached θ_0 and ending when the hip angle reversed direction at peak hip flexion (Figure 9B, bottom timeseries graphs). Without STATE 2, ZI output to the user, a fully passive device would resist user hip flexion, loading

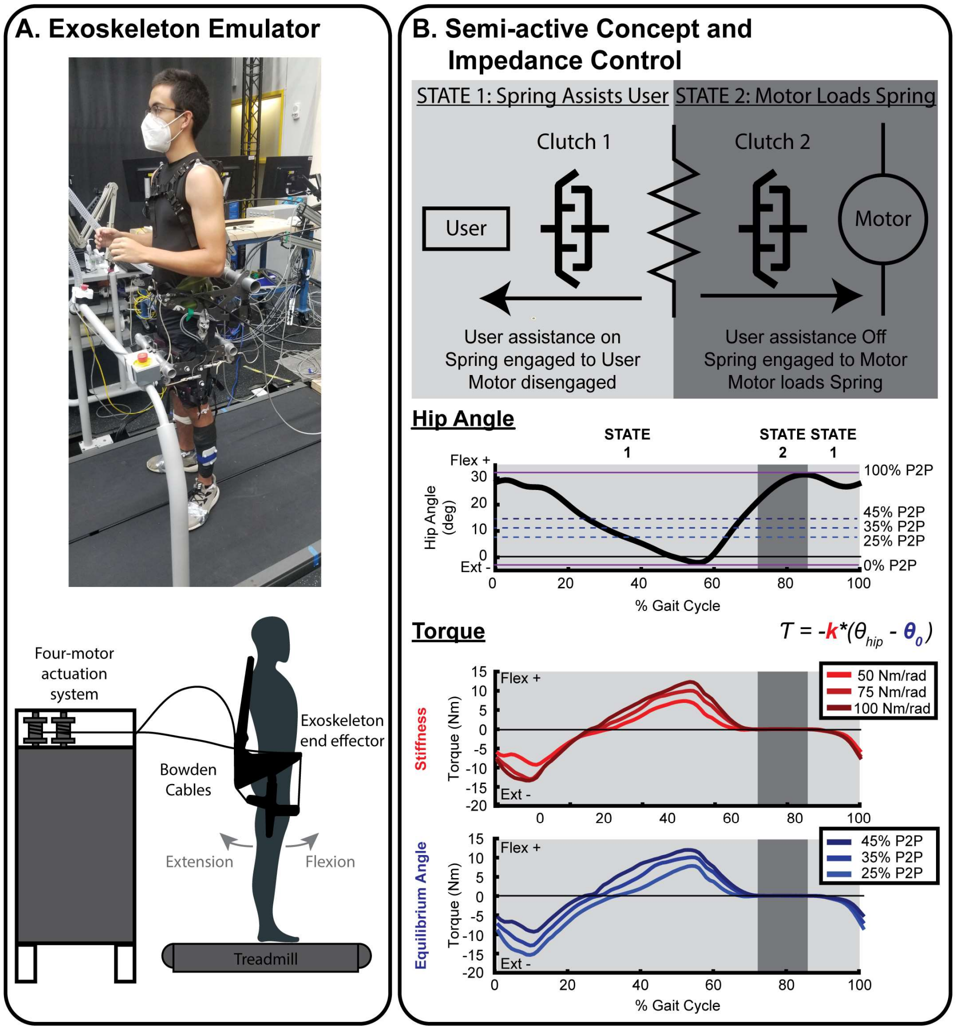

Figure 9 - Emulator-based evaluation of semi-active hip exoskeleton concept. A. We used a tethered, cable-driven hip exoskeleton to apply both extension and flexion assistance torque for each leg. Four offboard motors pulled on Bowden cables to apply flexion and extension to each leg. B. The applied torque profile was based on the concept of a semi-active device comprised of a motor, spring, and transmission with a two-state clutch mechanism. In State 1 (light gray), exoskeleton (exo) torque is transferred to the user according to a simple impedance (i.e., a virtual torsional spring) with a pre-set equilibrium angle (θ0) and stiffness (k) (Equation 2). In this state, exo stiffness, k, modulated the magnitude of both flexion and extension torque assistance. Equilibrium angle, θ0, was calculated as a percentage of a 5-step average peak-to-peak (P2P) hip angle with peak extension = 0% and peak flexion = 100%. θ0 modulated the timing of flexion torque onset/offset (smaller θ0= later flexion torque onset), as well as the relative magnitude of extension vs flexion torque (smaller θ0= larger extension torque bias at ground contact). In State 2 (dark gray), zero-impedance (ZI; no torque assisting or resisting the user) mode was engaged, starting when the hip angle flexed passed θ0 (~70% gait cycle) and ending with peak hip flexion. Simultaneously, a motor loading action was used to coil the virtual spring, developing extension torque internally, which was released by a clutch set to unlock at the onset of late swing hip extension (~90% gait cycle).

the spring while it applies extension torque, potentially impeding natural motion of the leg during swing [129]. Conceptually at the onset of STATE 2, the virtual Clutch 1 disengaged the spring from the user and Clutch 2 engaged the spring to the motor. this prevented extension torque transmission to the user via Clutch 1 and isolated motor-spring interaction through Clutch 2 The virtual motor then internally winded the exo spring (Figure 9B, top schematic). Finally, at the time of maximum hip flexion in late swing, coiled spring energy would be released to the user (State 2 --> State 1), by disengaging Clutch 2 and engaging Clutch 1, driving a pre-stance swing leg retraction to help propel the user via hip exo extension torque (Figure 9B, bottom timeseries graphs). A ramping function was implemented at extension torque onset to ensure high torques were not applied in a rapid manner, which was uncomfortable to some pilot participants. Exo stiffness (k) (Nm/rad) modulates the total torque range, increasing both flexion and extension peak torques with higher stiffnesses (Figure 9B, red). Exo equilibrium angle (θ_0) modulates the ratio between flexion and extension peak torques by shifting the torque along the vertical axis (Figure 9B, blue). To account for changes in range of motion with assistance, equilibrium angle was denoted as a percentage of a 5-step average peak-to-peak (P2P) range of motion, with peak flexion as 100% and peak extension as 0%. As equilibrium angle increased, the user experienced higher peak flexion torque, a lower peak extension torque, and flexion assistance starting earlier and ending later in the gait cycle.

We determined the ranges for stiffness and equilibrium angles based on pilot study data and peak torque. During pilot studies, we found parameter sets with higher than 60% equilibrium angle generated metabolic penalties compared to 60% and lower values. Having the range of equilibrium angles, we then tuned stiffness ranges to elicit peak torques

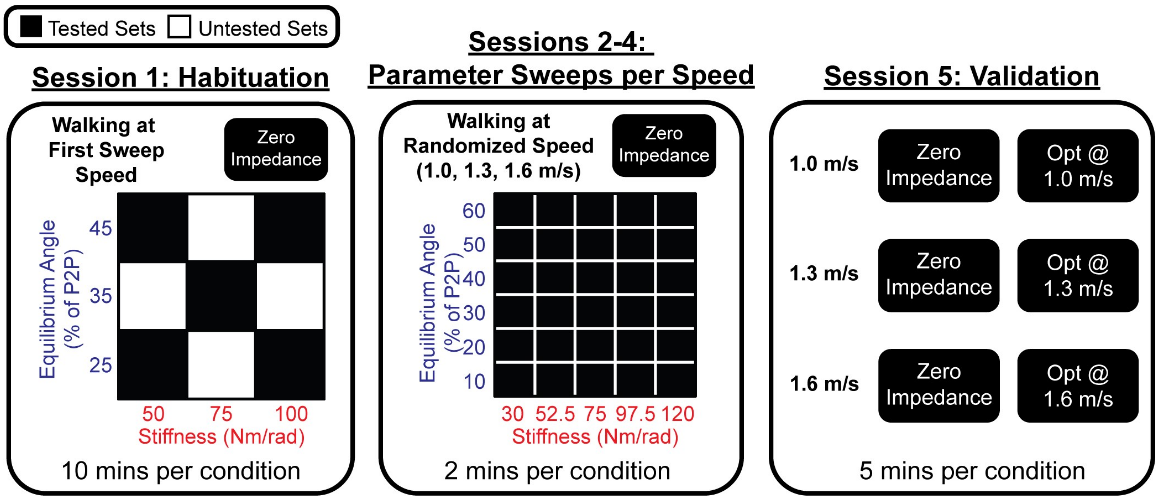

Figure 10 - Multi-session protocol to find optimal impedance parameters across speeds. The experimental protocol was split into 5 sessions. Session 1 (left) explored 5 spring parameter combinations and zero-impedance (ZI) for 10 minutes each, allowing the user to acclimate to walking with hip exo assistance at the first parameter sweep speed. Sessions 2-4 (middle) tested x30 parameter sets spanning the full range of k- θ0 impedance control space while recording users' metabolic rate and electromyography. A metabolic cost to exo parameter surface was created for each walking speed and the parameter set that minimized metabolic cost was used as the optimal for that speed (user-dependent). During Session 5 (right), users walked at all three speeds with zero-impedance and the user-dependent optimal condition for that speed to validate results.

from 5 Nm minimum to approximately 50 Nm maximum. The maximum limit was chosen based on [19] as their metabolically optimal hip only peak torque spline assistance was around 0.6-0.7 Nm/kg and the average weight of our pilot participants was around 70 kg. The inform increments between equilibrium angle and stiffness values were chosen to approximate 5Nm, the minimum change in torque seen to elicit metabolic cost differences around 4% or above.

3.2.2 *Study Protocol*

We recruited 10 healthy young adults to participate in the study (7M/3F; 67.76±10.62 kg, 172.2±9.4 cm). This study protocol was approved by the Georgia Institute of Technology Institutional Review Board (Protocol #: H18067 starting on June 14th, 2018) and all participants supplied voluntary consent to participate. For each participant, we implemented a 5-session protocol with three distinct purposes: (1) habituate the user to the device and measurement equipment, (2) create a metabolic cost to exoskeleton parameter landscape for a sweep of many (k- θ_0) combinations across a functional range of walking speeds (1.3-1.6 m/s), and (3) independently validate user metabolic performance with optimal exo settings across speeds (Figure 10).

3.2.2.1 Habituation

Session 1 involved user habituation to the device, the controller, and metabolic measurement system (explained in next section). Habituation, at least 25-30 mins, is necessary for the user to acclimate to wearing the exo and to develop efficient walking patterns utilizing assistance [43, 79]. To accommodate for the variety of assistance profiles the user would experience during the sweep sessions, we extended the habituation session to 60 minutes. Walking speed was chosen as the first of the randomized walking speeds (to be used as the sweep order in Sessions 2-4). Users first walked at a zero-impedance (ZI) condition (no assistance/resistance applied for the entire gait cycle), then at 5 randomized exo spring parameter sets ([50,25], [50,45], [75,35], [100,25], & [100,45] with [stiffness k, in Nm/rad, equilibrium angle θ_0 in % P2P range of motion]) for 10 minutes each (Figure 10, left).

3.2.2.2 Exo Spring Parameter Sweeps per Speed

To measure how metabolically optimal exo control parameters changed across walking speeds, we swept all combinations of 5 stiffness values (k = 30, 52.5, 75, 97.5, & 120 Nm/rad) and 6 equilibrium angles (θ_0 = 10, 20, 30, 40, 50, & 60%) at each of three walking speeds (1.0, 1.3, and 1.6 m/s) in randomized order (Figure 10, middle). Each parameter set and initial ZI condition was applied for 2 minutes while we measured metabolic rate and lower-limb muscle electromyography (EMG). To determine the metabolically optimal exo spring parameter set for each speed, a metabolic cost - exo parameter landscape was created using a 2nd order fit across stiffness, k, and a 3rd order fit across equilibrium angle, θ_0, a multidimensional application of [48]. Pilot testing revealed that this was the lowest order fit on each parameter that provided reasonably low error without overfitting. We then analytically solved for the k-θ_0 parameter combination that minimized the metabolic rate in the landscape and used this optimal set for validation. We pilot tested real-time or "body/human-in-the-loop" protocols using online optimization algorithms for this study [40, 41] but did not choose them as they would not consistently sample cost across the entire parameter space or provide optimal parameters within a lower number of samples for this lower multidimensional problem. If there were 3 or more parameters, we believe an online optimization algorithm would provide a more rapid optimal solution than our proposed method.

We note, for most participants, the optimal (k-θ_0) set was in between sweep values and thus was not experienced by the user before the validation session.

3.2.2.3 Validation

The final session (Session 5) was used to compare the metabolically optimal exo parameter set for each speed for each individual (user-dependent) to ZI at that speed (Figure 10, right). Testing by speed was done in the same randomized order as the sweeps, completing all conditions at that speed then moving to the next. Each condition lasted 5 minutes while we measured metabolic rate and lower-limb muscle electromyography (EMG).

3.2.3 Metabolic Cost Measurement

Metabolic cost was measured via indirect calorimetry. Breath-by-breath oxygen consumption and carbon dioxide production were measured and used to calculate body mass specific gross metabolic rate (W/kg) using the Brockway Equation [130]. For the exo parameter sweep sessions (Session 2-4), steady-state metabolic rate was estimated as the asymptote of a first order fit to 2 minutes of data [131]. For the validation session (Session 5), steady-state was calculated as the average metabolic rate from the last minute of each 5-minute bout. We conducted a metabolic cost comparison between user-dependent and user-independent impedance parameters, which we detail in Section IIE. We note, due to an equipment malfunction, the zero-impedance (ZI) trial for one participant during the 1.6 m/s validation session was only 3.5 minutes long due, so the average of the last 30s of the trial was used for the steady state metabolic rate. Study wide, we computed the percentage difference in metabolic rate using the ZI condition from that same session as baseline.

3.2.4 Electromyography

Muscle activity was measured via surface electromyography (EMG) for eight muscles: tibialis anterior (TA), medial gastrocnemius (MG), soleus (SOL), vastus medialis (VM), rectus femoris (RF), biceps femoris (BF), gluteus maximus (GMa), and gluteus medius (GMe). EMG sensors (Delsys, Inc.) were placed over each muscle on the left leg according to standard methods [132].

Raw EMG signals were processed through a bandpass Butterworth filter with cutoff frequencies of 20 and 400 Hz before being rectified. Each rectified signal was normalized by dividing by the peak magnitude of the corresponding signal (same speed, same muscle) from the zero-impedance (ZI) trial. Using ground reaction force (GRF) measurements, the EMG signals were then clipped to only include full strides in the analyses.

Next, each processed signal was integrated with respect to time; and the magnitude of the time-integral was divided by the total time of the processed signal to get the average normalized muscle activity for that trial. Then, to calculate the change in muscle activity due to each exo control parameter set, we subtracted the average muscle activity from the corresponding ZI trial in that session. For one participant walking in the 1.3 m/s condition, data from the ZI trial had an excessively low signal-to-noise ratio, so no analysis was done with the participant for that speed.

3.2.5 User-dependent vs. user- independent comparisons

Both user-dependent and user-independent approaches were used to report optimal exo parameter sets and the associated changes in metabolic cost across walking speeds (*e.g.*, see Figure 11). User-dependent measures (both optimal exo parameter sets (k-θ_0) and the estimated change in metabolic cost (Δ % from zero-impedance (ZI)) were defined using the global minimum of the fit to each individual user's metabolic cost landscape from the sweep grid points (Figure 40) and then averaged across participants. This approach accounts for each individual user's unique relationship between exo assistance parameters and metabolic cost while decreasing biasing effects from noisy metabolic measurements and estimations. User-independent measures were defined using a *single* across-participant average metabolic cost landscape in exo parameter space (k-θ_0). Thus, the user-independent metabolic cost minimum (Δ % from ZI) and the exo parameters that generated it (k-θ_0) were single values without any variance. As such, the user-independent approach assumes a 'generic' average user, and effectively smooths differences *between* participants, keeping only the major trends *across* participants intact.

3.2.6 Statistical analyses

We set out to examine whether the metabolically optimal hip exo parameters could reduce gross metabolic rate compared to zero-impedance (ZI) at each walking speed (Hypothesis 1); and whether the optimal exo parameters were different for different speeds (Hypothesis 2). Hypothesis 1 was tested using three separate within-speed, one-factor repeated measures ANOVA analyses (factor: exo condition: ZI, user-ind., user-dep., validation) (Figure 11A) with pairwise post hoc comparisons using a Bonferroni correction. Hypothesis 2 was tested using a single, two-way ANOVA across speed and exo condition (factors: speed: 1.0, 1.3, 1.6 m/s; exo condition: user-ind., user-dep.) (Figure 11B, C).

A post-hoc linear regression analysis was performed to examine the relationship between changes in users' muscle activity and metabolic cost due to exo assistance (*i.e.,* Δ's from ZI). The muscles used in the final linear regression were selected by first conducting regressions for each muscle, one-by-one, in a stepwise fashion. At each step, the muscle that yielded the highest increase in the adjusted r-squared of the overall fit was added to the regression (akin to sequential forward selection), yielding an ordering that produced the highest combined adjusted r-squared fit. This process was repeated until all eight recorded muscles were used in the regression (Figure 14, top). The combination of four muscles with the highest total adjusted r-squared fit was used for further analysis. We constrained the linear regression to have positive coefficients for each muscle; however, the value of the bias term was unconstrained. The participant-average fit equation, r-square, and p-value were computed using the fitted change in muscle activity vs. change in metabolic cost data at each walking speed (Figure 14, bottom).

3.3 Results

3.3.1 Metabolic Cost

Gross metabolic rate was significantly reduced with optimal semi-active hip exoskeleton impedance control settings (k-θ_0) for all walking speeds during sweep sessions, but not in

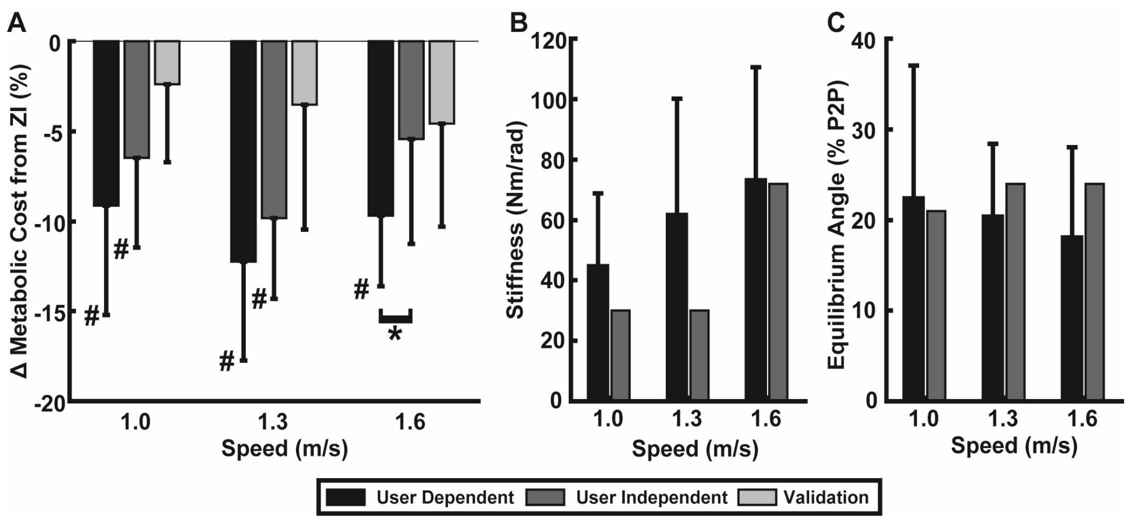

Figure 11 - Metabolic benefit and optimal hip exoskeleton impedance parameters (k- θ0) across walking speed. A. Optimal metabolic benefit (Δ% change from zero-impedance (ZI)) for each walking speed. User-dependent values (black) are mean ± SD taken from the fit to each individual participant's metabolic cost landscape (see Figure 40). User-independent value (dark gray) is taken from the grid point that yielded the minimum Δ metabolic rate from ZI for the metabolic cost surface fitted to the across-participant average data (hence no SD). Validation values (light gray) are from a follow-up test session using each participant's user-dependent minimum metabolic cost parameter set (k- θ0) at each speed. B. Optimal exo stiffness, k, (Nm/rad) and C. equilibrium angle, θ0, (%P2P) for each walking speed (m/s). User-dependent (black) and user-independent (dark gray) follow same convention as A. Statistically significant differences per speed from ZI are indicated by "#" and difference between conditions per speed are indicated by "*"

the validation session (Figure 11). During parameter sweep sessions, when compared to the zero-impedance (ZI) condition, user-dependent optimal parameters reduced gross metabolic rate from ZI by (mean ± standard deviation): -9.1 ± 5.7% ($p < 0.001$) at 1.0 m/s, -12.2 ± 5.2% ($p < 0.001$) at 1.3 m/s, and -9.7 ± 3.7% ($p < 0.001$) at 1.6 m/s. (Figure 11A (black), Figure 40 - Changes in metabolic cost across hip exoskeleton impedance parameter space (k-θ_0): Multidimensional polynomial fits to sampled percentage change from the zero impedance (ZI) condition (red= increase; blue= decrease) for each exoskeleton impedance parameter setting (a 5x6 stiffness (k) vs. equilibrium angle (θ_0) grid space) at each walking speed (1.0 m/s (top row), 1.3 m/s, 1.6 m/s (bottom row)). Columns represent different participants with the last column representing the across subject average at each speed (user-independent; Same as Figure 12 Right Column). In general, a semi-active hip impedance controller with low stiffness and equilibrium angle working at an intermediate walking speed had the most benefit while high stiffness and equilibrium angle had the least benefit. In contrast, there is substantial variation between participants, many of which gain maximum benefit from higher torques (Participants 8-10).) User-independent analysis indicated smaller but still significant metabolic reductions from ZI at all but the fastest walking speed: -6.5 ± 4.7% ($p = 0.021$) at 1.0 m/s, -9.8 ± 1.3% ($p = 0.001$) at 1.3 m/s, and -5.4 ± 5.5% ($p = 0.098$) at 1.6 m/s (Figure 11A (dark gray), Figure 13, right column).

Direct comparison of optimal hip exoskeleton impedance parameters indicated larger reductions in metabolic rate for the user-dependent versus user-independent settings for the fastest but not the slower speeds: $p = 0.054$ at 1.0 m/s, $p = 0.115$ at 1.3 m/s, and $p = 0.027$ at 1.6 m/s (Figure 11A, black versus dark grey).

During the validation test sessions (*i.e.,* a re-test of each user's speed-dependent best exoskeleton parameters from sweeps (see Figure 40)), we found no significant reduction in gross metabolic rate from ZI at any walking speed: -2.1 ± 4.2% ($p = 1.00$) at 1.0 m/s, -4.0 ± 6.7% ($p = 0.65$) at 1.3 m/s, and 4.5 ± 5.7% ($p = 0.24$) at 1.6 m/s.

3.3.2 Metabolically Optimal Exoskeleton Impedance Control Parameters

The hip exoskeleton impedance control parameters (k-θ_0) that minimized metabolic rate were highly variable across participants and showed no significant differences across walking speed (Figure 11 B&C; Figure 13, right column; Figure 40).

Optimal stiffness (k) ranged between 40-80 Nm/rad (User-dependent (mean ± standard deviation): 44.60 ±23.01 Nm/rad at 1.0 m/s; 61.75±36.45 Nm/rad at 1.3 m/s and 73.20±35.45 Nm/rad at 1.6 m/s) and increased with walking speed, albeit insignificantly (ANOVA: $p = 0.101$) (Figure 11B, black; Figure 13, right column). Optimal equilibrium angle (θ_0) was relatively constant around 20% of the peak-to-peak hip angle range of motion (User-dependent: 22.4±13.9 at 1.0 m/s; 20.4 ±7.6 at 1.3 m/s and 18.1±9.43 at 1.6 m/s) and tended to decrease (*i.e.,* became more extension biased) with increasing walking speed (ANOVA: $p = 0.707$) (Figure 11C, black; Figure 13, right column).

The significant amount of variability between participants for both optimal stiffness (k) (Figure 11B, Figure 40) and equilibrium angle (θ_0) (Figure 11C, Figure 40) was reflected in differences between user-dependent and user-independent optimal values, especially for stiffness (k) at low walking speeds (Figure 11. black vs. dark grey bars).

3.3.3 Muscle Activity

Muscle activity was reduced for a subset of muscles, local to the assisted joint, by metabolically optimal semi-active hip exoskeleton impedance control settings (k-θ_0) for all walking speeds (Figure 13, Figure 14, bottom). Representative time-series data show that reductions in muscle activity were driven by the hip and knee extensors (GMa, BF, and

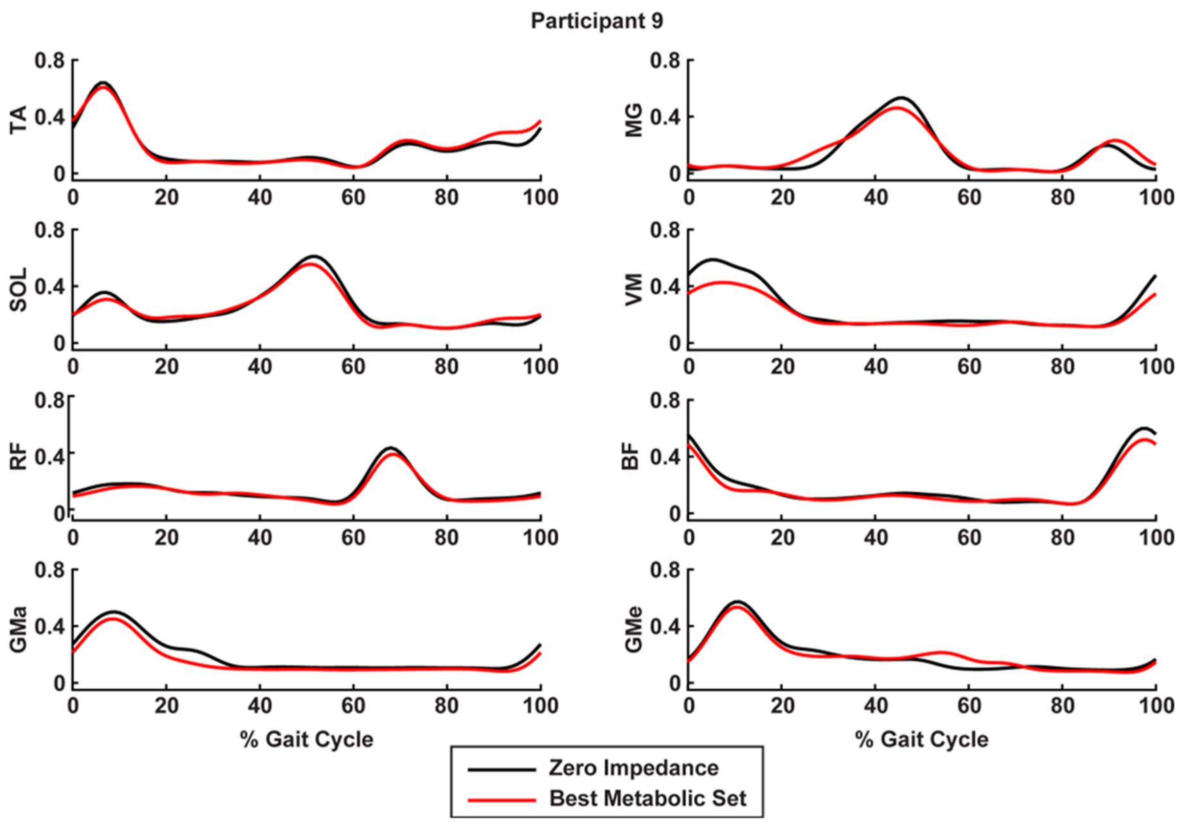

Figure 12 - Muscle activity time-series for the hip exoskeleton impedance parameters (k- θ0) with the lowest (best) metabolic cost and zero impedance (no assistance or resistance applied to the user). Representative gait cycle (0% heel strike, 60% end stance, to 100% end swing) averaged muscle activity taken from surface electromyography records for Participant 9 during the 1.3 m/s exo parameter sweep session. Black curves are from the zero-impedance condition and red curves are from the condition with exo parameters that were metabolically optimal (k=120 Nm/rad and θ0= 13% P2P). Muscle activity was recorded from 8 lower limb muscles (ordered from distal-to-proximal, anterior-to-posterior): tibialis anterior (TA), medial gastrocnemius (MG), soleus (SOL), vastus medialis (VM), rectus femoris (RF), biceps femoris (BF), gluteus maximus (GMa), and gluteus medius (GMe). The optimal assistance strategy showed reduced hip and knee extensor (e.g., GMa, BF, and VM) activity in early stance and reduced hip flexor activity in early swing (e.g., RF) as well as reduced plantarflexor activity at push-off (e.g., SOL and MG).

VM, respectively) early in the gait cycle, the hip flexors in early swing (RF) and the ankle plantarflexors (MG, SOL) at push-off. (Figure 12).

Stepwise, iterative regression analysis revealed that only the four most significant muscles were necessary to characterize the relationship between changes in metabolic cost and changes in muscle activity, as the adjusted r-squared value did not meaningfully increase when more than four muscles were included in the model (Figure 14, top).

The muscles that most influenced predicted changes in metabolic rate from changes in muscle activity due to hip exoskeleton assistance depended on walking speed. Iterative linear regression indicated: GMa, BF, VM, GMe at 1.0 m/s; BF, VM, RF, and GMe at 1.3 m/s; and BF, GMa, VM, and SOL at 1.6 m/s (Figure 14, top). BF and VM were present at all speeds; GMa and GMe present at 2 speeds each.

Participant average fits of the 4 'best'-muscle linear regression models indicated a significant relationship ($p<0.0001$) between changes in muscle activity and changes in gross metabolic rate due to hip exoskeleton impedance control when compared to zero-impedance (ZI) for all walking speeds (Figure 14, bottom). Correlations were strong at all speeds with r-squared values of 0.65, 0.88 and 0.70 at 1.0, 1.3 and 1.6 m/s, respectively.

3.3.4 Data Archive

The study data set can be found at: https://sites.gatech.edu/hpl/archival-data-from-publications/.

3.4 Discussion

We used a lab-based emulator to evaluate a semi-active hip exoskeleton concept (*i.e.,* motor, spring, clutch system) (Figure 9) and measured the physiological response of human

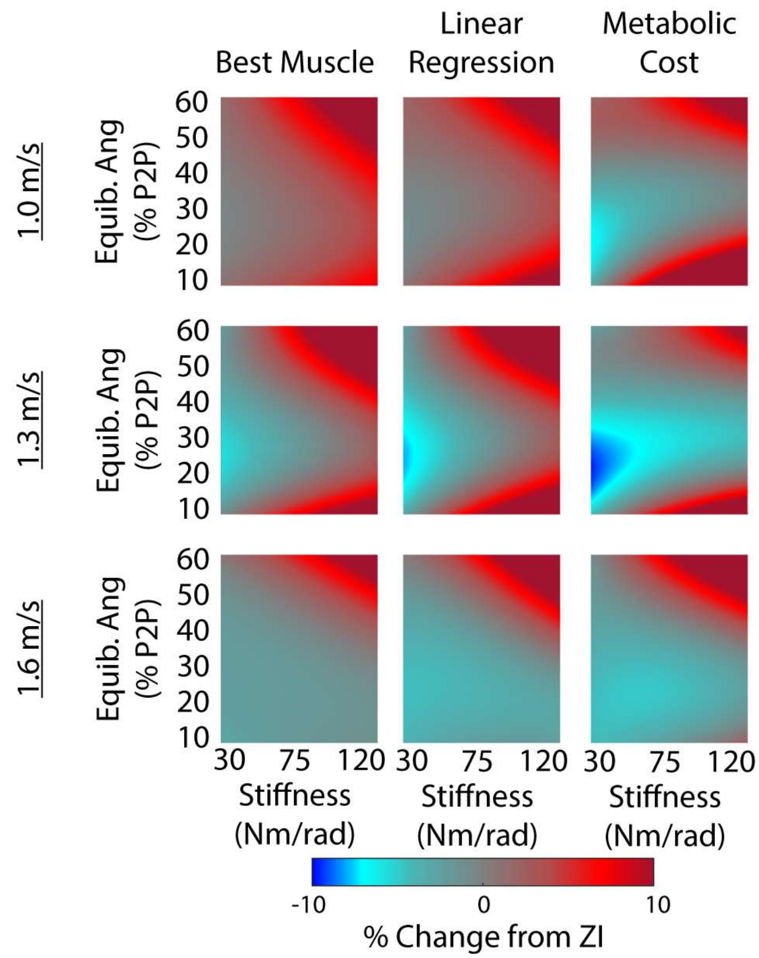

Figure 13 - User-independent changes in muscle activity and metabolic cost across hip exoskeleton impedance parameter space (k-θ0): Across-participant averaged (i.e., user-independent) multidimensional polynomial fits to sampled percentage change (red= increase; blue= decrease from the zero-impedance (ZI) condition) for each exoskeleton impedance parameter setting (a 5x6 stiffness (k) vs. equilibrium angle (θ0) grid space) at each walking speed (1.0 m/s (top row), 1.3 m/s, 1.6 m/s (bottom row)). Columns represent different outcome measures. (Left) Total muscle activity from the muscle with the best linear regression fit to metabolic cost (Best Muscle), (Middle) Linear regression fit using the 4 muscles with the best combined fit to metabolic cost (Linear Regression), and (Right) metabolic cost. The muscles selected per speed for the Best Muscle and Linear Regression fits can be found in Figure 13 top row. The method of selecting muscles for the linear regressions is discussed in Section IIE. In general, a semi-active hip impedance controller with low stiffness and equilibrium angle working at an intermediate walking speed had the most benefit. Study-wide, changes in muscle activity corresponded well with changes in metabolic rate.

users to examine whether: (*i*) optimal impedance settings (spring stiffness, k and equilibrium angle, θ_0) could reduce metabolic cost across a range of walking speeds (1.0-1.6 m/s), and (*ii*) whether impedance settings (k, θ_0) for metabolically optimal performance depended on walking speed (Figure 11) .

First, we hypothesized that walking with a hip exoskeleton using metabolically optimal impedance settings (k, θ_0) would provide metabolic benefit compared to zero-impedance (ZI) mode at each speed. Indeed, the user-dependent parameter set with the lowest metabolic cost provided significant benefits that ranged from 9-12% depending on walking speed (Figure 11A, Figure 40). Second, we hypothesized that the metabolically optimal impedance parameters (k, θ_0) would change across walking speed, mirroring physiological increases in hip joint quasi-stiffness and peak extension moment with speed [103]. Trends in our data supported this idea, as the optimal stiffness (k) increased from ~40 N-m/rad to ~80 N-m/rad (Figure 11B) and the optimal equilibrium angle θ_0 decreased from >20% to <20% of the P2P hip angle (*i.e.,* larger extensor torque bias) (Figure 11C) as speed increased from 1.0 to 1.6 m/s.

Optimal hip exoskeleton impedance parameters (k, θ_0) followed observed trends in biological moments and quasi-stiffness observed in humans walking at faster and faster speeds. Physiological hip moments increase in both extension and flexion with increasing walking speed [11, 133]. This increase in peak-to-peak moment is accompanied by an increase in the flexion quasi-stiffness of the joint, or the ratio change in hip joint moment to change in hip joint angle during early swing [7]. Our metabolically optimal hip exo stiffness (k) also increased with speed, causing higher peak flexion and extension hip exo assistance torques. Similar trends have been reported for passive elastic ankle exoskeletons, where the metabolically optimal stiffness also follows physiological changes in ankle joint quasi-stiffness with increasing walking speed [9], [20]. More broadly, these results suggest that semi-active exoskeletons design that rely on spring-like elements might be nominally set to match trends in the physiological quasi-stiffness of the target joint across locomotion modes (*e.g.,* surface incline, or roughness). Conversely, human-in-the-loop optimizations of powered (not semi-active) exoskeletons to maximize metabolic cost savings while walking has shown that non-physiological torque profiles are optimal for each lower-limb joint [43, 95, 98, 134]. Perhaps semi-active devices, with both powered and passive elements, should take inspiration from both physiological and optimized torque/impedance information to provide the most benefit to users.

Notably, speed dependent shifts in optimal hip exoskeleton impedance parameters (for k or θ_0) did not reach statistical significance. This was mostly because of high variability in optimal impedance settings between participants (Figure 11B, C; Figure 40), and highlights the potential importance of focusing on tuning exo control parameters to each individual user to maximize performance (*i.e.,* user-dependent controller settings). Indeed, differences between hip exo impedance parameter (k, θ_0) - metabolic cost landscapes derived using a *user-dependent* (*i.e.,* per-each individual, or customized) (Figure 40) versus a *user-independent* (*i.e.,* averaged across-individuals or generalized) (Figure 13) analysis approach points to the potential benefit of tuning assistance to each unique user (*i.e.,* personalized control). For example, for the metabolically optimal stiffness (k), the user-dependent values increased steadily with walking speed while the user-independent values only appeared to increase at 1.6 m/s (Figure 11B). This suggests that the effect of increased stiffness (k), (*i.e.,* higher hip exo torque for both flexion and extension) did not yield a large generalized metabolic benefit for most users across speed, but instead, a subset of users benefited greatly from increased stiffness (*k*), when moving from 1.0 to 1.3 m/s (Figure 40, Participants 4, 7, 8, 9). Thus, using a semi-active device hip exo with stiffness tuned for the average user (*i.e.,* user-independent) at intermediate speed would leave some users with a glaring lack of metabolic benefit. Indeed, user-dependent assistance tended to provide more metabolic benefit than user-independent stiffness at every walking speed (Figure 11A). Other studies comparing user-dependent (customized) vs. user-independent (generalized) torque profiles with powered ankle exoskeletons also show increased benefits from a user-dependent approach - both for increasing preferred walking speed [38] and reducing metabolic cost [43, 95] compared to a user-independent 'one-size-fits all' approach. Taken together, these data suggest that perhaps commercial exoskeletons could apply a generalized 'best' assistance profile for 'out-of-the-box use' but that control settings should then be customized per user to provide highest possible benefit.

Muscles ultimately consume the metabolic energy that moves us, and exoskeletons reduce metabolic cost principally by reducing muscle force and activation [82, 85, 135]. Our data strongly support this idea, as changes in activity of the lower-limb muscles had strong correlation with changes in metabolic cost due to torque assistance from our semi-active hip exoskeleton concept (Figs. 5, 6). The strength of the fits from our linear regression analyses at all walking speeds (Figure 14, bottom) supports the validity of using a multi-channel surface electromyography (EMG) approach to model metabolic cost of exoskeleton users rather than direct measurements via indirect calorimetry [136, 137]. Using changes in EMG as a proxy for changes in metabolic cost could allow for faster online tuning of exoskeletons control parameters than what is offered by traditional human-in-the loop approaches.

Changes in activity of the muscles spanning the hip joint (*e.g.,* GMa, GMe, BF, RF) were shown to be most significant in predicting changes in metabolic cost (Figure 13, top); perhaps not surprising given the primary action of the exo is about the hip. Indeed, many

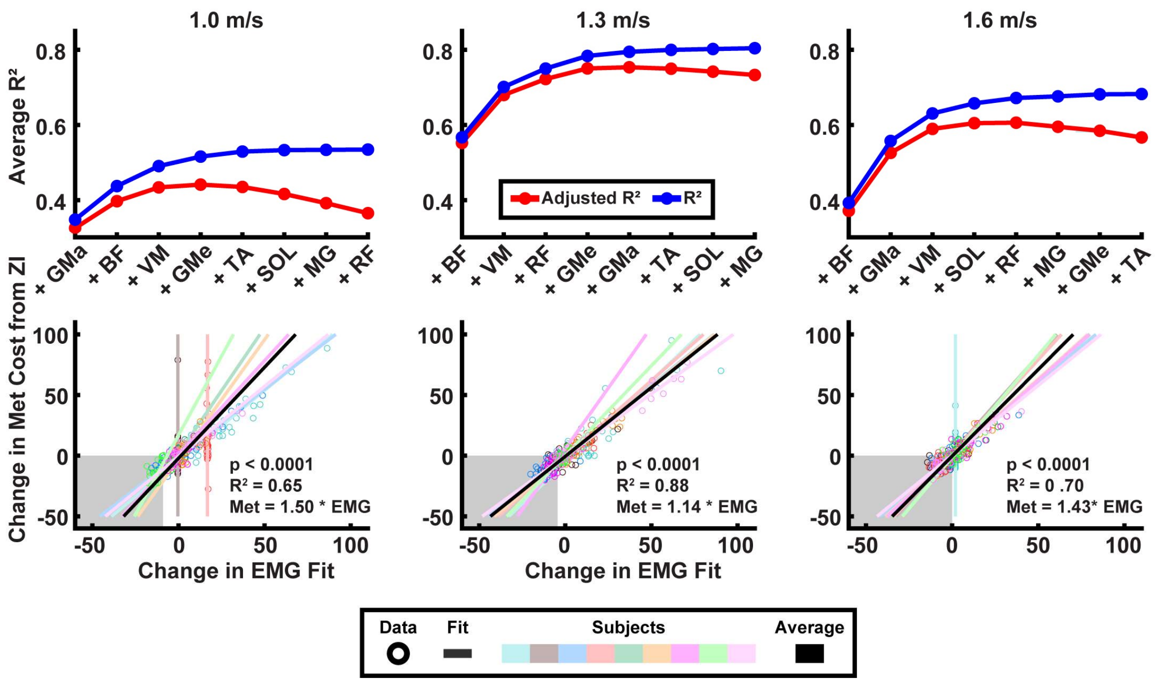

Figure 14 - Association between changes in users' lower-limb muscle activity and metabolic cost across hip exoskeleton impedance parameter space (k- θ0): (Top) Participant average r-squared and adjusted r-squared values produced in an iterative regression process, relating changes in gait cycle averaged muscle activity (%) and changes in gross metabolic rate (%) compared to the zero-impedance (ZI) condition. On the x-axis, the muscles included in the model are cumulative from left to right, so that each muscle's plotted r-squared point corresponds with a model that also includes all muscles in the preceding columns. Data are separated by walking speed (1.0 m/s, 1.3 m/s, 1.6 m/s form left to right). (Bottom) Linear regression fits using the four most significant muscles (i.e., four 'best' fits) per participant (colored lines) and the averaged across participants (black lines) for walking at 1.0 m/s, 1.3 m/s, and 1.6 m/s (left to right). Grey boxes highlight the areas in which there was a reduction in metabolic rate with respect to the corresponding zero-impedance (ZI) trial. Study-wide, changes in muscle activity corresponded well with changes in metabolic rate and participants who derived metabolic benefit had reduced muscle activity, especially at faster walking speeds.

other studies have shown that when robotic exoskeletons target the knee or ankle joint, the muscles that are more closely associated with those joints tend to respond most and drive changes in users' metabolic cost [20, 62, 138]. However, it is interesting to note that hip assistance also helped reduce activity in the knee extensors (VM) during early stance and the plantarflexors (SOL, MG) in late stance (Figure 12), re-emphasizing results from previous studies showing that exos at the hip [139] and ankle [67] can have non-local effects on muscle effort.

The metabolic benefit shown for optimal semi-active hip exoskeleton parameters (k, θ_0) of the metabolic cost landscape across parameters from the comprehensive sweep sessions did not transfer to the validation session for any walking speed (Figure 11A). We believe the lack of translation was due to the limited time given for re-habituation to optimal exoskeleton assistance from the sweep sessions at each walking speed. Habituation to exoskeleton assistance can occur in as little as 20 minutes [56, 62, 79, 140] but on average probably takes much longer, especially for metabolic rate to reach a new-steady state [43]. Much less is known about how habituation persists across multiple use-sessions separated by a significant time (*i.e.,* retention from one session to another) and/or how long is needed to re-habituate. Our results provide some evidence that re-habituation may be crucial. One could posit that our results from the sweep session were biased by measurement noise inherent when using indirect calorimetry to measure metabolic rate and further exacerbated by 2-minute estimations of steady-state cost, rather than effects of the exoskeleton control parameters themselves. To avoid this problem, we fit a multi-polynomial surface to the change in metabolic rate versus zero-impedance (ZI) across the grid of exoskeleton impedance parameters (k, θ_0), and then selected the optimal parameters based on the estimated metabolic minimum of the fit. Thus, the optimal set (k, θ_0), was influenced by all data points in the measurement set that generated fitted surface, decreasing bias from outliers and/or measurement noise (assumed to be normally distributed). Further, the difference in metabolic rate from ZI for our optimal parameter sets is much larger than the noise associated with measures of metabolic rate from indirect calorimetry [131, 141]. Strong correlations between changes in metabolic cost and changes in muscle activity (R^2=0.52-0.78) provide some physiological evidence that our measured changes were due to the exoskeleton and not measurement noise or bias.

Our study was not without some limitations. First, our hip exoskeleton end effector hardware was designed to handle over 200 Nm of torque applied at the hip [128]. Considering this, the added mass of the exoskeleton was much larger than what would be expected for a portable, autonomous semi-active version of the device. To accommodate for this difference, we compared gross metabolic rate in active impedance trials to that of wearing the exoskeleton in zero-impedance (ZI) mode, but we note that the bulk of the emulator may have affected the measured metabolically optimal assistance parameters (k, θ_0) themselves. Second, our emulator did not perfectly reproduce the semi-active device due to safety adjustments made to the onset of extension torque and imperfect torque tracking. As mentioned in Section IIA, we implemented a ramp function to decrease the speed of extension torque onset from ZI mode as some pilot users found this uncomfortable. The consequence of this ramp was decreased peak extension torques. The root-mean-squared-error of torque tracking across conditions was ~3Nm, which equated to <15% of peak-to-peak torque. We believed this was reasonable to conduct the study as torques generally followed the desired passive spring torque, but we acknowledge this does not perfectly emulate the proposed semi-active device. Last, this study was conducted on a treadmill rather than overground, which could have limited user adaptation via free adjustments in walking speed. Exoskeleton assistance has been shown to alter preferred walking speed along with changes in metabolic cost [38, 111]. Thus, it is possible that metabolic benefits could be higher for walking speeds outside the range we tested. future studies could explore optimizing the global cost of transport (*i.e.,* energy consumption per distance travelled), where both metabolic rate and preferred walking speed can equally contribute. This scenario might better represent user behavior outside of the lab, as humans tend to select their preferred walking speed to minimize cost of transport [36] in real-time [89, 90]. In our future work, rather than using an in the lab emulator to perform brute force exoskeleton controller parameter sweeps during treadmill walking at fixed speed, we plan to conduct optimizations using autonomous devices outside the lab under real-world conditions that better represent an average user's daily activities.

CHAPTER 4. OPTIMAL HIP AND ANKLE EXOSKELETON ASSISTANCE TO ENHANCE SELF-SELECTED WALKING SPEED

4.1 Introduction

Older adults become more sedentary and less able to partake in physical activity [3, 4] which leads to decreasing quality of life and independence over time and increasing fall risk, morbidity, and mortality [5-10]. The declining health of older adults increases the burden on our healthcare system, substantially contributing to U.S. healthcare costs [142]. As a proxy for physical ability in older adults, clinicians use an efficient and low intensity measurement of self-selected walking speed (SSWS) [143]. Slowing SSWS has been correlated with physical ability along with increased health issues [5-10]. Experimental studies have investigated physiological factors correlated with declining SSWS including increased energy expenditure during walking, decreased muscle strength, decreased ankle power generation, and increased reliance on the hip joint [3, 24-33]) but none have noted a causal link. Without a clear focus, therapeutic interventions developed have inconsistent results improving SSWS or do so in a non-ideal manner [5, 26, 32, 144, 145]. Wearable devices may provide an avenue to increase mobility in older adults without understanding the causal factors.

While exoskeletons (exos) provide an exciting new opportunity to enhance walking ability in older adults, it is unclear whether returning function to the source of the biomechanical changes with aging (ankle) or assisting at the joint of compensation (hip) would be more effective at increasing walking speed. Studies applying exoskeleton assistance at the ankle have successfully lowered metabolic cost compared to walking in the unpowered device [21, 146] but failed to increase SSWS [21]. This may be due to the high metabolic cost of distal loading while walking [22]. Both passive (spring-based) and powered assistance at the hip have successfully decreased metabolic cost and increased SSWS [23, 147]. In terms of medical device prescription, it is important to know which target joint would be best to assist to decrease patient costs. With only a few studies applying exos to improve SSWS with no direct comparisons, it is still unclear if assistance at the hip or the ankle would be more beneficial. To understand the maximal benefits of lower limb exo assistance for a proper comparison, assistance must be optimized.

Human-in-the-loop optimization (HILO) has the potential to enhance exo performance outcomes in older adults, but special accommodations must be considered. In younger adults, HILO has been used to maximize metabolic benefits at each lower limb joint [39-41] and SSWS at the ankle [18, 38]. Further, studies have found individually optimized (*i.e.,* individualized, user-dependent) exo torque assistance provides more metabolic benefit than generic (*i.e.,* user-independent) assistance [41-43]. Individualization of assistance may be increasingly important for older adults as muscle activation and gait parameters vary more with age [45, 46]. Fatiguability also increases with age [47], jeopardizing the ability of older adults to complete strenuous or lengthy HILO protocols. Among the HILO algorithms tested [40, 41, 48], Bayesian optimization has provided the shortest amount of time to reach globally optimal parameters for cost landscapes with multiple local minima (i.e., non-convex). Task selection is also important to consider in terms of testing duration and translatability. Optimizing using overground SSWS measurements, compared to metabolic cost, would decrease optimization times by ~75% [38, 41, 42]. Additionally, overground compared to treadmill walking speed selection would provide higher clinical comparability [148] and, from our pilot studies, higher comfort when walking with an experimental device. Optimized exo assistance may be an effective method to increase SSWS in older adults.

We designed an overground HILO protocol to realize an effective exoskeleton assistance strategy for both hip and ankle joints to increase SSWS in older adults and tested this novel protocol with younger and older adults. This is the first overground HILO protocol focused on optimizing SSWS performance and the first study to include older adults with HILO for both hip and ankle assistance. We expect the optimized (user-dependent) exo assistance strategies (at each joint) will provide increased SSWS compared to generic (user-independent) assistance. The optimized profiles provided from this study will inform future exo development for community ambulation. Our study will also provide a head-to-head comparison between ankle and hip assistance to identify the most effective exo target, providing valuable insight for future exo prescription and SSWS interventions. We hypothesize applying assistance to the ankle joint will yield the largest increase in SSWS compared to walking without an exo by increasing total torque output at the ankle which has been suggested as the "SSWS bottleneck" {Conway, 2018 #232}.

4.2 Methods

4.2.1 Participants

We recruited 3 65+ year old adults (3F, Age: 66.67±1.53; Weight: 57.92±4.91 kg, Height: 159.6±4.87 cm) and 8 young adults (6M/2F; Age: 21.43±1.72; Weight: 73.82±19.04 kg, Height: 176.47.2±12.46 cm). The participants provided written informed consent prior to participation in accordance with Georgia Institute of Technology Institutional Review Board requirements (Protocol H20533).

4.2.2 Exoskeleton Control

For the hip, we designed an exoskeleton (Figure 15) capable of matching peak torque assistance of the Dephy ExoBoot. The in-house exoskeleton applied spline torque at the

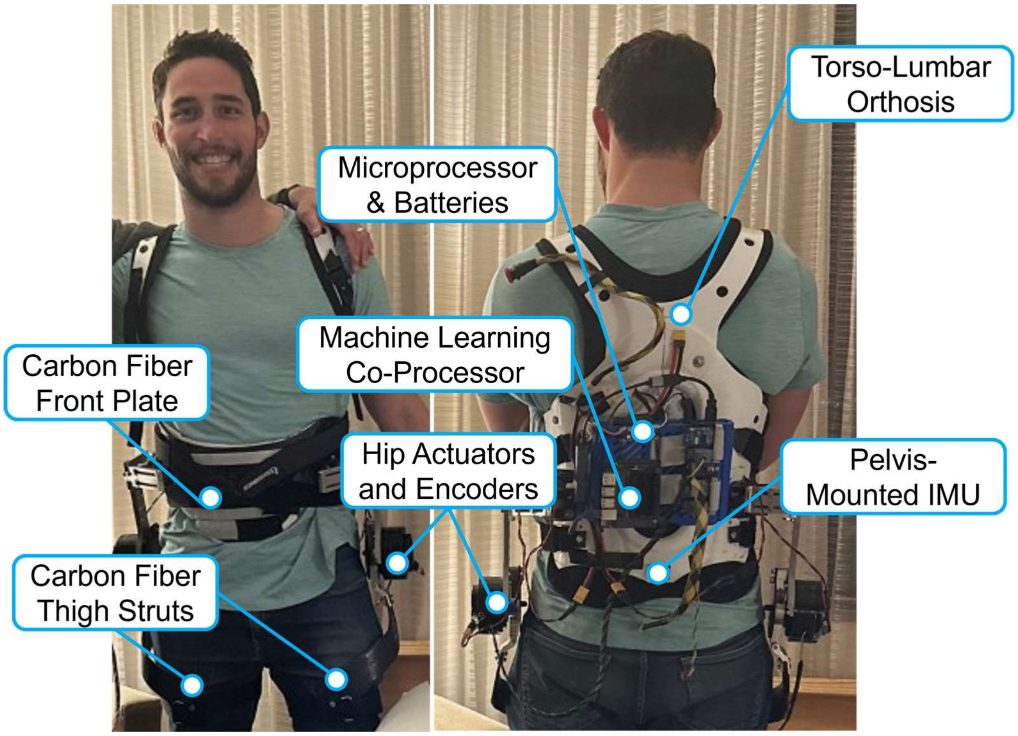

Figure 15 - Georgia Tech in-house hip exoskeleton and component labels seen from the front (Left) and back (Right).

hip using gait phase estimates via a convolutional neural network model driven by a lower back mounted IMU and encoder measurements from motors (T-MOTOR, Jiangxi, China). Desired torque was communicated to the motors via a MyRio (National instruments, Austin, TX, USA), which allowed real-time modulation of hip assistance using 5 parameters (peak torque duration, extension peak time, flexion torque duration, flexion peak time, and peak torque (extension).

For the ankle, the Dephy ExoBoot (Dephy Inc, Boxborough, MA USA) applied plantarflexor assistance based on a spline torque profile across gait phase. We estimated gait phase using a Convolutional Neural Network (CNN) model driven by IMU and encoder measurements from each boot and run on a Jetson Nano (NVIDIA, Santa Clara, CA USA) [43]. Using a Raspberry Pi (Raspberry Pi Foundation, Cambridge, UK), we

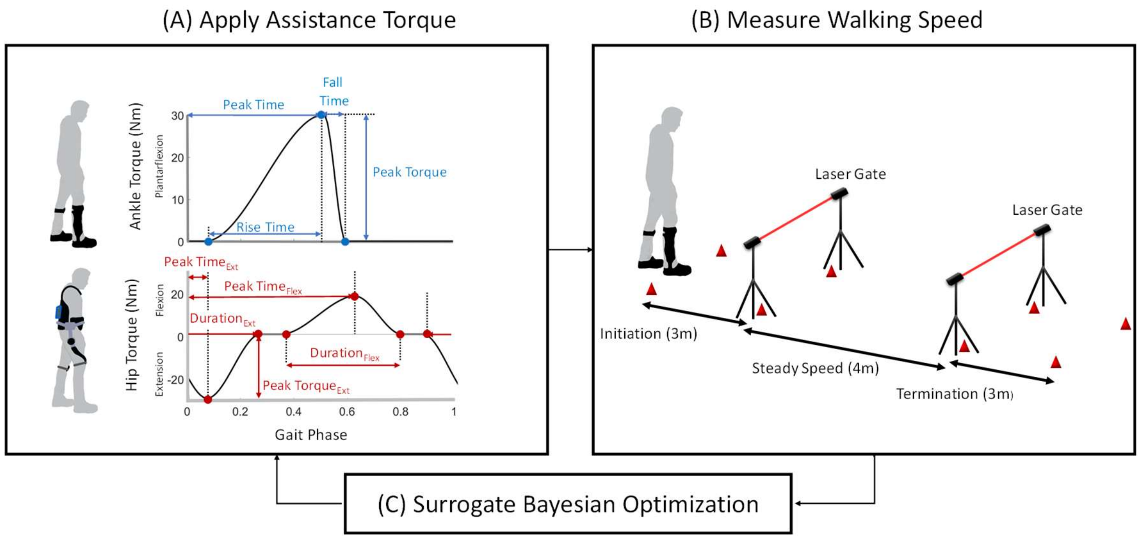

Figure 16 - Ankle and hip exoskeleton torque assistance and human in the loop optimization protocol. Hip and ankle torque profiles are generated using splines with specified magnitude and timing parameters (A). Ankle assistance is modulated by 4 parameters: Peak Torque, Rise Time, Peak Time, and Fall Time. Hip assistance is modulated by 5 parameters: Peak Torque, Extension Peak Time, Flexion Peak Time, Extension Duration, and Flexion Duration. Each exo undergoes assistance optimization on a separate day. First, assistance is set to a generalized parameter set and self-selected walking speed is measured using the 4-meter walk test (B) and the associated parameters are input to the Surrogate Bayesian Optimization algorithm (C). The algorithm supplies the next parameter set to be tested and this cycle repeats for 30 iterations or until parameter convergence.

modulated the desired torque assistance along the gait cycle using 4 adjustable parameters: start time, peak torque, peak time, and end time (Figure 16A).

4.2.3 Overground self-selected walking speed measurement

We used the 4m walk test (4MWT) protocol for overground self-select-walking speed (SSWS) measurement (Figure 16B) [45]. The participant walked a straight 10m distance. The distance was separated into 3 zones: initiation (3m), steady speed (4m), and termination (3m). The time to walk through the steady speed zone was measured using laser gates. The participants walked back and forth 3 times per SSWS measurement (6 speed calculations). The last 4 speeds were averaged for the final SSWS measurement.

4.2.4 Human-in-the-loop optimization algorithm

We maximized assisted SSWS using the Surrogate optimization algorithm in Matlab (MathWorks, Apple Hill Campus, MA, USA). To minimize the number of measurements needed for optimization and reduce walking time for participants, we conducted an offline comparison between Surrogate and previously published algorithms for human-in-the-loop optimization (HILO), including Bayesian, and covariance matrix adaptation evolution strategy (CMAES) algorithms, based on optimization speed and accuracy {Kim, 2019 #344}{Zhang, 2017 #160}. We found Surrogate converged with the lowest required measurements and comparable accuracy to the other optimizers (Figure 41).

4.2.5 Data collection protocol

We separated the data collection into 2 sessions. The first session was to allow the user to habituate to the exoskeleton assistance and then conduct HILO. In the second session, users rehabituated to their optimized assistance profile and then we measured SSWS across exoskeleton conditions.

4.2.5.1 Session 1

First, we habituated the subjects to exo assistance. We fitted the exoskeleton to the participants and then measured their SSWS while walking without assistance (NoPwr). We habituated users to exo assistance using a user-independent metabolically optimized profile (GEN) from a previous study [40]. Habituation was conducted on a treadmill then overground. On the treadmill, participants walked at their overground NoPwr SSWS without assistance for 1 minute and then with peak ankle plantarflexor/hip extensor torque beginning at 6Nm and increasing 4Nm/min until 30Nm or a maximum comfortable torque was reached. The participants then walked with this maximum torque for 21 minutes. After completing the treadmill portion, participants returned to the overground area. We started with a 4MWT while walking with the GEN assistance. Once complete, we input their SSWS and the associated parameters to begin a round of optimization. The user walked for 9 more iterations, having the chance to learn walking with various assistance profiles. After these 10 iterations, we measured GEN SSWS again and compared this to the initial value. If speed changed by more than 0.1 m/s, we interpreted this as a lack of habituation and restarted the optimization. The optimization process was restarted no more than twice per participant.

After habituation (continuing after the first 10 iterations), participants walked with assistance for 20 iterations (i.e., parameter sets/assistance profiles) or until parameters converged (next parameter within 5% of previous) (Figure 16A). In each iteration, assistance parameters were generated by the algorithm and applied to the participant while completing a 4mWT. The associated measurement was input to the algorithm and a new parameter set was generated for testing.

4.2.5.2 Session 2

For re-habituation, we first measured SSWS while the participants walked without wearing the exoskeleton (NoExo). Then participants walked on the treadmill with OPT at 4 speeds (0%, ±33%, and -67% of $SSWS_{NoExo}$) in random order for 3 minutes each. For each speed, we increased peak ankle plantarflexor/hip extensor torque as in habituation until the optimal or max comfortable torque was reached. Then, the participant walked overground for ten 10m passes. This accumulated to 30-40 minutes of rehabituation time, similar to values suggested in literature to get users acquainted with exoskeleton assistance and reduce measurement variability [149].

To validate our SSWS measurements, the participants completed 4MWTs while walking with NoPwr, the GEN assistance, and the OPT assistance with conditions randomized in ABCCBA order.

4.2.6 Statistical Analyses

To determine if optimized exo assistance can enhance SSWS and which joint target provided the largest enhancement, the SSWS measurements during Session 2 of each condition (NoExo, GEN, OPT) were averaged across participants for each target joint (ankle and hip). We used a two-way ANOVA with post-hoc comparisons to determine any significant differences in SSWS between any of the conditions and joints. We used the same statistical analysis on the percent difference of SSWS from the NoExo condition to compare GEN and OPT conditions and across joints. To determine any significant linear relationships between ankle and hip parameter sets and SSWS within subject groups, we used linear regressions for each parameter from optimization session data.

4.3 Results

4.3.1 Self-selected walking speed (SSWS)

For each exoskeleton (exo) target joint (ankle or hip), there were no significant effects for changes in self-selected walking speed (SSWS) across conditions (without the exo (NoExo), with exo powered off (NoPwr), with exo generalized assistance (GEN), and with exo individually optimized assistance (OPT) (Figure 17). The following differences are discussed qualitatively.

4.3.1.1 Ankle

Wearing the ankle exoskeleton without assistance (NoPwr) reduced walking speed (NoPwr-NoExo, -0.04 +/- 0.09 m/s) (Figure 17). Both GEN and OPT assistance increased walking speed from NoExo and NoPwr (GEN-NoExo: 0.05 +/- 0.12 m/s; OPT-NoExo: 0.03 +/- 0.13 m/s; GEN-NoPwr: 0.09 +/- 0.09 m/s; OPT-NoPwr: 0.07 +/- 0.10 m/s). OPT and GEN assisted walking speeds were nearly identical on average (OPT-GEN: -0.00 +/- 0.02 m/s).

4.3.1.2 Hip

Wearing the hip exoskeleton without assistance (NoPwr) reduced walking speed (Change from NoExo, -0.10 +/- 0.05 m/s) (Figure 17). Both GEN and OPT assistance decreased walking speed from NoExo (GEN-NoExo: -0.01 +/- 0.13 m/s; OPT-NoExo: -0.01 +/- 0.11 m/s). Both GEN and OPT assisted speeds were increased from NoPwr walking speed (GEN-NoPwr: 0.09 +/- 0.14 m/s; OPT-NoPwr: 0.09 +/- 0.12 m/s). OPT and GEN walking speeds were nearly identical on average (OPT-GEN: -0.00 +/- 0.05 m/s).

4.3.1.3 Between Target Joints

For both ankle and hip joints, assistance increased SSWS from NoPwr for each joint (Figure 17). The proportional cost of the wearing the exo to SSWS was higher for the hip exo than the ankle exo (Hip NoPwr-NoExo (mean +/- stdev): -6.85% +/- 2.89%; Ankle NoPwr-NoExo: -3.25% +/- 6.67%). Assistance at the ankle and hip generated faster

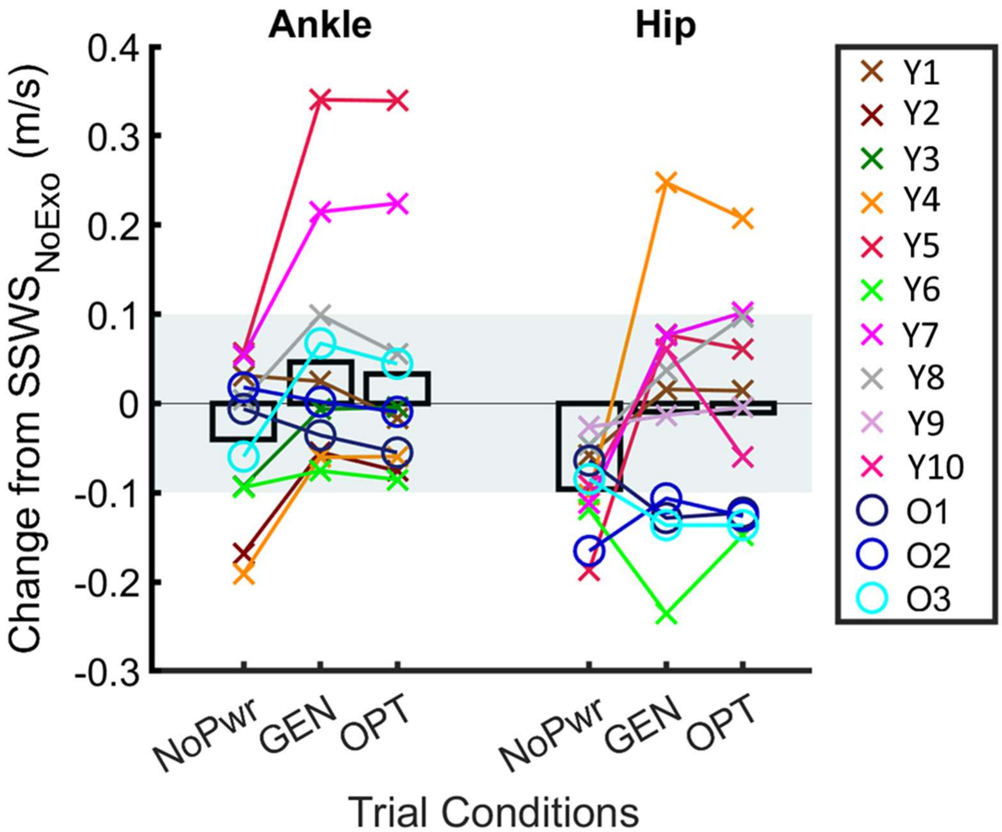

Figure 17 - Self-selected walking speed changes for NoPwr, GEN, and OPT trial conditions versus SSWS without the exoskeleton (NoExo)]. Black outlined bars represent group averaged absolute SSWS differences from the NoExo condition. Individual subject data points are included to show the distribution within the group. The gray area denotes the region below the minimal clinically significant difference, which is ±0.1 m/s from NoExo SSWS. Statistically significant differences between conditions or exo joints are indicated by "*".

walking speeds compared to NoPwr similarly (Ankle GEN-NoPwr: 7.09% +/- 6.57%; Ankle OPT-NoPwr: 5.97% +/- 7.05%; Hip GEN-NoPwr: 6.83% +/- 10.63%; Hip OPT-NoPwr: 7.05% +/- 9.28%). That said, only the ankle could generate assisted walking speeds faster than walking in normal shoes (Ankle GEN-NoExo: 3.56% +/- 9.39%; Ankle OPT-NoExo: 2.48% +/- 9.77%; Hip GEN- NoExo: -0.62% +/- 8.91%; Hip OPT- NoExo: -0.41% +/- 7.70%).

4.3.2 Optimal Parameters

Across groups and exo target joints, optimal parameters fell within designated upper and lower bounds of the optimization.

4.3.2.1 Ankle

Optimal absolute plantarflexion torque magnitudes (Figure 18A) were distributed across the upper half of the optimization range (15-30 Nm) with an average mass-normalized torque of .39 +/- .15 Nm/kg (Figure 18B). Rise time averaged within the bottom half of the range, 27.2 +/- 7.9 %GC, and optimal values were spread across the range (Figure 18C). Similarly, optimal values for Fall time were spread across the range (Figure 18C) and

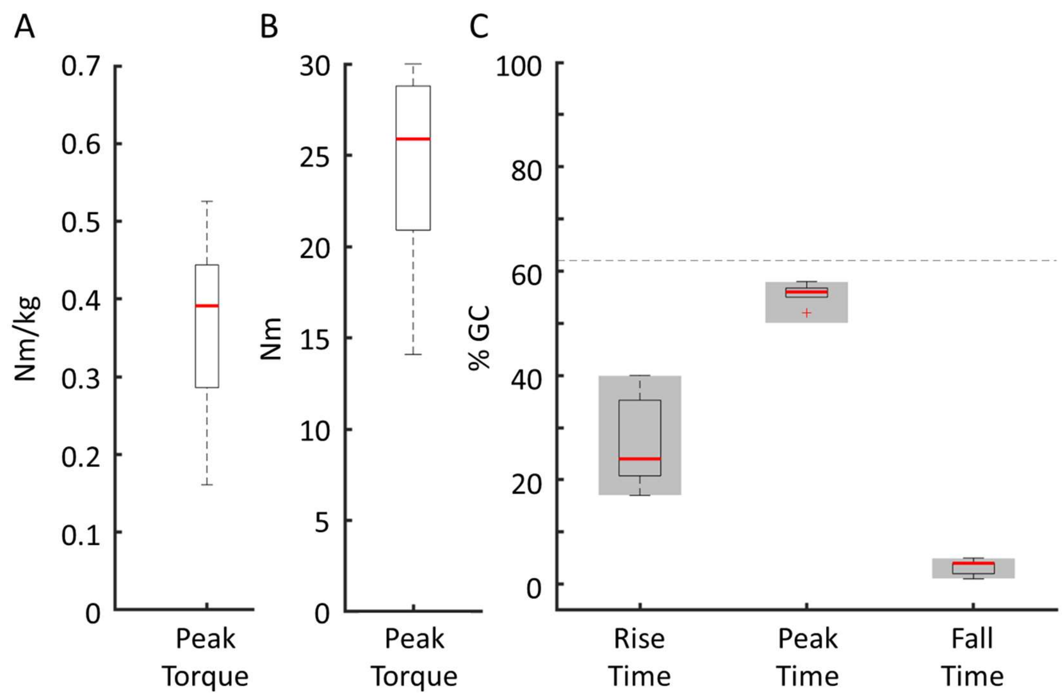

Figure 18 - Ankle exoskeleton optimal parameter distributions. Peak torque is shown as both normalized to subject mass (A) and absolute (B). Timing parameters (C) are shown in terms of percentage of the gait cycle (%GC) where 0% and 100% represent heel strike. Toe off was estimated at 62% of the gait cycle and shown as the grey dotted line. Parameter value ranges used in the optimization are the shaded regions for the timing parameters. Peak torque ranged between 0-30 Nm.

averaged at 3.3 +/- 1.2 %GC. Peak time averaged at 55.9 +/- 1.6 %GC and with a much smaller distribution compared to the other parameters (Figure 18C).

4.3.2.2 Hip

Optimal absolute torque magnitudes ranged from 3-30 Nm, averaging 18.9 +/- 8.8 Nm or 0.29 +/- 0.16 Nm/kg (Figure 19A&B). Optimal extension peak times ranged from 10-20 GC (upper 50 of optimization range) with one outlier at the earliest time (Figure 19C). Flexion peak times varied across the optimization range with the majority of participants optimized after toe-off (62 %GC) (Figure 19C). Optimal extension assistance was shorter

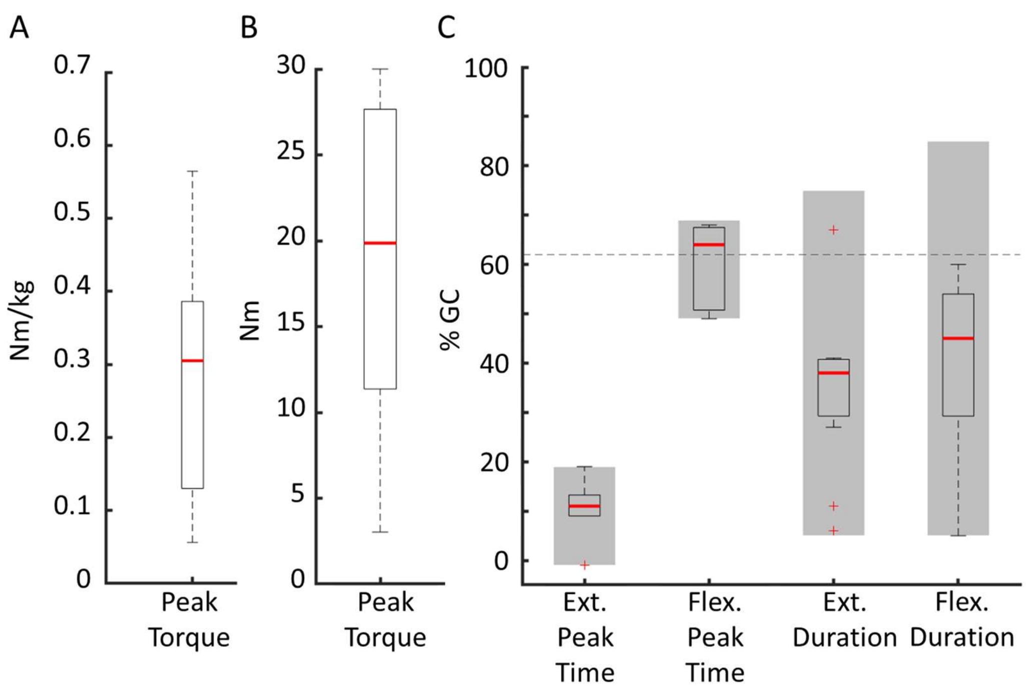

Figure 19 - Hip exoskeleton optimal parameter distributions. Peak torque is shown as both normalized to subject mass (A) and absolute (B). Timing parameters (C) are shown in terms of percentage of the gait cycle (%GC) where 0% and 100% represent heel strike. Toe off was estimated at 62% of the gait cycle and shown as the grey dotted line. Parameter value ranges used in the optimization are the shaded regions for the timing parameters. Peak torque ranged between 0-30 Nm.

than flexion assistance and varied much less (Figure 19C). Excluding outliers, extension duration ranged between 25-42.5 %GC while flexion duration ranged between 15-60 %GC.

4.3.3 Parameter Sensitivity Analysis

4.3.3.1 Ankle

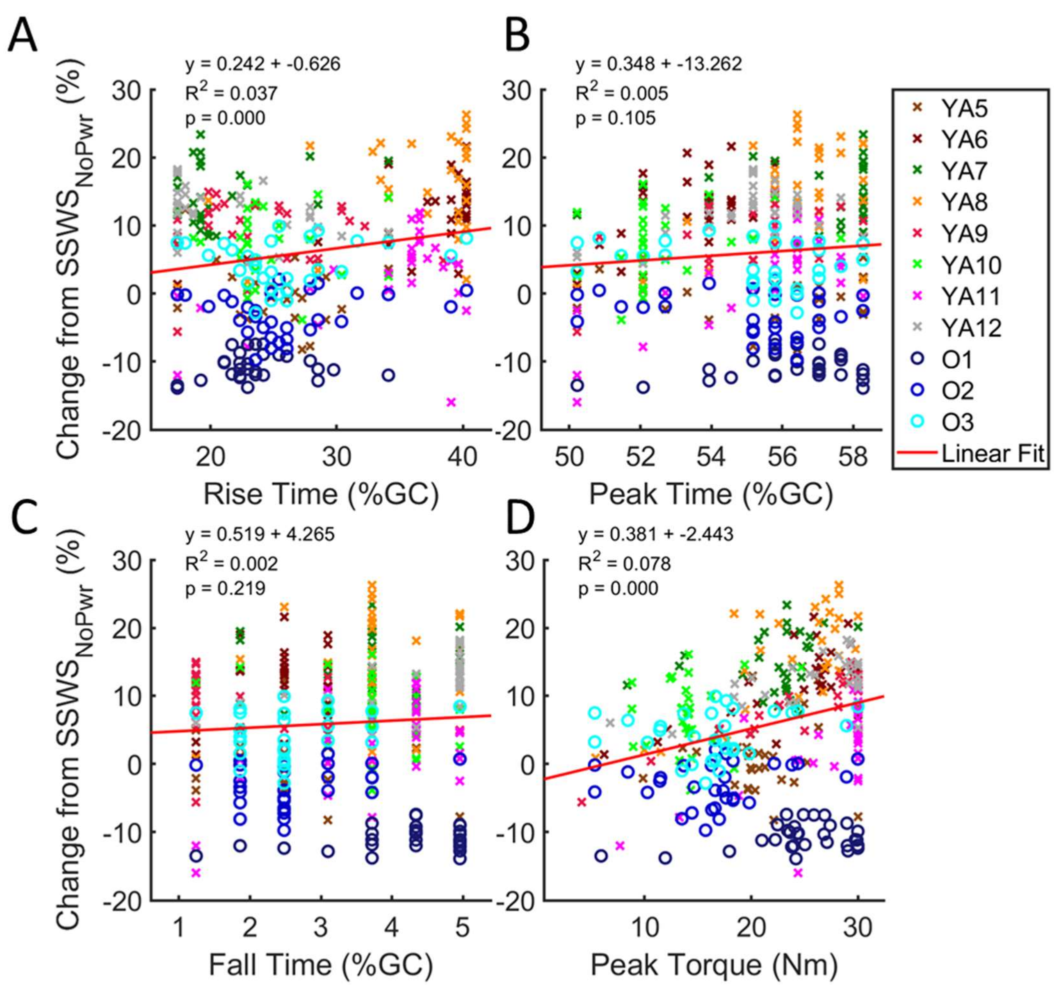

Figure 20 - Linear regressions between ankle exoskeleton commanded spline torque parameters and percent changes in walking speed from walking in the exo with no assistance (NoPwr) during the optimization session. The overall fit is shown as the red line. Participants are shown in separate colors as labelled, with the older adults in shades of blue and circle markers.

Rise Time and Peak Torque parameters were significantly associated with changes in walking speed ($p < 0.001$ each) while Peak Time and Fall time were not ($p = 0.10$ and 0.291, respectively) (Figure 20). Each were weakly associated with percentage changes in SSWS (Peak Torque: $R^2 = 0.078$; Rise Time: $^2 = 0.037$). These correlations seem to be driven by the younger adult participants.

4.3.3.2 Hip

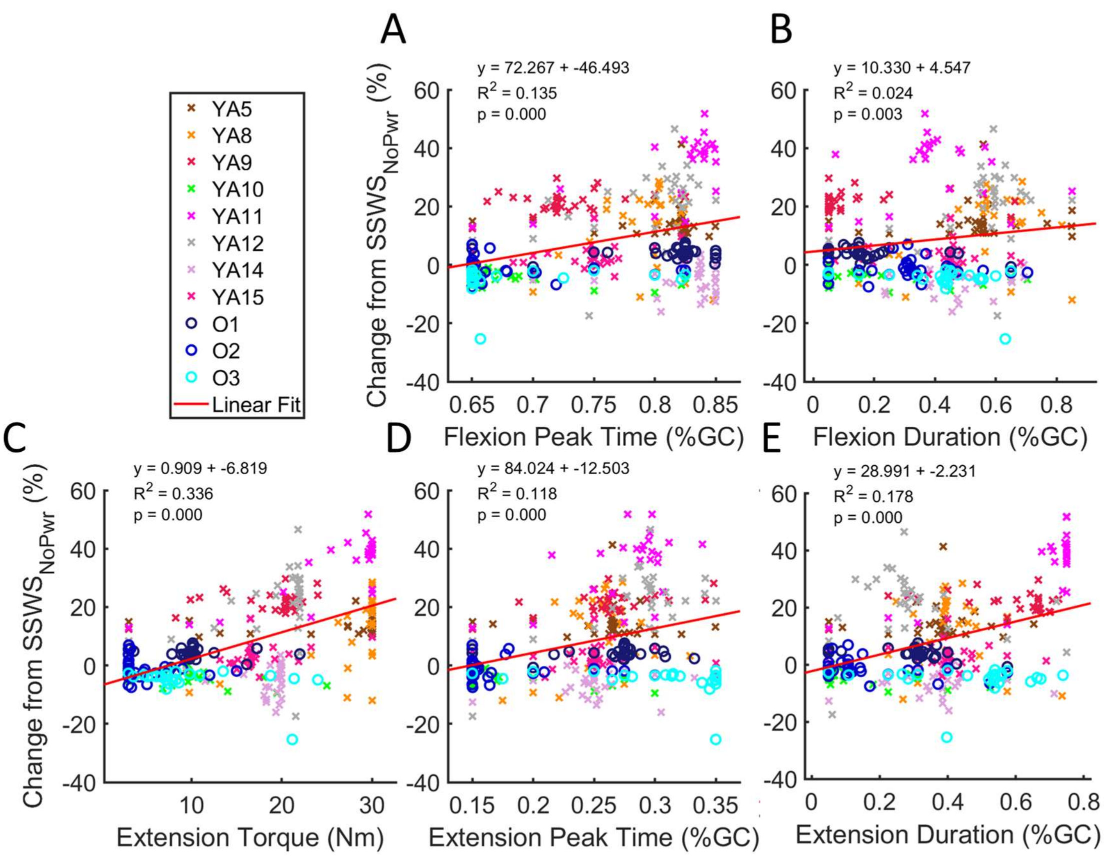

Figure 21 - Linear regressions between hip exoskeleton commanded spline torque parameters and percent changes in walking speed from walking in the exo with no assistance (NoPwr) during the optimization session. The overall fit is shown as the red line. Participants are shown in separate colors as labelled, with the older adults in shades of blue and circle markers.

All hip assistance parameters were significantly and positively associated with changes in SSWS from walking with the unpowered exoskeleton (NoPwr) with varying degrees of correlation (Figure 21). Extension torque magnitude (which also scaled flexion assistance proportionally) had the strongest correlation (R^2 = 0.336, p <0.001) (Figure 21C). Extension Duration, Flexion Peak Time, and Extension Peak Time (Figure 21EA&D) all had similar associations (Extension Duration: R^2 = 0.178, p <0.001; Flexion Peak Time:

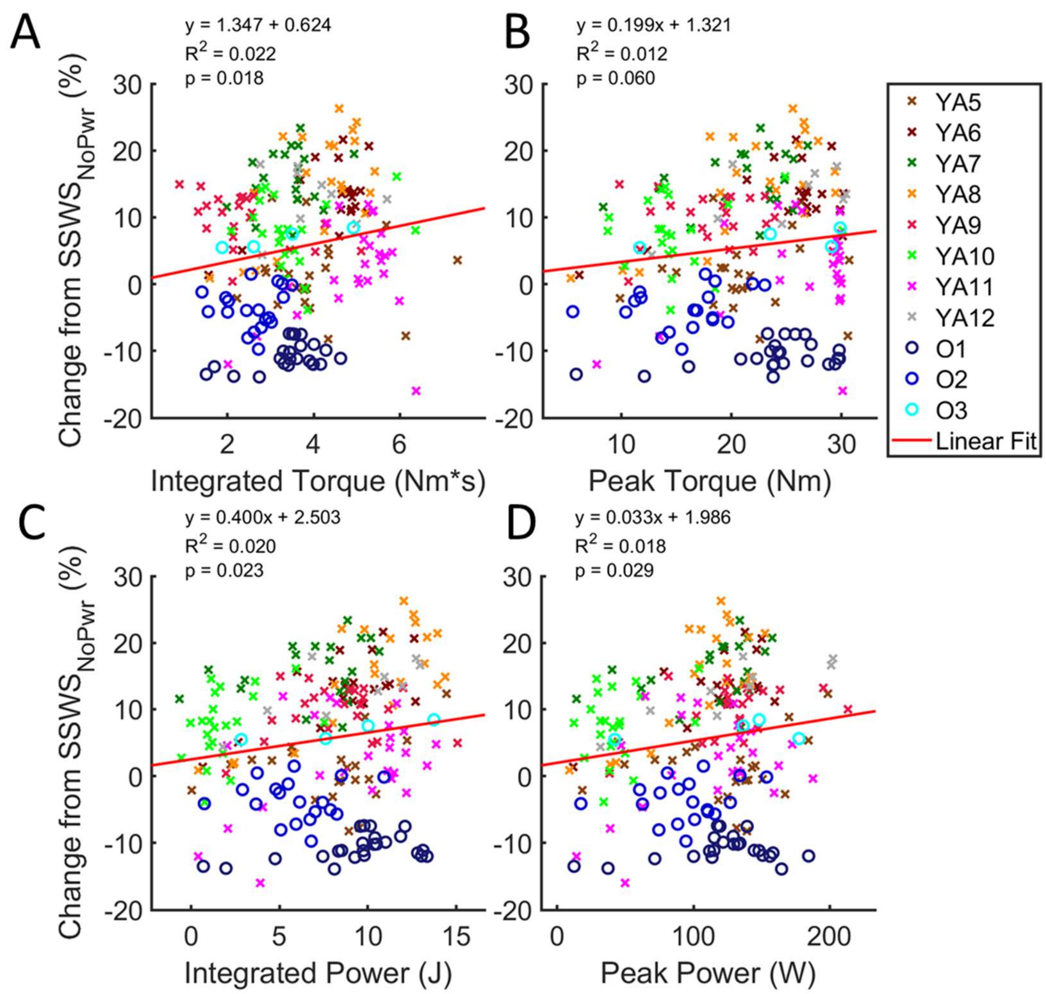

Figure 22 - Linear regressions between ankle exoskeleton mechanical factors and percent changes in walking speed from walking in the exo with no assistance (NoPwr) during the optimization session. The overall fit is shown as the red line. Participants are shown in separate colors as labelled, with the older adults in shades of blue and circle markers.

R^2 = 0.135, p <0.001; Extension Peak Time: R^2 = 0.118, p <0.001). Flexion Duration (Figure 21B) had the weakest correlation (R2 = 0.024, p = 0.003) similar to ankle assistance parameters discussed in the previous section.

4.3.4 Mechanical Sensitivity Analysis

4.3.4.1 Ankle

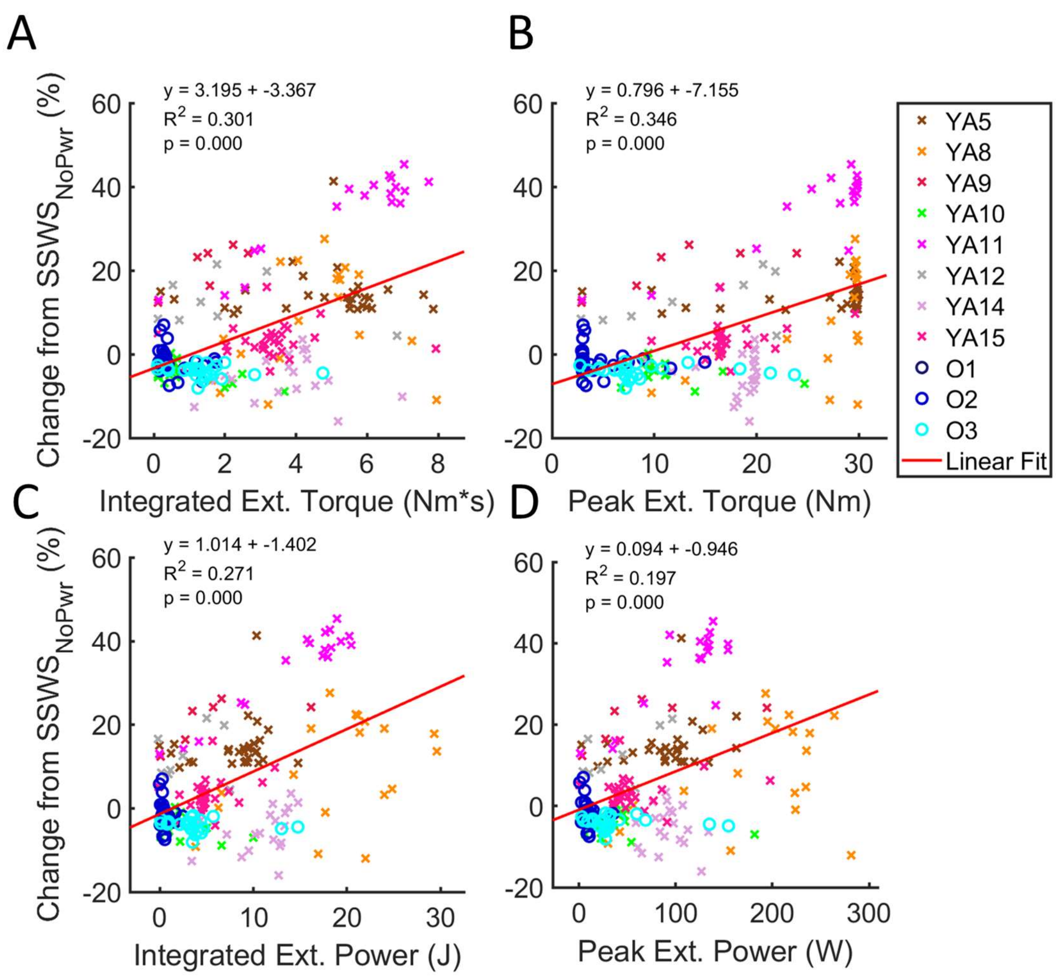

Figure 23 - Linear regressions between hip extension exoskeleton mechanical factors and percent changes in walking speed from walking in the exo with no assistance (NoPwr) during the optimization session. The overall fit is shown as the red line. Participants are shown in separate colors as labelled, with the older adults in shades of blue and circle markers.

Of the mechanical factors measured during the optimization sessions, integrated ankle assistance torque (Figure 22A) was the only significantly correlated factor with changes in walking speed from NoPwr ($R^2 = 0.022$, $p = 0.018$). All other factors were insignificantly correlated with assisted walking speeds (Figure 22BCD). Older adults seemed to decrease the significance of these correlations by having a smaller range of walking speed changes and possible opposite correlations compared to the younger adults.

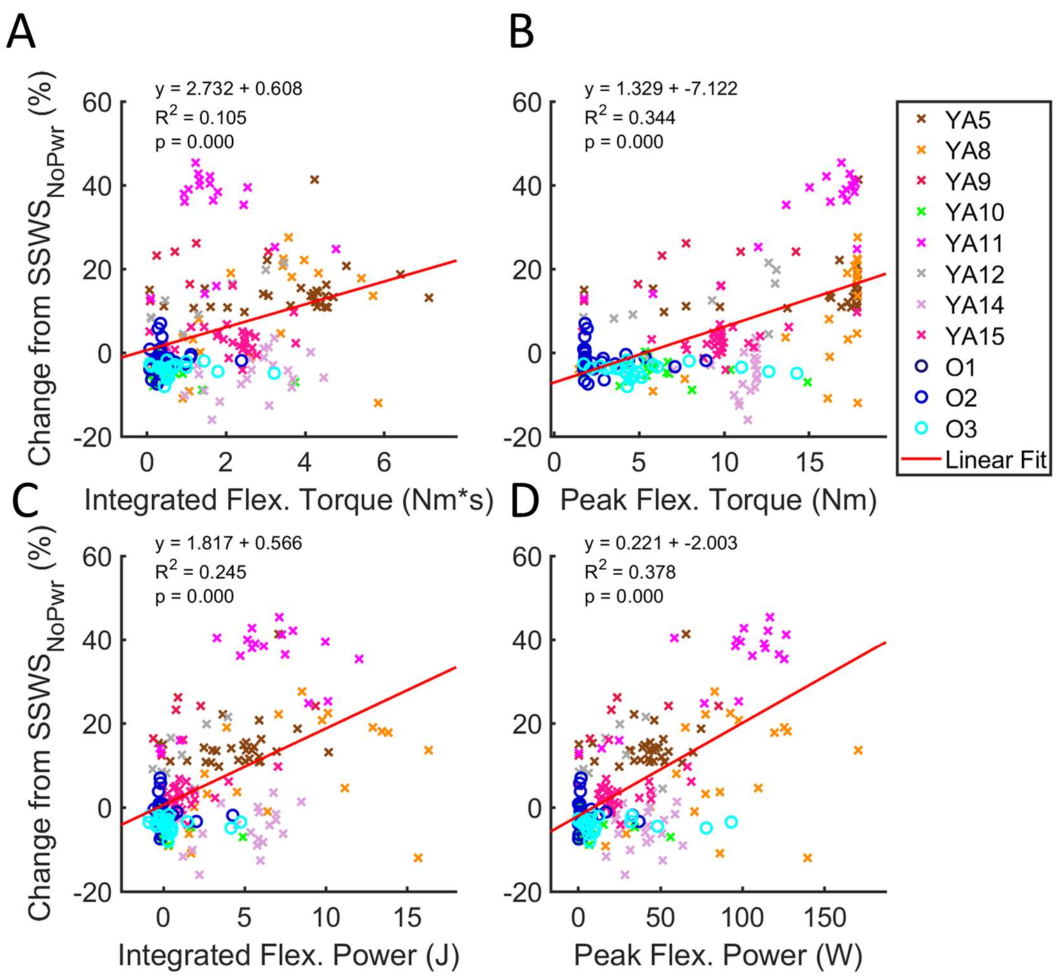

Figure 24 - Linear regressions between hip flexion exoskeleton mechanical factors and percent changes in walking speed from walking in the exo with no assistance (NoPwr) during the optimization session. The overall fit is shown as the red line. Participants are shown in separate colors as labelled, with the older adults in shades of blue and circle markers.

4.3.4.2 Hip

All 8 measured hip exo assistance mechanical factors (integrated torque, peak torque, integrated power, and peak power for both extension and flexion) were significantly correlated with changes in walking speed from wearing the unpowered exoskeleton (Figure 23 and Figure 24. Flexion peak power (Figure 24D) had the strongest correlation to changes in SSWS ($R^2 = 0.378$, $p < 0.001$). Peak Extension Torque (**Error! Reference source not found.**B) and Peak Flexion Torque (Figure 24B) had similar correlations (Peak Extension Torque: $R^2 = 0.346$, $p < 0.001$; Peak Flexion Torque: $R^2 = 0.344$, $p < 0.001$). Extension Integrated Torque (**Error! Reference source not found.**A), Extension Integrated Power (**Error! Reference source not found.**C), Flexion Integrated Power (Figure 24C), and Extension Peak Power (**Error! Reference source not found.**D) had moderate correlations (Extension Integrate Torque: $R^2 = 0.301$, $p < 0.001$; Extension Integrated Power: $R^2 = 0.271$, $p < 0.001$; Flexion Integrated Power: $R^2 = 0.245$, $p < 0.001$; Extension Peak Power: $R^2 = 0.197$, $p < 0.001$). Flexion Integrated Torque (Figure 24A) had the weakest correlation with changes in SSWS ($R^2 = 0.105$, $p < 0.001$).

4.4 Discussion

In this study, we optimized torque assistance for ankle and hip exoskeletons in younger and older adults based on overground self-selected walking speed. Our goal was to determine which exoskeleton joint would be more effective at changing SSWS and if an overground optimization could increase SSWS beyond metabolically optimized assistance on a treadmill.

First, we predicted that ankle exo assistance would provide faster SSWS than hip assistance compared to NoExo and found no significant changes to SSWS between target joints ($p = 0.987$) (**Error! Reference source not found.**). Some trends were interesting although insignificant. Despite a larger SSWS cost to wear the hip exoskeleton without assistance (NoPwr), assisted SSWS benefits proportional to NoPwr were similar between the ankle and hip powered conditions. This suggests that ankle and hip assistance may have similar benefits to SSWS when using weight match devices. With our older adults, we see that ankle assistance may be more readily accepted than hip exo assistance as SSWS decreased with hip assistance while ankle assistance elicited similar or increased SSWS compared to NoExo. We matched torque application characteristics between the hip and ankle exos, yet it is apparent more studies with weight matched devices are needed to make accurate conclusions on whether ankle or hip assistance is better for increasing SSWS in younger and older adults as weight may have different effects across age groups.

Second, we predicted that the OPT assistance would provide faster SSWS compared to the GEN condition for both ankle and hip target joints. There were no significant differences in walking speed between ankle conditions (walking without the exo (NoExo), in the exo unpowered (NoPwr), with generic assistance (GEN), and with optimized assistance (OPT)) ($p = 0.821$) or between hip conditions ($p = 0.70$) (**Error! Reference source not found.**). We believe there are 2 factors that could have contributed to this result: (1) the optimization may not have been successful and (2) lack of carry-over from optimization to validation measurements. To reduce walking fatigue in our older adult participants, we used a modified Bayesian algorithm that showed similar accuracy and quicker convergence than traditional Bayesian and CMAES algorithms used in other human-in-the-loop optimization

(HILO) applications {Zhang, 2017 #160}{Kim, 2019 #344} during offline simulations. One limitation to Bayesian algorithms is a lack of adaptability to time-variant cost functions {Venter, 2010 #751}. SSWS is volitionally controlled, unlike metabolic cost, and participants often changed their SSWS while assisted with the same torque profile. Optimizations could have converged to a parameter set which was the faster than GEN due to the participant's volitional state rather than the assistance leading to suboptimal assistance. We attempted to mitigate this risk by using precise walking instructions and restarts of the optimization when the SSWS with identical assistance changed substantially. Using a genetic optimization algorithm like CMAES would mitigate the risk of suboptimal convergence but at the cost of lengthier optimization sessions. Since SSWS is dependent on the participant's volitional state, lack of habituation during the validation session could have reduced the effect size of powered assistance on SSWS. Our habituation times for this study were based on assisted walking periods that minimized metabolic cost variability {Galle, 2013 #708}. Using a more volatile measure (like overground SSWS), may require more habituation time to ensure the highest measurement precision. Future studies should compare optimization algorithm performance directly and determine if habituation times vary for performance measures with a volitional component.

Assistance may need to be more individualized for hip assistance than ankle assistance. The number of tuneable parameters between the hip and ankle were similar (5 and 4 respectively) and motor performance (peak torque, power, etc.) was matched, yet all 5 hip parameters were significantly associated with SSWS compared to only 2 parameters at the ankle (Figure 20 and Figure 21). In fact, parameters that had higher optimal value distribution (more different across participants were more likely to have a significant effect on SSWS, with the exception of ankle Fall Time (Figure 18 and Figure 19). This may be due to each parameter's effects on mechanical assistance factors at each joint. At the ankle, Rise Time and Peak Torque were each positively correlated with SSWS (Figure 20). Peak Time across participants was tightly distributed, suggesting one value could work for all users. If fact, ankle assisted SSWS was significantly correlated with Integrated Torque, Integrated Power, and Peak Power, all of which are affected by changes in Rise Time and Peak Torque. To maximize assisted SSWS with ankle assistance, more torque should be applied during plantarflexion regions. At the hip, we assisted in both extension and flexion. For hip extension assistance, Integrated Torque was more corelated with SSWS than Integrated Power and both had a stronger correlation than Peak Power. This suggests that hip extension and ankle plantarflexion assistance appear to have a similar function for increasing SSWS. Hip flexion assistance Peak Power had the strongest effect on SSWS than all other factors (Figure 24D). It is apparent that the timing peak hip flexion velocity varies more across participants than ankle plantarflexion or hip extension in that peak flexion timing varied across 100% of the optimization range. Thus, it is most important to tune hip flexion assistance timing to maximize assisted SSWS benefits then hip extension timing, and ankle plantarflexion timing.

The timing of ankle exoskeleton assistance optimized for overground SSWS is similar to metabolically optimized profiles and SSWS optimized profiles on the treadmill. We used modifiable ankle spline torque parameters based on [19] (Figure 18). To start our optimizations, we began with their across subject average parameter set based on metabolic human-in-the-loop optimization while walking at 1.25 m/s on a treadmill (GEN). Our torque optimization resulted in unique parameter sets per participant which were also different from GEN (Figure 18). Peak Time and Rise Time were nearly identical (55% and 27%, respectively). In contrast, optimal Fall Time was much shorter for overground SSWS (3.4%) compared to the metabolic optimal (17%). Overground metabolic ankle assistance tuning generated similar Rise and Peak Times with shorter Fall Times closer to the ones found in this study (9.98%) [18]. It seems that overground walking requires plantarflexion assistance to end earlier. Exo assistance mechanical analysis for treadmill SSWS optimization presented significant correlations with Peak Torque magnitude and Peak Power matching our results. Maximizing the power of assistance while avoiding disruption of natural foot raising seems to be important for enhancing overground SSWS compared to profiles based on treadmill and metabolic performance.

Future studies could benefit hardware that is more similar in weight and form factor across target joints. Our in-house developed hip exoskeleton matched assistance outputs with the Dephy Exoboots but took longer to put on and was much heavier. This may have resulted in less comfort with the device and slower walking speed beyond the effects of carrying a heavy load. The cost to SSWS performance was overcome in the younger adult group but persisted in the older adult group. Future studies could also benefit from using optimization algorithms that are robust to time variant cost functions such as SSWS. We selected the Surrogate Bayesian algorithm based on an offline comparison of optimization speed and accuracy with 2 established human-in-the-loop optimization algorithms (traditional Bayesian [40] and CMAES [41]) tuning a model to estimate biological torques while walking. In this time invariant test, Surrogate was the quickest to optimize with results comparable to the other algorithms. This was essential to our study as we needed to minimize walking effort for the older adult group. That said, walking speed is much more variable than metabolic cost as it relies on the psychological state of the walker and can be controlled volitionally. Using an algorithm robust to time-variant measurements would give more optimal torque profiles that may further increase SSWS performance. Nevertheless, OPT assistance provided comparable SSWS to GEN and speeds at or above NoExo. Qualitatively, when asked which assistance profile was more comfortable, 100% of the users stated the OPT assistance was better than the GEN assistance despite no difference in SSWS performance. Focusing on SSWS instead of metabolic cost to tune exo assistance could be more user friendly and practical for real-world applications.

CHAPTER 5. USING EXOSKELETONS TO DETERMINE THE PHYSIOLOGICAL BASES FOR SELF-SELECTED WALKING SPEED ACROSS AGE

5.1 Introduction

As we get older, our locomotor ability declines, subsequently diminishing physical health and the ability to safely move inside and outside the home (i.e., crossing the street) [1, 7, 8]. To monitor physical decline, geriatricians measure overground self-selected walking speed (SSWS) which is correlated with important outcomes such as quality of life and independence in older adults [5-8]. While the relationship between SSWS and aging has been extensively studied, it is still unclear what causes age-related slowing of SSWS [3, 9, 10, 24, 25, 27-29, 34, 35]. Experimental studies have investigated factors correlated with declining SSWS (i.e., increased energy expenditure during walking, decreased muscle strength, and decreased ankle power generation [3, 24-33]) but none have noted a causal link. Without guidance on how to increase SSWS, the efficacy of current interventions is limited [5, 26, 144, 150].

Humans naturally walk at a speed that minimizes their metabolic cost of transport (COT) or energy per unit distance [36]. When comparing COT in older and younger adults, COT increases across all walking speeds with aging but the speed that minimizes COT does not {Martin, 1992 #64}. Meaning, older adults choose a self-selected walking speed (SSWS) slower than the speed that minimizes COT [3, 25, 35]. Assuming we are still optimizing gait as we age, there must be a different physiological measure being used. Since humans do not use respiratory gases to measure their COT and optimize gait [151], we believe they could be optimizing their relative muscle activation or load (as a percentage of maximum voluntary contraction). Simulations that have implemented age-related changes to the muscles and nerves of a walking model, determined that muscle load more accurately predicts SSWS compared to COT in older adults [29]. An examination of joint-level muscular changes with aging may support this hypothesis.

The ankle and hip joints are the primary positive power producers while walking [11]. At each joint with aging we see decreased kinetic outputs (torque and power) and a significantly larger deficit at the ankle compared to the hip during walking [12, 13]. These deficits at the ankle are considered primary contributors of slowing walking speed with age [13]. To compensate, older adults shift power generation from the ankles to the hips [14, 15] despite incurring a metabolic penalty [16]. The increased load at the hip significantly affects COT, but the decreased loading at the ankle has no effect [16]. Further, it follows that using ankle musculature less during walking results in a more rapid decline of ankle strength and power generation compared to the hip over time. It is safe to assume that power generation at the hip would require less muscle load, proportional to max loading, than at the ankle. These data posit there is a disconnect between COT and muscle load in older adult walking that could manifest differences in optimal speed that are driven by age-related changes at the ankle joint. To determine if muscle load better predicts changes in SSWS compared to COT, we employed exoskeleton (exo) assistance from the previous chapter to change the SSWS-COT/CMAPD relationship.

The objective of this study was to understand how well muscle load across walking speeds predicts SSWS in older adults. We applied optimized hip and ankle exo assistance modify muscle load, COT, and speed compared to walking in normal shoes (NoExo) providing a broad context for comparison. We hypothesized optimal muscle load speed will (1) significantly correlate with SSWS across groupings (age, exo condition, and target joint) and (2) have a stronger correlation with SSWS compared to optimal COT speed in older adults compared to younger adults.

5.2 Methods

5.2.1 Participants

We recruited 3 older (65+ years old) adults (3F, Age: 66.67±1.53; Weight: 57.92±4.91 kg, Height: 159.6±4.87 cm) and 7 young adults (6M/1F; Age: 21.43±1.72; Weight: 73.82±19.04 kg, Height: 176.47.2±12.46 cm). The participants provided written informed consent prior to participation in accordance with Georgia Institute of Technology Institutional Review Board requirements.

5.2.2 Exoskeleton Control

We implemented spline control (torque assistance profile over percentage gait) for both the hip and ankle exoskeletons (Figure 25). A 3-node spline was used to determine ankle plantarflexion assistance of the Dephy Exoboot (Dephy Inc, Boxborough, MA, USA) by optimizing all 4 parameters: start time, peak time, end time, and peak torque. Gait phase during the ankle exo condition was estimated via a previously trained machine learning model {Kang, 2021 #83} using bi-lateral ankle joint angles, ankle joint velocities, and shank 6 degree-of freedom IMU data. To control our in-house designed hip exoskeleton, we used a 6-node spline and optimized the 5 parameters (Extension peak time, extension

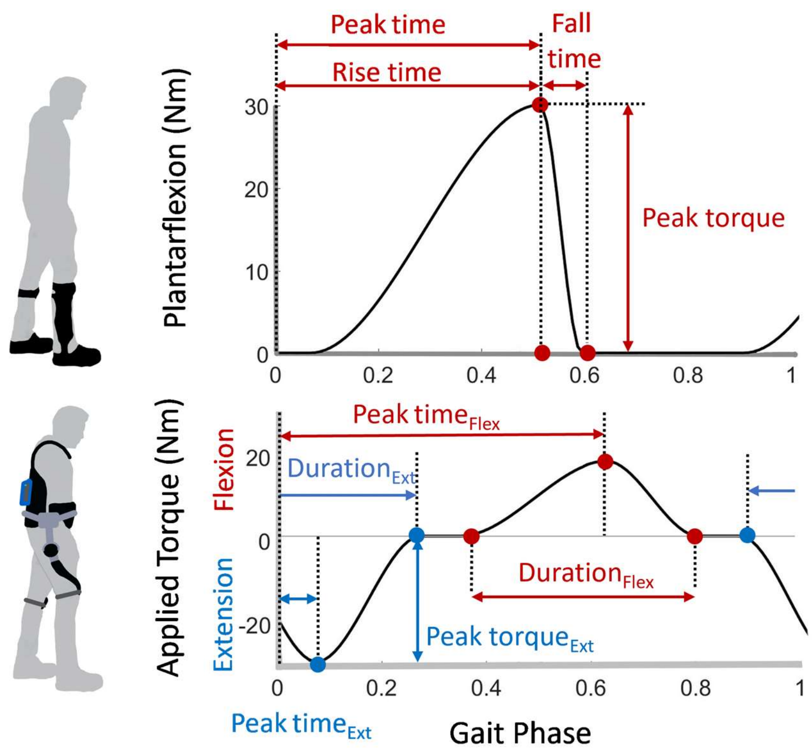

Figure 25 - Ankle and hip exoskeleton torque assistance and human in the loop optimization protocol. Hip and ankle torque profiles are generated using splines with specified magnitude and timing parameters. Ankle assistance is modulated by 4 parameters: Peak Torque, Rise Time, Peak Time, and Fall Time. Hip assistance is modulated by 5 parameters: Peak Torque, Extension Peak Time, Flexion Peak Time, Extension Duration, and Flexion Duration. All timing parameters are in gait phase where 0 and 1 are equivalent to heel strike.

duration, flexion peak time, flexion duration, and extension peak torque). Peak hip extension torque was set to the ankle device limit of 30 Nm. Parameters not optimized were set to the average metabolically optimal parameters found in {Bryan, 2021 #325}. We also estimated gait phase with a convolutional neural network driven by encoder measurement from the motors (bilateral hip angle, hip velocity) and pelvis 6 degree of freedom IMU data [152, 153].

5.2.3 Overground self-selected walking speed measurement

To measure short-distance overground self-selected walking speed we used the 4 m walk test (4MWT) protocol [148]. Subjects walked 6 passes on a straight 10 m walkway. The time to traverse the middle 4 m was measured and converted to walking speed. The average of the last 4 passes was used as the final SSWS measurement.

5.2.4 Data collection protocol

We separated the data collection into 2 sessions. The first session was to allow the user to habituate to the exoskeleton assistance and then conduct HILO. In the second session, users rehabituated to their optimized assistance profile and then we measured SSWS across exoskeleton conditions on the treadmill and overground.

5.2.4.1 Session 1

To habituate the user to exoskeleton (exo) assistance, we fitted the exoskeleton to the participant and measured their SSWS while walking without assistance (NoPwr). We habituated users to exo assistance using a user-independent metabolically optimized profile (GEN) from a previous study [40]. Habituation was conducted on a treadmill then overground. On the treadmill, participants walked at their overground NoPwr SSWS without assistance for 1 minute and then with peak ankle plantarflexor/hip extensor torque beginning at 6 Nm and increasing 4 Nm/min until 30 Nm or a maximum comfortable torque was reached. The participants then walked with this maximum torque for 21 minutes. Overground, we started the optimization and ran it for 10 assistance profiles starting with GEN. We then re-measured GEN SSWS. If speed changed by more than 0.1 m/s, we interpreted this as a lack of habituation and restarted the optimization process. We restarted no more than twice per participant.

After habituation (continuing after the first 10 iterations), participants walked with assistance for 20 iterations (i.e., parameter sets/assistance profiles) or until parameters converged (next parameter within 5% of previous). In each iteration, assistance parameters were generated by the algorithm and applied to the participant while completing a 4mWT. The associated measurement was input to the algorithm and a new parameter set was generated for testing.

5.2.4.2 Session 2

Sessions were separated by at least 24 hours. To start re-habituation, we measured SSWS while the participants walked without wearing the exoskeleton (NoExo). Then participants walked on the treadmill with OPT at 5 speeds ($SSWS_{NoExo}$, $SSWS_{NoExo}$ ±33%, and -67%) in random order for 3 minutes each. For each speed, we increased peak ankle plantarflexor/hip extensor torque as in habituation until the optimal or max comfortable torque was reached. Then the participant walked overground for 10 10 m passes. This accumulated to 30-40 minutes of rehabituation time similar to values suggested in literature users to get acquainted with exoskeleton assistance and reduce measurement variability [4].

After rehabituation, participants wore a metabolic mask (See Metabolics Section) and surface electromyography sensors (See Electromyography Section) on their dominant leg (Figure 26). Participant started with a standing trial to obtain a reference metabolic cost. Then, participants walked 5 speeds ($SSWS_{Exo}$, $SSWS_{NoExo}$, $SSWS_{NoExo}$ ±33%, and -67%) in random order for both NoExo and Exo for a total of 10 trials, 5 minutes for each.

5.2.5 Metabolics

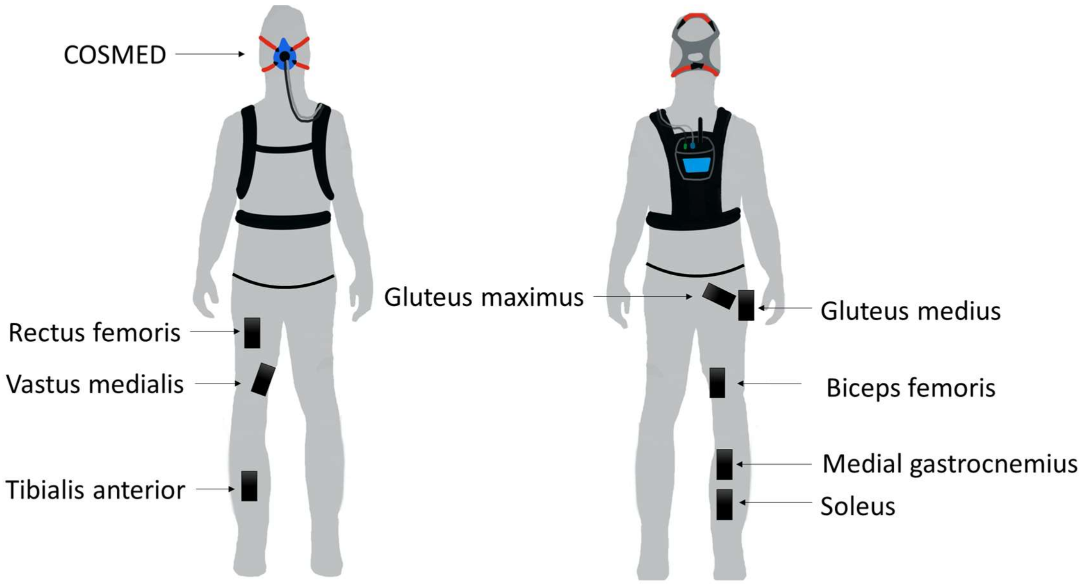

Figure 26 – Metabolic and muscle activation data acquisition setup. COSMED K5 for measuring metabolic cost and 8 electromyographic electrode placed on 8 lower limb muscles (dominant leg only). These muscles cover all sagittal plane movements for each joint.

Metabolic measurements were collected using indirect calorimetry via the COSMED K5 (COSMED USA Inc., Concord, CA, USA). On a breath-by-breath basis, consumed volume of oxygen and expired volume of carbon dioxide were measured and used to calculate metabolic cost via the Brockway equation [46]. On the treadmill, metabolic cost was computed for each trial as the average of the last 1.5 minutes. Metabolic cost of transport (COT) was calculated by dividing the metabolic cost by the walking speed.

5.2.6 Electromyography

Surface EMG was collected from the dominant leg for 8 muscles (Tibialis Anterior, Soleus, Medial Gastrocnemius, Vastus Medialis, Rectus Femoris, Biceps Femoris, Gluteus Medius, and Gluteus Maximus) using Delsys Avanti sensors (Delsys Inc., Natick, MA, USA) (Figure 26). Raw signals passed through a 3rd order highpass (fc = 100 Hz)

Butterworth filter, rectified, then passed through a 3rd order lowpass (fc = 6 Hz) Butterworth filter. Timeseries data was divided into gait cycles using heel strikes identified by ground reaction forces recorded by an instrumented split-belt treadmill (Motek Medical B.V., Houten, Netherlands). Gait cycle data for each muscle was normalized by the peak activity during the NoExo condition at SSWSnoexo. The normalized gait cycle data was integrated and divided by walking speed to provide cumulative muscle activity per distance (CMAPD) [45]. And then we summed the CMAPD across all muscles to calculate sCMAPD for each trial.

5.2.7 Optimal Walking Speed

Our dataset includes COT and CMAPD data across 5 speeds for NoExo and Exo conditions across 2 target joints (hip and ankle) for 11 subjects each. For each subject and target joint, we fit a quadratic curve to each physiological measure (COT & CMAPD) and target joint across five speeds for NoExo and Exo. We derived the minimum of each quadratic function to determine the optimal speed and percentage difference. For each subject, we fit a quadratic curve for all combinations of physiological measure (2 total), target joint (2 total), and condition (2 total), resulting in 23 or 8 total optimal speed data points (i.e., the speeds that minimized the quadratic functions). We used this data to correlate SSWS with optimal COT and CMAPD speeds.

5.2.8 Statistical analyses

To compare SSWS, across conditions (NoExo, NoPwr, GEN and OPT) within one exo joint target (hip, ankle), we conducted a two-way ANOVA using a Bonferroni correction for multiple comparisons. To compare SSWS, metabolic cost, COT, and CMAPD across

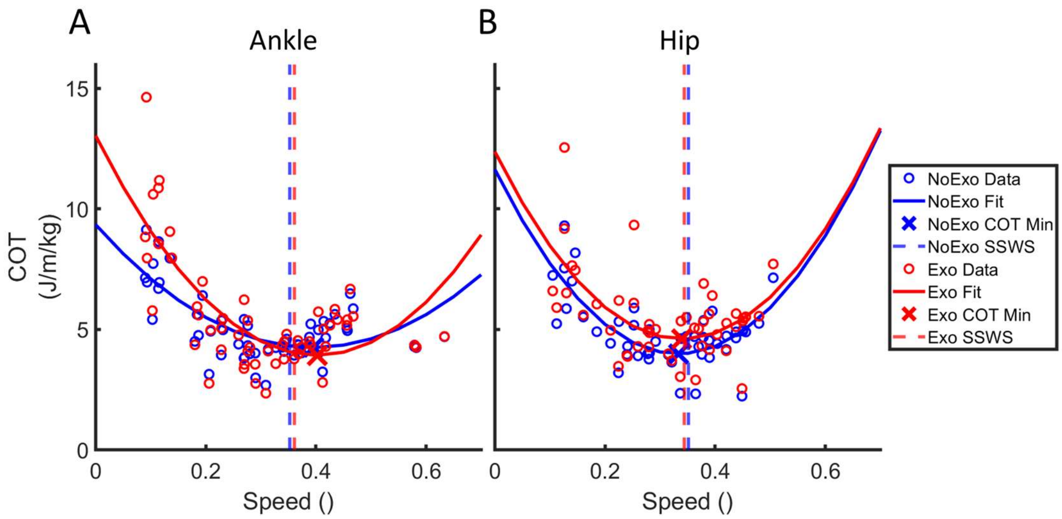

Figure 27 – Group COT-Speed landscapes for ankle (A) and hip (B) exoskeletons. For each joint, we fit all subject data points for NoExo and Exo conditions with a quadratic curve and the minimum of that curve was calculated. For comparison, the average SSWS for each joint-condition pairing are also included. Speeds were nondimensionalized by dividing by the square root of the product of gravitational acceleration and height.

target joints for both indoor and outdoor collections, we calculated the percentage difference from NoExo for each joint's OPT condition then conducted students t-test using a Bonferroni correction for multiple comparisons. To determine physiological measure best correlates with changes in SSWS, we ran a linear regressions between each COT & CMAPD optimal speed and SSWS (both nondimensionalized to account for height differences by dividing speed by the square root of gravitational acceleration (m/s2) times height (m) [38]) across all data, age groups, exo condition, and exo target joints. Significance was considered for p values <= 0.05.

5.3 Results

5.3.1 Cost of Transport (COT)

Self-selected walking speed (SSWS) optimized ankle and hip exoskeleton (exo) assistance had different effects on COT across speeds. Ankle assistance trended to increase COT at extreme walking speeds (slowest and fastest) and decrease COT near the speed that minimized COT across all subjects (Figure 27A). Hip assistance trended to increase COT for all speeds (Figure 27B). When pooling minimum COT speed (MinCOTSpeed) and paired SSWS data for all subjects (young (Y) and old (O)) across target joints (ankle and hip) and exoskeleton conditions (Exo and NoExo), there was a significant ($p<0.001$) correlation of 0.662 (Figure 28). Running separate linear regressions for the O and Y groups (Figure 31), each had a significant correlation (O: $p<0.001$ and Y: $p<0.001$).

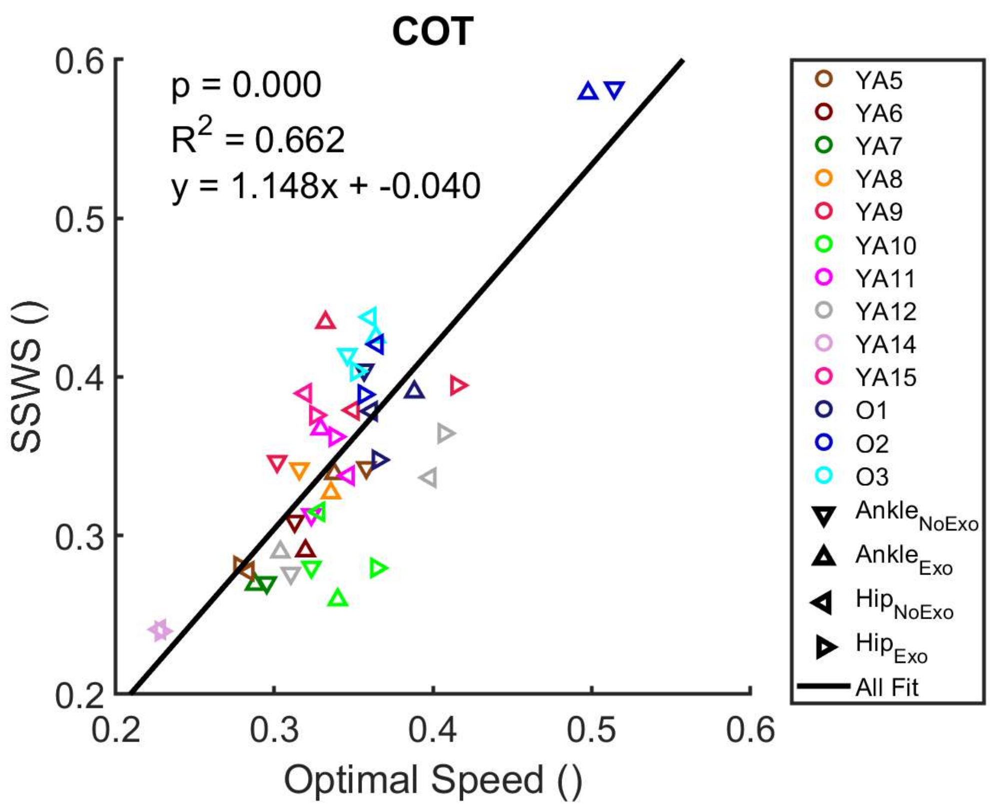

Figure 28 - Linear Regressions between the optimal speed to minimize COT and SSWS, both nondimensionalized to account for changes in height. The overall linear regression is shown as a black line. Individual participants are shown in separate colors with older adults in shades of blue. The 4 conditions (Exo and NoExo for Ankle & Hip each) are shown with different marker shapes.

MinCOTSpeed was more strongly correlated (R^2 = 0.828) with SSWS in the O group compared to the Y (R^2 = 0.346). Separating Exo and NoExo trials for each group, exo condition, and target joint, each had a significant correlation (Exo: $p<0.001$ and NoExo: $p<0.001$) (Figure 31). MinCOTSpeed was more strongly correlated (R^2 = 0.716) with SSWS in Exo condition compared to NoExo (R^2 = 0.600). When examining assistance at the Ankle and Hip with all subjects, minCOTSpeed and SSWS were significantly correlated for each target joint (Ankle: p = 0.001, Hip: p = 0.022) (Figure 31). Ankle assistance resulted in a larger correlation (R^2 = 0.721) than the Hip (R^2 = 0.439).

5.3.2 Summed Cumulative Muscle Activation per Distance (sCMAPD)

SSWS optimized ankle and hip exo assistance had different effects on sCMAPD across speeds. Ankle assistance trended to increase sCMAPD at extreme walking speeds (slowest and fastest) and decrease sCMAPD near the speed that minimized sCMAPD across all

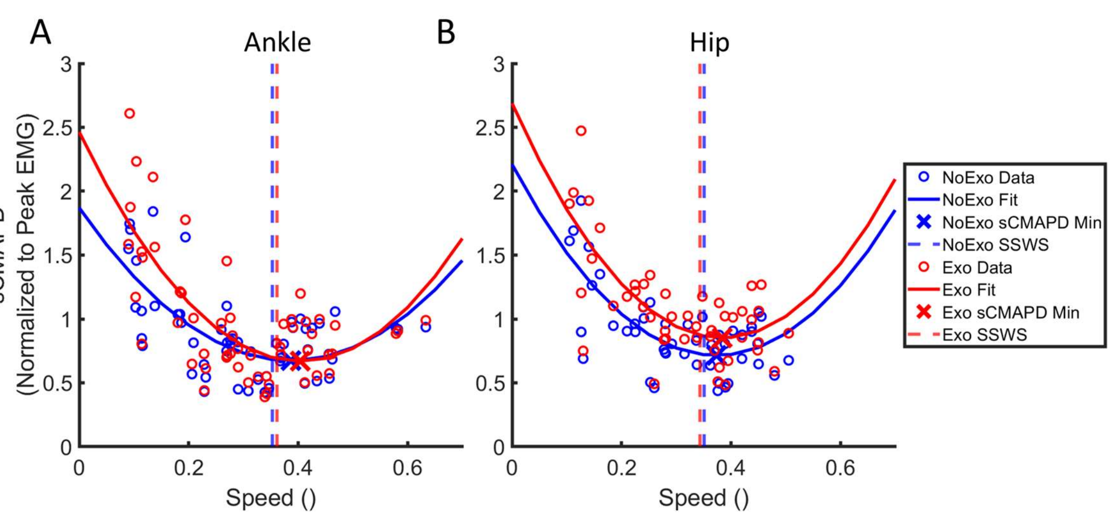

Figure 29 - Group summed CMAPD-Speed landscapes for ankle (A) and hip (B) exoskeletons. For each joint, we fit all subject data points for NoExo and Exo conditions with a quadratic curve and the minimum of that curve was calculated. For comparison, the average SSWS for each joint-condition pairing are also included. Speeds were nondimensionalized by dividing by the square root of the product of gravitational acceleration and height.

subjects (Figure 29A). Hip assistance trended to increase sCMAPD for all speeds (Figure 29B). When pooling minimum sCMAPD speed (minCMAPDspeed) and paired SSWS data for all subjects (young (Y) and old (O)) across target joints (ankle and hip) and exoskeleton conditions (Exo and NoExo) there was a significant ($p < 0.001$) correlation of 0.534 (Figure 30). Running separate linear regressions for the O and Y groups, each had a significant correlation (O: $p = 0.022$ and Y: $p = 0.001$) (Figure 31). MinCMAPDSpeed was more strongly correlated ($R^2 = 0.364$) with SSWS in the O group compared to the Y ($R^2 = 0.315$). Separating Exo and NoExo trials for each group, exo condition, and target joint, each had a significant correlation (Exo: $p<0.001$ and NoExo: $p<0.001$) (Figure 31).

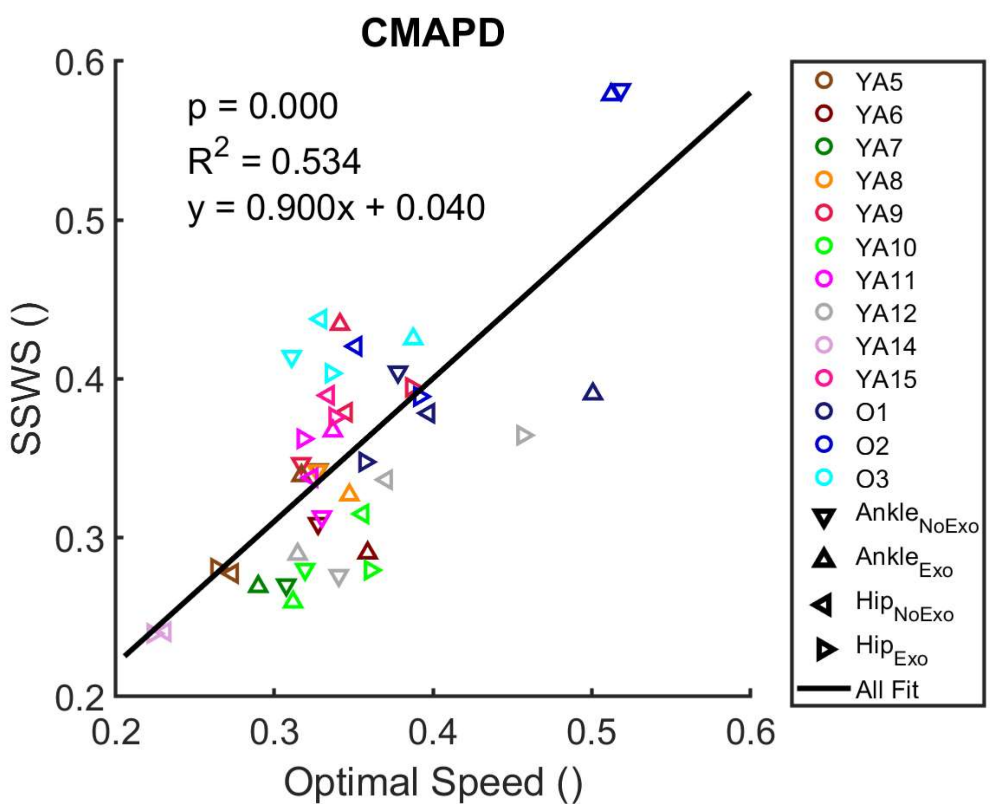

Figure 30 - Linear Regressions between the optimal speed to minimize summed CMAPD and SSWS, both nondimensionalized to account for changes in height. The overall linar regression is shown as a black line. Individual participants are shown in separate colors with older adults in shades of blue. The 4 conditions (Exo and NoExo for Ankle & Hip each) are shown with different marker shapes.

MinCMAPDSpeed was more strongly correlated (R^2 = 0.595) with SSWS in NoExo condition compared to Exo (R^2 = 0.498). When examining assistance at the Ankle and Hip with all subjects, minCMAPDSpeed and SSWS were significantly correlated for each target joint (Ankle: p = 0.006, Hip: p = 0.039) (Figure 31). Ankle assistance resulted in a larger correlation (R^2 = 0.539) than the Hip (R^2 = 0.362).

5.3.3 Comparing SSWS estimation between COT and sCMAPD

For the complete dataset of all subjects (young (Y) and old (O)) across target joints (ankle and hip) and exoskeleton conditions (Exo and NoExo), minimum speed for COT was more associated with SSWS (R^2 = 0.662) than the minimum speed for sCMAPD (R^2 = 0.534)

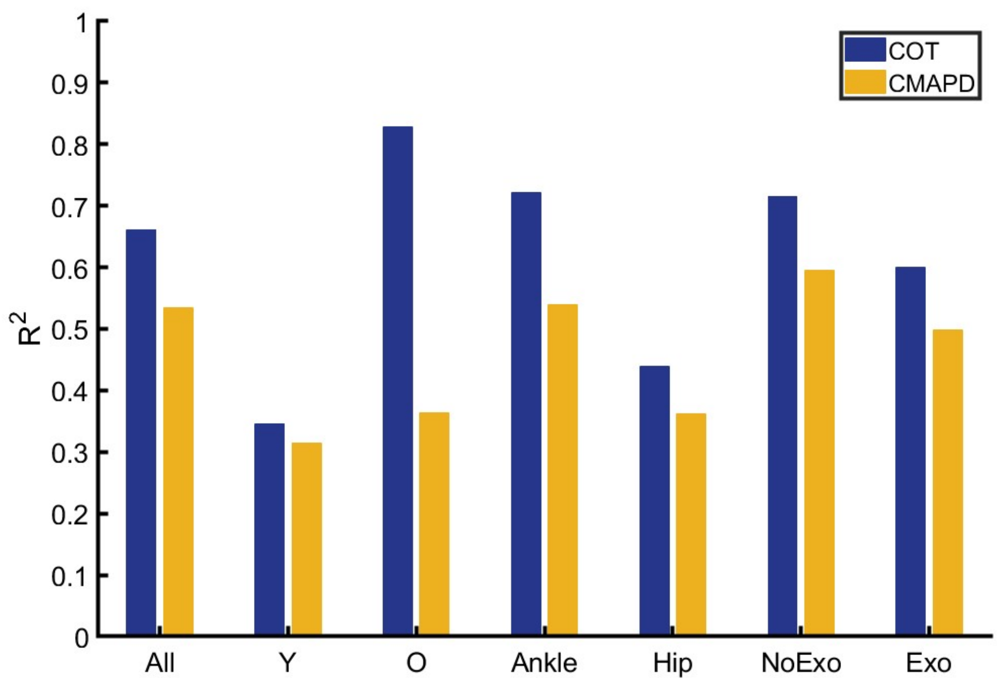

Figure 31 - Pearson correlation coefficients for statistically significant ($p < 0.05$) context linear regressions. Comparisons between the correlations for cost of transport (COT) and summed cumulative muscle activation per distance (sCMAPD) were made for the entire dataset (ALL). Young adults (Y), Older adults (O), Ankle target joint, Hip target joint, walking without an exoskeleton (NoExo, and walking with exoskeleton assistance (Exo)

(Figure 31). This trend repeated for all subsequent grouped analyses: Y, O, Ankle, Hip, NoExo, and Exo; See **Error! Reference source not found.** for details.

5.4 Discussion

In this study, we measured cost of transport, cumulative muscle activation, and self-selected walking speed across a broad set of contexts (age, exoskeleton assistance, and exo target joint) to determine if optimal COT or sCMAPD speeds would better predict SSWS. We hypothesized that (1) optimal sCMAPD speed would significantly correlate with SSWS and (2) optimal sCMAPD speeds would correlate more strongly with SSWS compared to COT in older adults. We found that SSWS does indeed significantly correlate with optimal CMAPD speeds across the entire data set ($p < 0.001$) and within each grouping (Old: $p = 0.022$, Young: $p = 0.001$, Exo: $p < 0.001$, NoExo: $p < 0.001$, Ankle: $p = 0.006$, Hip $p = 0.039$) (Figure 30 and **Error! Reference source not found.**). By employing our unique ability to shift the optimal speeds of COT and CMAPD across contexts, we were able to ascertain how each correlated with SSWS. Compared to CMAPD in older adults, COT optimal speed was more correlated with SSWS (COT: $R^2 = 0.828$, CMAPD: $R^2 = 0.364$) (Figure 31). This is in contrast to literature [3, 25, 35] suggesting older adults walked at a non-economical speed and used muscle loading to select walking speed. In fact, we found COT guided SSWS selection more than CMAPD across age and exo conditions. Nevertheless, CMAPD is still important to SSWS, and these data suggest focusing on lowering both COT and CMAPD at higher speeds would generate the highest benefit for device and therapeutic interventions.

It is more likely that humans optimize COT rather than sCMAPD when selecting walking speed, including older adults (Figure 31). While selecting gait parameters by optimizing for COT has been well established [3], there has been debate on whether this still holds for older adults and whether, instead, limb level measures of muscle activity/load are optimized by humans during gait selection [29, 154]. This is the first study providing evidence that older adults indeed select economical speeds in contrast to literature stating optimal COT speeds were unchanged with age while SSWS significantly changed [3, 25, 29]. This holds true across the contexts of wearable assistance as well (Figure 31). For both younger and older adults, SSWS was selected economically for walking with and without exo assistance. Across target joints, there was less correlation between COT and SSWS with hip assistance than ankle assistance suggesting that wearing the hip exo in this study may have affected the user's gait selection in ways beyond economy (Figure 31).

Wearable robotic devices are valuable tools to shift motor behavior and deepen our understanding of human gait. While energetic measures like COT strongly drive gait selection, they do not explain it completely and we would be naïve to say there are no other factors at play. In fact, in certain situations like acutely perturbed gait, energetic minimization is not evident [155]. Muscle loading factors seem to have more importance compared to COT in these situations and humans have been shown to trade off some energy efficiency for neuromuscular optimality [37]. This study has shown that neither energetics nor muscle loading completely explains changes in SSWS, suggesting we need to examine alternative measures.

This study was able to demonstrate humans optimize both COT and muscle activation while walking, and that older adults continue to select energetically economical speeds in a variety of situations including exoskeleton assistance at 2 different joints. That said, exoskeleton assistance did not change SSWS on average from walking without the exoskeleton for either target joint. Future studies should focus on the benefits of assistance versus the cost of wearing the exoskeleton unpowered. Larger differences in SSWS would increase the power of these analyses and provide a more precise look at what drives changes in walking speed. In this study, our physiological measurements were taken on the treadmill and SSWS was measured overground. We elected to use the overground SSWS as older adults were less comfortable walking on the treadmill, especially with the unknown speed changes of the self-pacing mode. This may have decreased the power of our regressions as differences between overground and treadmill SSWS are known. Future studies could spend more time habituating their older users to the treadmill and modifying their self-paced treadmill to ensure comfort and minimize walking time.

CHAPTER 6. CONCLUSION

6.1 Contributions of this work

In this work, we explored various exoskeleton (exo) control schemes across hip and ankle joints with multiple performance goals. We first examined the viability of neuromuscular model based (NMM) control at the ankle to provide metabolic benefits controller and how the controller affects user energetics, muscle activity, and biomechanics. We found the control scheme to be constrained mechanically, not being able to independently modulate average torque and net power, leading to a lack of metabolic benefit. However, this assistance at the ankle was able to reduce user ankle joint moment while simultaneously increasing total joint moment. Next, we implemented impedance control at the hip to determine how a semi-active device would need to modulate assistance across speeds based on optimal metabolic cost benefits. Impedance assistance trended toward increasing extension assistance with speed and was able to reduce metabolic cost at each speed compared to walking with the exo unpowered. Further, we found hip assistance benefitted user energy consumption by reducing muscle activity local to the exo. To increase translation of our work beyond the lab and with clinical populations, we implemented spline-based control schemes with autonomous ankle and hip exos and developed an overground human-in-the-loop protocol to maximize self-selected walking speed (SSWS) in younger and older adults. Due to the large amount of variability across subjects, we found no significant differences in SSWS across exo conditions (walking without the exo (NoExo), in the exo unpowered (NoPwr), with generic (GEN) or optimized (OPT) assistance) or target joints (ankle or hip). Insignificantly, the optimized assistance increased

SSWS beyond the NoPwr condition for both joints. By using powered exoskeletons to change SSWS, we were able to probe how younger and older adults optimally select their walking speed. Metabolic cost of transport (COT; energy consumed per unit distance) mainly dictates walking speed while lower limb muscle loading (cumulative muscle activity per unit distance (CMAPD)) plays a significant yet less substantial role. Each of the experiments detailed in this document contributed to increasing the effectiveness exoskeleton assistance during walking at different target joints, with different populations, and different performance goals through detailed examination of the physiological effects of assistance.

6.2 The importance of versatile exoskeleton control

Exoskeleton control schemes can start with an effective generic assistance strategy but must be uniquely tuned across real-world contexts (e.g., performance goals, clinical populations, individual differences, etc.) to be viable and accepted outside the lab. To do this, controllers need to be flexible and able to tune their mechanical outputs appropriately, Passive and some active control strategies, like the ankle NMM mentioned previously, are too constrained to modulate performance effectively. When optimizing assistance torque for different performance measures and tasks (like metabolic cost on the treadmill and overground SSWS), there are different average optimal profiles and thus different mechanical factors that associate with task benefit. Within the same task of maximizing overground SSWS, optimized assistance varied as well as the beneficial mechanical factors. Older adults displayed faster SSWS when walking with powered ankle assistance compared to hip assistance while younger adults walked faster than NoPwr with powered assistance at each joint. Further, younger adults benefitted more from assistance with higher peak power while older adults benefitted from higher impulse. Within each group at the hip joint, there were substantial variability in assistance profiles and while there were no significant SSWS differences from walking with the generic assistance, every user found individualized assistance to be more comfortable and preferred. Other studies using metabolic cost to tune assistance have also noted similar trends that individualization matters. Future exoskeleton studies need to keep this in mind and develop control strategies that are flexible enough to independently modulate mechanical properties of assistance. Further, starting with a generic, user-independent controller is a good starting point for beneficial assistance but ways to individualize assistance during real-world use continue to be necessary to provide the most benefit to their unique user based on the task and goal.

6.3 SSWS as an optimization outcome

As exoskeleton hardware is becoming more viable in real-world and clinical applications, a wider scope of performance measures must be investigated and compared to provide more effective assistance to users. Energetic measures like COT guide how younger and older adults select their walking speed and muscle activity/loading plays a significant part in how COT/SSWS is modulated. By using SSWS as an optimization goal, exo assistance is tuned based on user preference, COT, and muscle loading simultaneously. Furthermore, SSWS can be measured simply, without expensive equipment, in virtually any setting making it a viable measure for exo tuning outside the lab. In this work, we were able to employ SSWS as an optimization goal in older adults. Through this work, we provide preliminary data supporting that ankle assistance given by a light and aesthetically pleasing exo may be more readily accepted by older adults than hip assistance from a heavier, experimental exo. Exo powered SSWS outcomes were clearly influenced by non-physiological effects having to do with the exo beyond mechanical assistance, which has not been studied. Exo assistance can also be used to casually perturb walking to provide insight on walking physiology and motor control. By comparing changes in energetics and muscle activity from hip and ankle assistance we can determine how changes at the joint level can affect walking performance and guide future interventions (i.e., focusing on the joint of disability or the compensating joint). It is important for the exo field to continue investigating SSWS as a performance outcome across target joints to better understand the physiological and psychological effects of this assistance on the user.

6.4 Future directions for exoskeleton design

The exoskeleton field must have a bigger focus on user acceptance and translation outside the lab and examine this through more direct comparison studies. Over the past 10 years, exoskeleton assistance has been successful at providing energetic benefits within the lab but these results are still rarely tested in real-world settings. Few studies have tested exoskeleton systems outside the lab let alone of the treadmill, Treadmill optimized exoskeleton torque profiles need to be tested outside the lab to see if the metabolic benefits translate to real world settings where users will not be limited to a specific speeds or gait kinematics. To do this, autonomous exoskeleton designs need to be improved to be more lightweight with lower form factors and increased ease of use. This would mainly be through mechanical hardware design, but additional computational hardware and control algorithm safety must also be explored. Machine learning provides the opportunity for adaptive, optimal control across the various locomotion modes seen in daily life. While high accuracy classifiers are available, the risk of misclassification is still likely due to the number of classifications that would be made daily. Machine learning based controllers need implementations that safely provide assistance when misclassifications occur. Alternatively, analytical algorithms like spline, or impedance-based controllers may not provide as much possible benefit but reduce risk due to their continuous nature. Direct comparison between data-driven and analytical controllers must be made. Once we realized an exoskeleton system that can be tested in the real-world, longitudinal testing can occur with performance outcomes and user preference evaluations. As exos become more commercially available, it is more evident that performance enhancement is not enough to drive user acceptance. Other factors such as thermal comfort, assistance predictability, form factor, etc., are the bottleneck that is blocking wearable devices from being used and more projects being funded. More research on what factors matter to user acceptance across tasks, joints, and populations needs to be done to release this bottleneck. Exoskeletons have the potential to provide significant locomotor enhancement across professions and clinical populations but more work needs to focus on hardware design and user acceptance before the true benefits of exoskeletons are realized.

APPENDIX A.CHAPTER 2 SUPPLEMENT

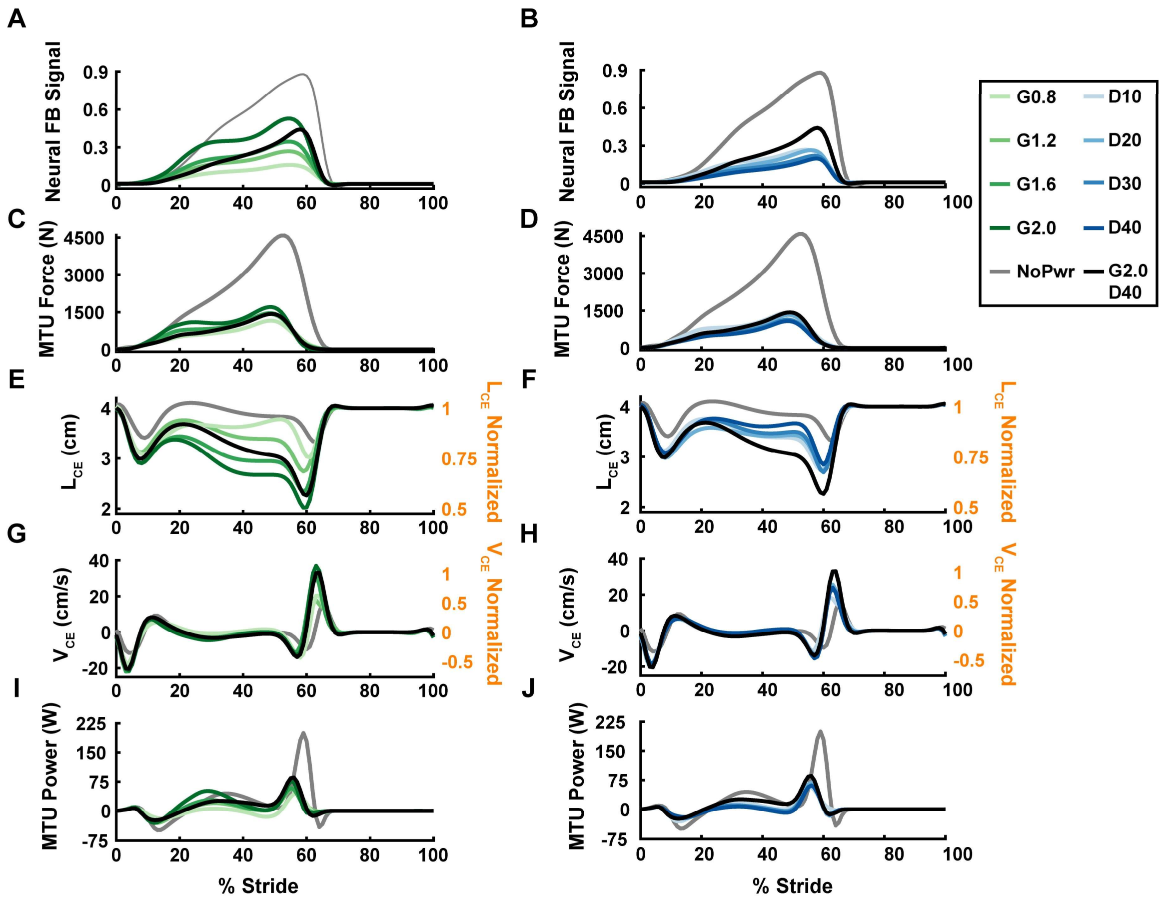

Figure 32 - Neuromuscular model (NMM) muscle-tendon (MT) dynamics over a stride cycle. Records of the input and output signals to and from the ankle exoskeleton neuromuscular model controller (Figure 2). The neural feedback (FB) signal for activating the Hill-type muscle (A and B), the output force generated by the virtual muscle-tendon unit (MTU) (C and D), the length (LCE) [with right axis normalized to the muscle optimal length] (E and F) and velocity (VCE) [with right axis normalized to the maximum muscle velocity (shortening is negative)] (G and H) of the virtual muscle contractile element (CE) and the mechanical power generated by the virtual MTU (I and J). All data were first averaged across many strides per participant and then across all participants (N=9) per condition. Records across Gain conditions can be seen on the left (A, C, E, G, I) and across Delay conditions on the right (B, D, F, H, J). Conditions are abbreviated and color coded as follows: NMM reflex Gains of 0.8, 1.2, 1.6, and 2.0 all with reflex Delay = 10ms (G0.8, G1.2, G1.6, and G2.0, respectively) (green), NMM reflex Delays of 10, 20, 30, and 40ms all with a reflex Gain = 1.2 (D10, D20, D30, D40, respectively) (blue), and a high-Gain-high-Delay condition (G2.0 D40) (black).

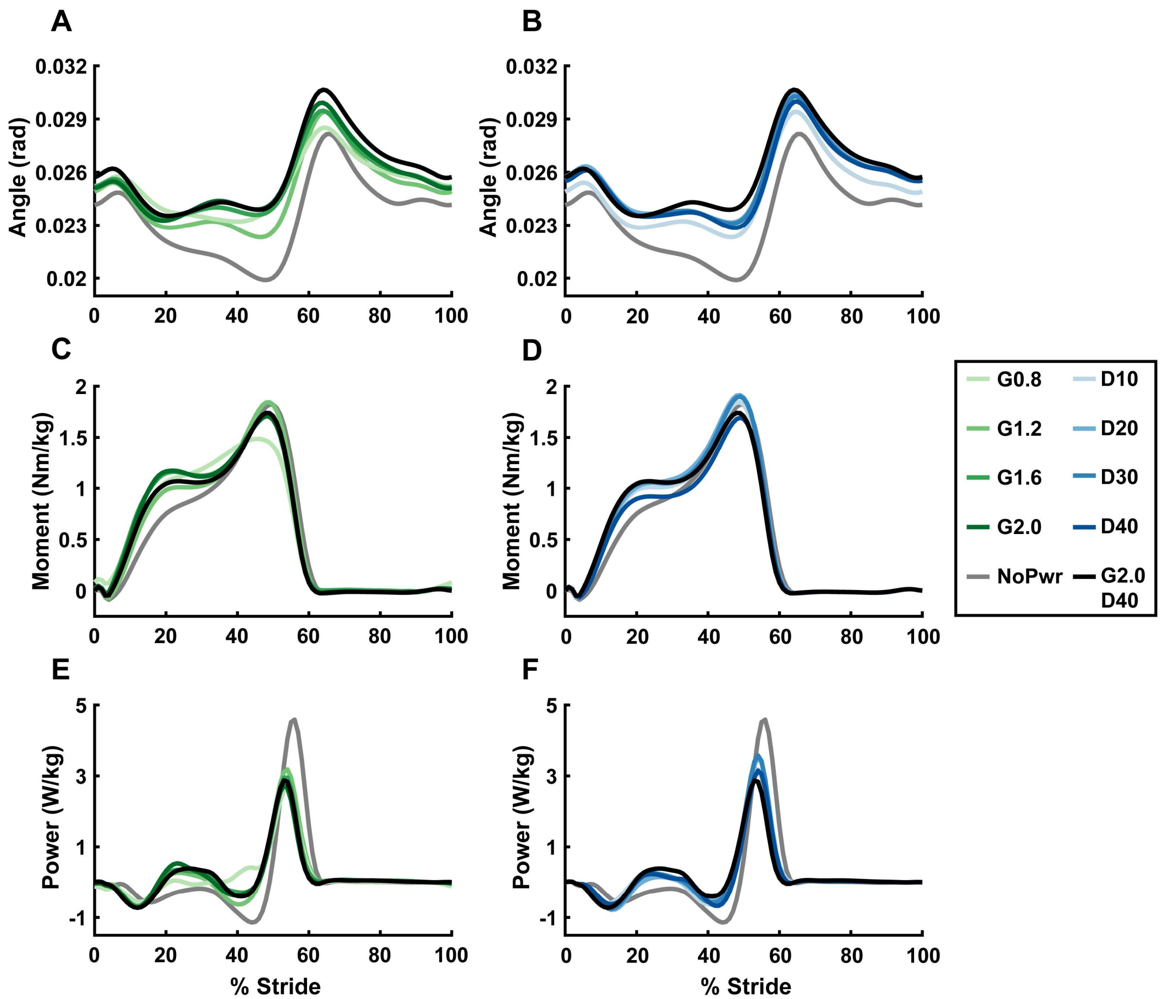

Figure 33 - Users' total (bio + exo) ankle kinematics and kinetics over a stride cycle. Measurements of users' ankle angle (A and B), total ankle moment (C and D), and total ankle power (E and F) over a stride from heel strike (0%) to heel strike (100%) of the same leg are shown. Ankle plantarflexion is depicted as positive and dorsiflexion as negative for the angle and moment plots. All data were first averaged across many strides per participant and then across all participants (N=9) per condition. Time-series data across Gain conditions can be seen on the left (A, C, and E) and across Delay conditions on the right (B, D, and F). Conditions are abbreviated and color coded as follows: unpowered (NoPwr)(gray), NMM reflex Gains of 0.8, 1.2, 1.6, and 2.0 all with reflex Delay=10ms (G0.8, G1.2, G1.6, and G2.0, respectively) (green), NMM reflex Delays of 10, 20, 30, and 40ms all with a reflex Gain=1.2 (D10, D20, D30, D40, respectively) (blue), and a high-Gain-high-Delay condition (G2.0 D40) (black).

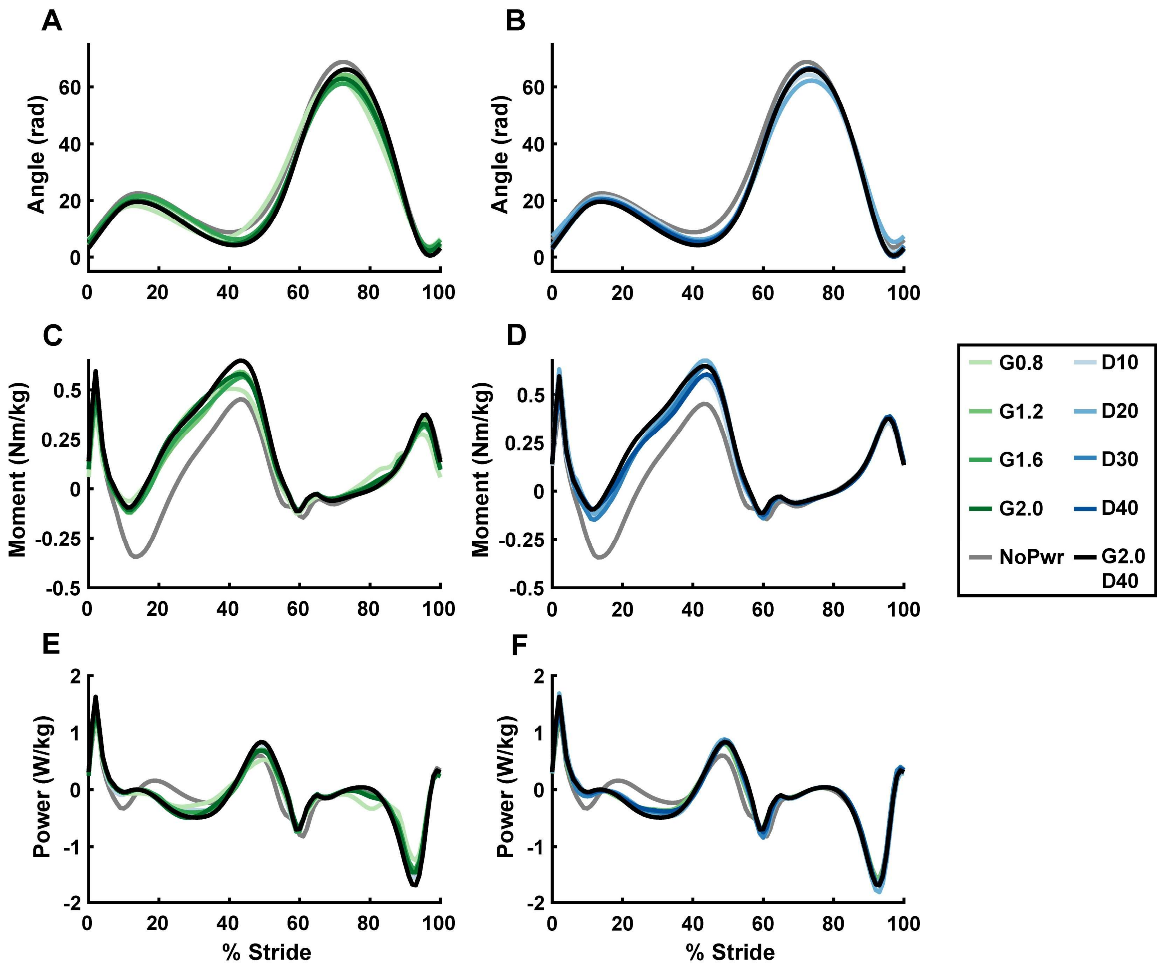

Figure 34 - Users' knee kinematics and kinetics over a stride cycle. Measurements of users' knee angle (A and B), knee moment (C and D), and knee power (E and F) over a stride from heel strike (0%) to heel strike (100%) of the same leg are shown. Knee flexion is depicted as positive and extension as negative for the angle and moment plots. All data were first averaged across many strides per participant and then across all participants (N=9) per condition. Time-series data across Gain conditions can be seen on the left (A, C, and E) and across Delay conditions on the right (B, D, and F). Conditions are abbreviated and color coded as follows: unpowered (NoPwr)(gray), NMM reflex Gains of 0.8, 1.2, 1.6, and 2.0 all with reflex Delay=10 ms (G0.8, G1.2, G1.6, and G2.0, respectively) (green), NMM reflex Delays of 10, 20, 30, and 40 ms all with a reflex Gain=1.2 (D10, D20, D30, D40, respectively) (blue), and a high-Gain-high-Delay condition (G2.0 D40) (black).

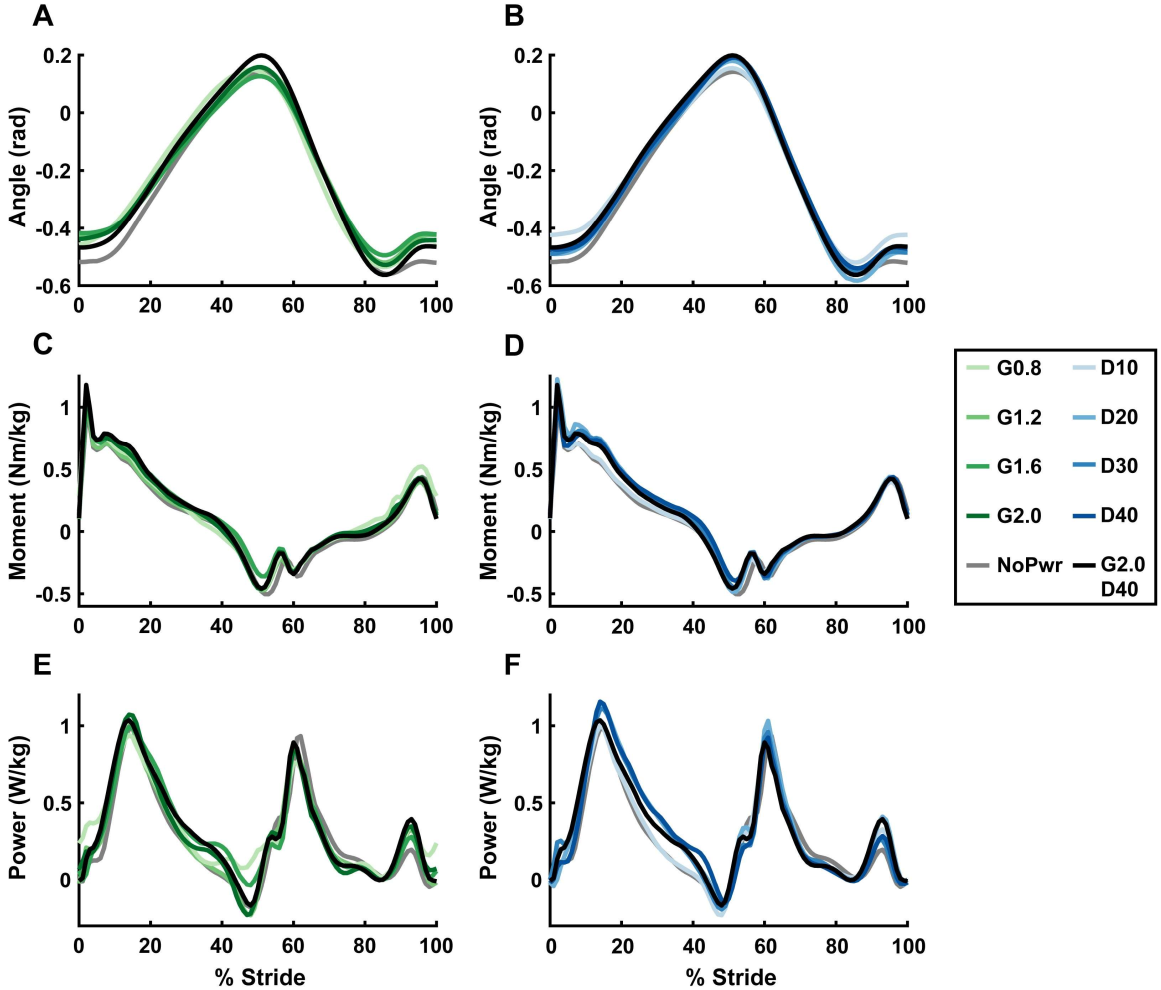

Figure 35 - Users' hip kinematics and kinetics over a stride cycle. Measurements of users' hip angle (A and B), hip moment (C and D), and hip power (E and F) over a stride from heel strike (0%) to heel strike (100%) of the same leg are shown. Hip flexion is depicted as negative and extension as positive for the angle and moment plots. All data were first averaged across many strides per participant and then across all participants (N=9) per condition. Time-series data across Gain conditions can be seen on the left (A, C, and E) and across Delay conditions on the right (B, D, and F). Conditions are abbreviated and color coded as follows: unpowered (NoPwr) (gray), NMM reflex Gains of 0.8, 1.2, 1.6, and 2.0 all with reflex Delay=10 ms (G0.8, G1.2, G1.6, and G2.0, respectively) (green), NMM reflex Delays of 10, 20, 30, and 40 ms all with a reflex Gain=1.2 (D10, D20, D30, D40, respectively) (blue), and a high-Gain-high-Delay condition (G2.0 D40) (black).

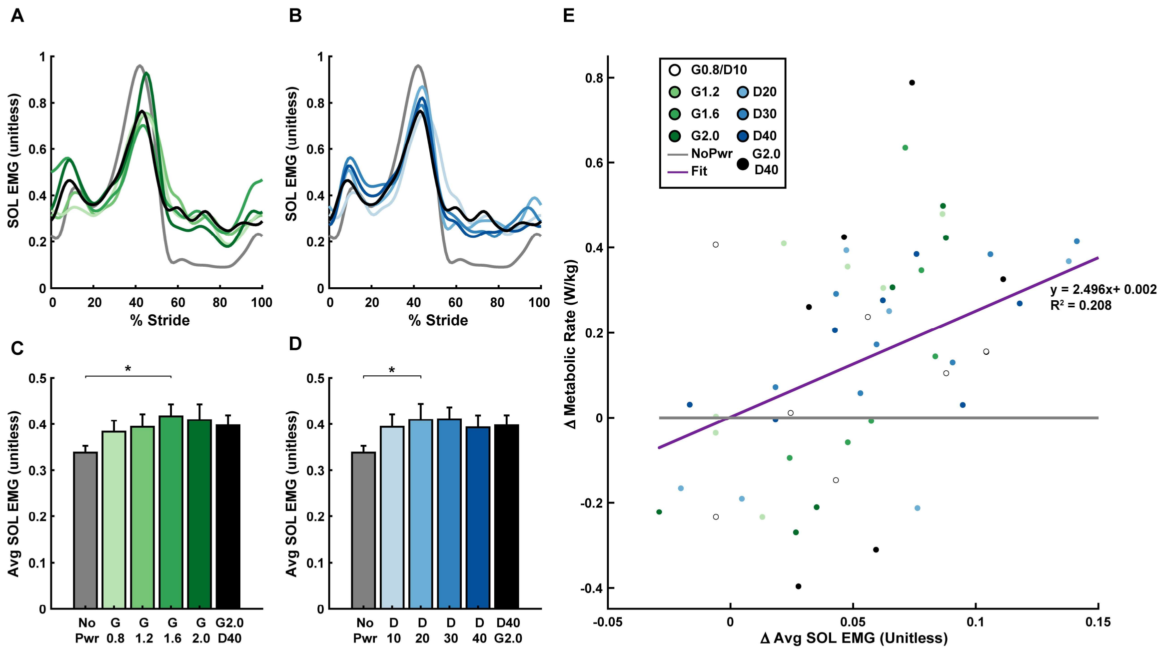

Figure 36 - Measurements of users' normalized soleus (SOL) electromyography (EMG) over a stride from heel strike (0%) to heel strike (100%) of the same leg are shown (A, B). Bar graphs are averages of the normalized SOL EMG signal over the stride (C and D). All measurements are averages across the study participants (N=9) in each condition with varying neuromuscular model (NMM) controller reflex Gain (green) in left panel (A, C) and Delay (blue) in the right panel (B, D). Linear regression between the change in metabolic rate versus the change in average SOL EMG with respect to the unpowered (NoPwr) condition (E). * denotes pairwise significant difference of $p < .05$. R2 value is denoted with a "~" if the linear regression was not statistically significant. Conditions are abbreviated and color coded as follows: unpowered (NoPwr) (gray), NMM reflex Gains of 0.8, 1.2, 1.6, and 2.0 all with reflex Delay=10 ms (G0.8, G1.2, G1.6, and G2.0, respectively) (green), NMM reflex Delays of 10, 20, 30, and 40 ms all with a reflex Gain=1.2 (D10, D20, D30, D40, respectively) (blue), and a high-Gain-high-Delay condition (G2.0 D40) (black).

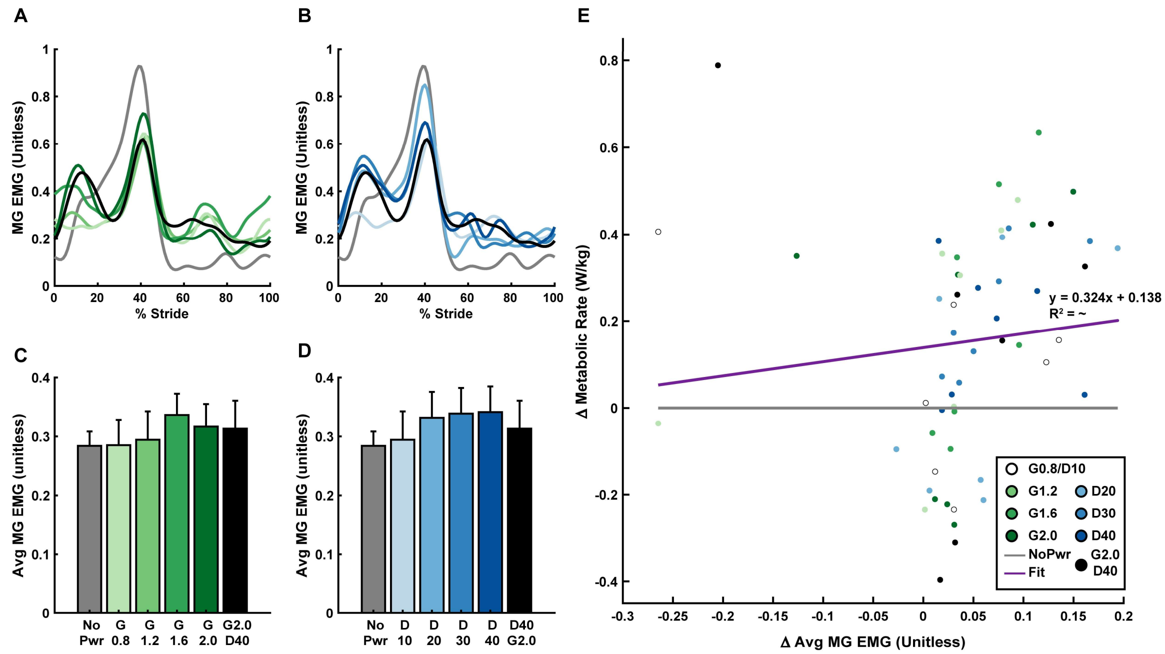

Figure 37 - Measurements of users' normalized medial gastrocnemius (MG) electromyography (EMG) over a stride from heel strike (0%) to heel strike (100%) of the same leg are shown (A, B). Bar graphs are averages of the normalized MG EMG signal over the stride (C and D). All measurements are averages across the study participants (N=9) in each condition with varying neuromuscular model (NMM) controller reflex Gain (green) in left panel (A, C) and Delay (blue) in the right panel (B, D). Linear regression between the change in metabolic rate versus the change in average SOL EMG with respect to the unpowered (NoPwr) condition (E). * denotes pairwise significant difference of p < .05. R2 value is denoted with a "~" if the linear regression was not statistically significant. Conditions are abbreviated and color coded as follows: unpowered (NoPwr) (gray), NMM reflex Gains of 0.8, 1.2, 1.6, and 2.0 all with reflex Delay=10 ms (G0.8, G1.2, G1.6, and G2.0, respectively) (green), NMM reflex Delays of 10, 20, 30, and 40 ms all with a reflex Gain=1.2 (D10, D20, D30, D40, respectively) (blue), and a high-Gain-high-Delay condition (G2.0 D40) (black).

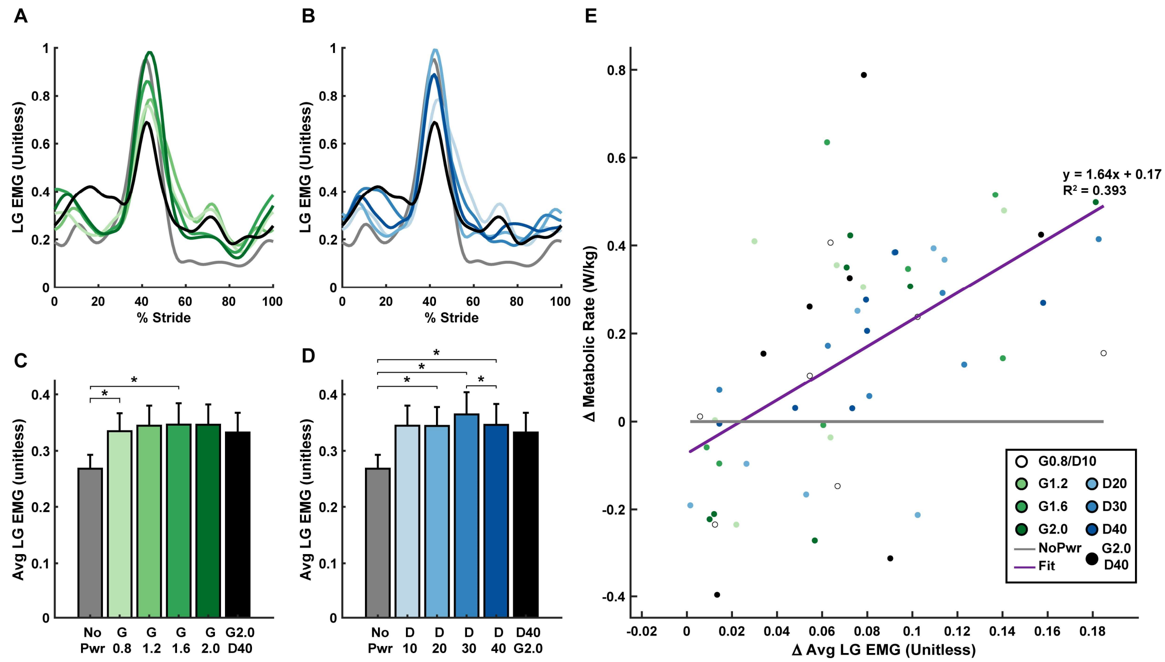

Figure 38 - Measurements of users' normalized lateral gastrocnemius (LG) electromyography (EMG) over a stride from heel strike (0%) to heel strike (100%) of the same leg are shown (A, B). Bar graphs are averages of the normalized LG EMG signal over the stride (C and D). All measurements are averages across the study participants (N=9) in each condition with varying neuromuscular model (NMM) controller reflex Gain (green) in left panel (A, C) and Delay (blue) in the right panel (B, D). Linear regression between the change in metabolic rate versus the change in average LG EMG with respect to the unpowered (NoPwr) condition (E). * denotes pairwise significant difference of p < .05. R2 value is denoted with a "~" if the linear regression was not statistically significant. Conditions are abbreviated and color coded as follows: unpowered (NoPwr) (gray), NMM reflex Gains of 0.8, 1.2, 1.6, and 2.0 all with reflex Delay=10ms (G0.8, G1.2, G1.6, and G2.0, respectively) (green), NMM reflex Delays of 10, 20, 30, and 40ms all with a reflex Gain=1.2 (D10, D20, D30, D40, respectively) (blue), and a high-Gain-high-Delay condition (G2.0 D40) (black).

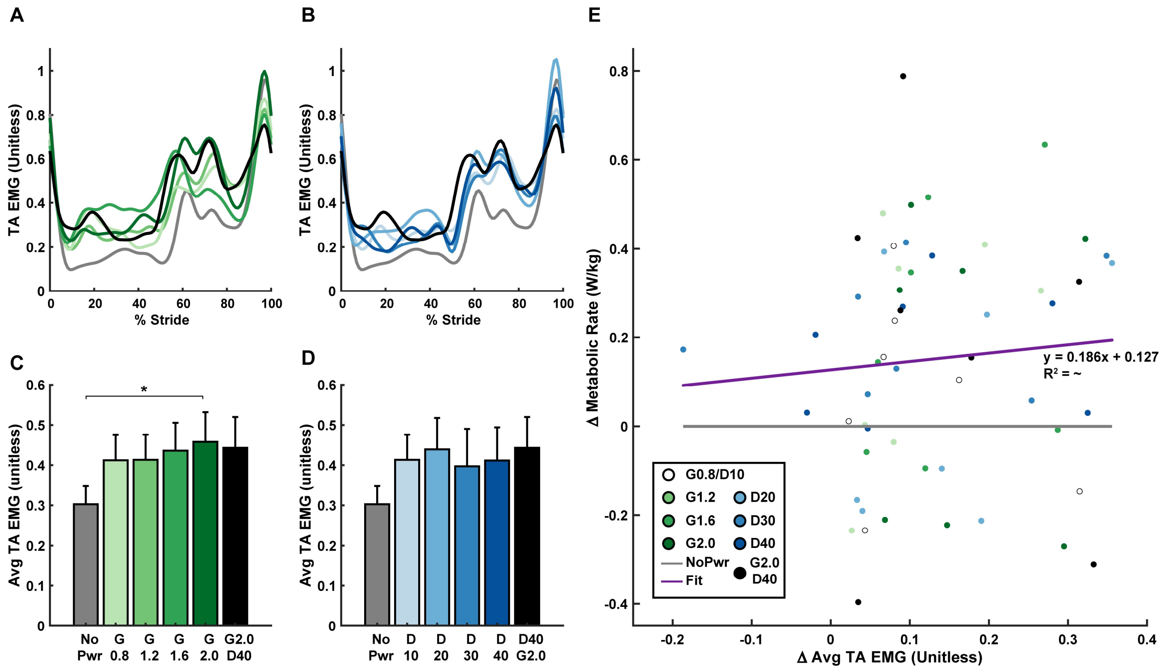

Figure 39 - Users' tibialis anterior muscle activity. Measurements of users' normalized tibialis anterior (TA) electromyography (EMG) over a stride from heel strike (0%) to heel strike (100%) of the same leg are shown (A, B). Bar graphs are averages of the normalized TA EMG signal over the stride (C and D). All measurements are averages across the study participants (N=9) in each condition with varying neuromuscular model (NMM) controller reflex Gain (green) in left panel (A, C) and Delay (blue) in the right panel (B, D). Linear regression between the change in metabolic rate versus the change in average TA EMG with respect to the unpowered (NoPwr) condition (E). * denotes pairwise significant difference of $p < .05$. R^2 value is denoted with a "~" if the linear regression was not statistically significant. Conditions are abbreviated and color coded as follows: unpowered (NoPwr) (gray), NMM reflex Gains of 0.8, 1.2, 1.6, and 2.0 all with reflex Delay=10 ms (G0.8, G1.2, G1.6, and G2.0, respectively) (green), NMM reflex Delays of 10, 20, 30, and 40 ms all with a reflex Gain=1.2 (D10, D20, D30, D40, respectively) (blue), and a high-Gain-high-Delay condition (G2.0 D40) (black).

APPENDIX B. CHAPTER 3 SUPPLEMENT

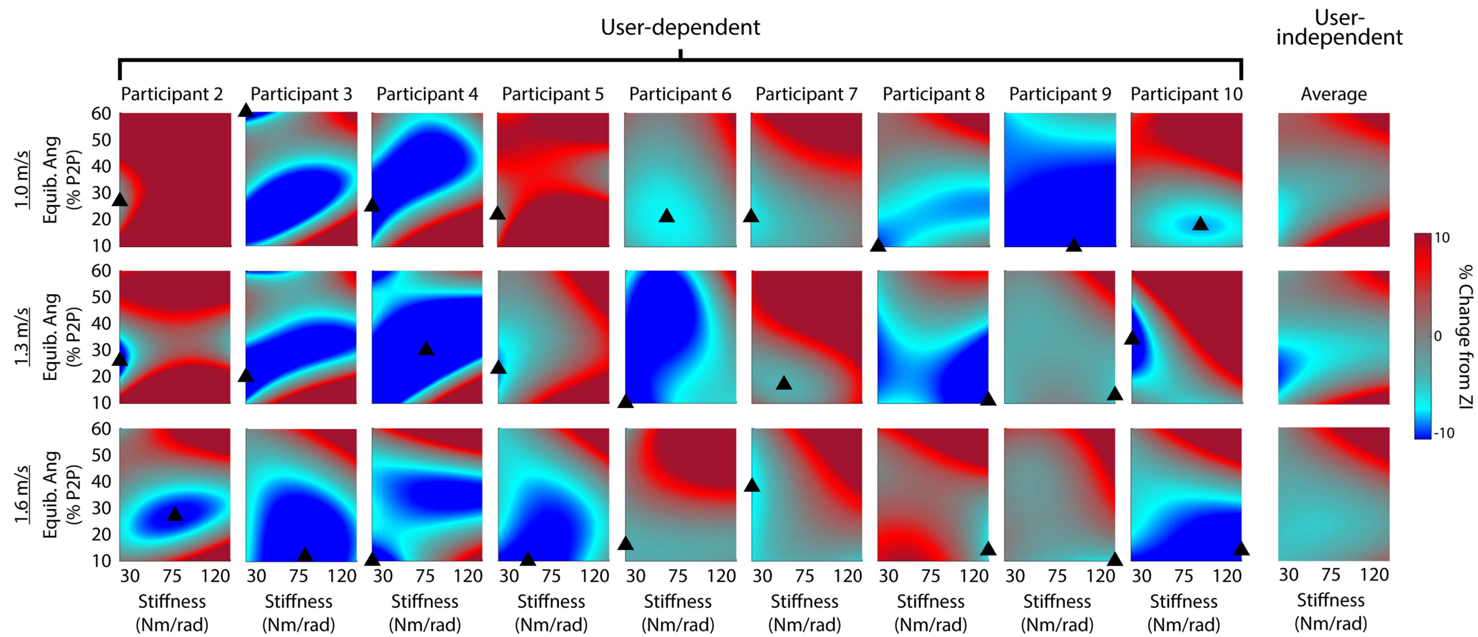

Figure 40 - Changes in metabolic cost across hip exoskeleton impedance parameter space (k-θ_0): Multidimensional polynomial fits to sampled percentage change from the zero impedance (ZI) condition (red= increase; blue= decrease) for each exoskeleton impedance parameter setting (a 5x6 stiffness (k) vs. equilibrium angle (θ_0) grid space) at each walking speed (1.0 m/s (top row), 1.3 m/s, 1.6 m/s (bottom row)). Columns represent different participants with the last column representing the across subject average at each speed (user-independent; Same as Figure 12 Right Column). In general, a semi-active hip impedance controller with low stiffness and equilibrium angle working at an intermediate walking speed had the most benefit while high stiffness and equilibrium angle had the least benefit. In contrast, there is substantial variation between participants, many of which gain maximum benefit from higher torques (Participants 8-10).

APPENDIX C.CHAPTER 4 SUPPLEMENT

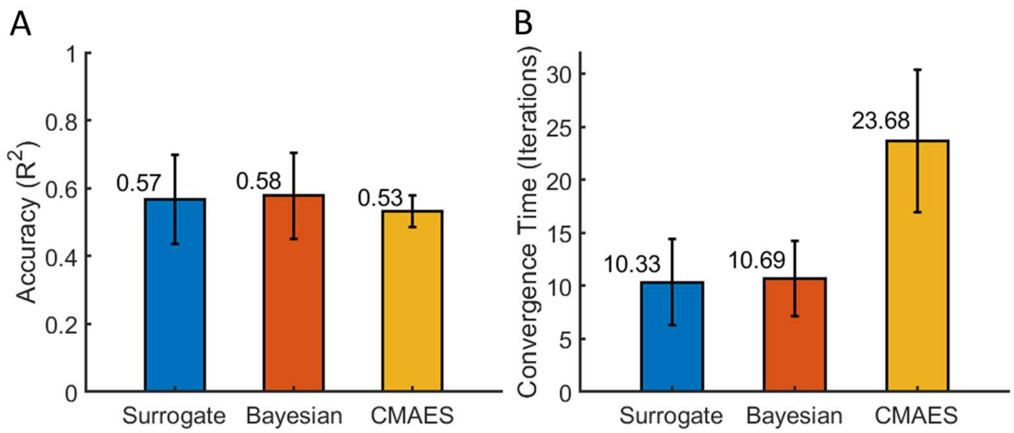

Figure 41 - Human-in-the-loop optimization algorithm offline comparison results (average +/- standard error). Accuracy (A) and convergence time (B) performance between Surrogate Bayesian Optimization (Surrogate), Traditional Bayesian Optimization (Bayesian), and Covariance Matrix Adaptation Evolution Strategy (CMAES) algorithms. The task was to tune 8 parameters of a neuromuscular model and maximize linear correlation (R^2) between the model torque and inverse dynamic generated torques for 5 subjects across 7 grades each within 30 iterations (comparable to 1 hour of 2-minute metabolic cost estimations) and repeated 5 times. Accuracy of each optimization was measured as the R^2 of the 30^{th} (final) iteration. Convergence time was considered the first iteration of a 3-iteration window that had predicted optimal parameter sets with R^2-values within +/-5% of the final iteration. Since CMAES only provides predicted optimal parameter sets after each generation (10 iterations or only 3 predicted optimal sets) the first set to be within 5% of the final was taken for convergence time. Final Accuracy (R^2) and Convergence Times were averaged across all grades and repeats then across all subjects for each algorithm.

REFERENCES

[1] L. J. Melton Iii, "Epidemiology of hip fractures implications of the exponential increase with age," *Bone,* vol. 18, no. 3, pp. S121-S125, 1996.

[2] A. M. Coimbra, N. A. Ricci, I. B. Coimbra, and L. T. Costallat, "Falls in the elderly of the Family Health Program," *Arch Gerontol Geriatr,* vol. 51, no. 3, pp. 317-22, Nov-Dec 2010, doi: 10.1016/j.archger.2010.01.010.

[3] P. E. Martin, D. E. ROTHSTEIN, and D. D. LARISH, "Effects of age and physical activity status on the speed-aerobic demand relationship of walking," *J. Appl. Physiol.,* vol. 72, no. 1, pp. 200-206, 1992.

[4] E. J. Bassey, M. J. Bendall, and M. Pearson, "Muscle strength in the triceps surae and objectively measured customary walking activity in men and women over 65 years of age," *Clin Sci (Lond),* vol. 74, no. 1, pp. 85–89, 1988, doi: https://doi.org/10.1042/cs0740085.

[5] J. Lim and J. Y. Lim, "Responsiveness of Gait Speed to Physical Exercise Interventions in At-risk Older Adults: A Systematic Review and Meta-Analysis," *Annals of Geriatric Medicine and Research,* vol. 21, no. 1, pp. 17-23, 2017, doi: 10.4235/agmr.2017.21.1.17.

[6] E. A. Awick, D. K. Ehlers, S. Aguinaga, A. M. Daugherty, A. F. Kramer, and E. McAuley, "Effects of a randomized exercise trial on physical activity, psychological distress and quality of life in older adults," *Gen Hosp Psychiatry,* vol. 49, pp. 44-50, Nov 2017, doi: 10.1016/j.genhosppsych.2017.06.005.

[7] D. H. Paterson, D. Govindasamy, M. Vidmar, D. A. Cunningham, and J. J. Koval, "Longitudinal study of determinants of dependence in an elderly population," *Journal of the American Geriatrics Society,* vol. 52, no. 10, pp. 1632-1638, 2004.

[8] S. Perera *et al.*, "Gait Speed Predicts Incident Disability: A Pooled Analysis," *J Gerontol A Biol Sci Med Sci,* vol. 71, no. 1, pp. 63-71, Jan 2016, doi: 10.1093/gerona/glv126.

[9] A. Aboutorabi, M. Arazpour, M. Bahramizadeh, S. W. Hutchins, and R. Fadayevatan, "The effect of aging on gait parameters in able-bodied older subjects: a literature review," *Aging Clin Exp Res,* vol. 28, no. 3, pp. 393-405, Jun 2016, doi: 10.1007/s40520-015-0420-6.

[10] L. Alcock, N. Vanicek, and T. D. O'Brien, "Alterations in gait speed and age do not fully explain the changes in gait mechanics associated with healthy older women," *Gait Posture,* vol. 37, no. 4, pp. 586-92, Apr 2013, doi: 10.1016/j.gaitpost.2012.09.023.

[11] D. J. Farris and G. S. Sawicki, "The mechanics and energetics of human walking and running: a joint level perspective," *J R Soc Interface,* vol. 9, no. 66, pp. 110-8, Jan 7 2012, doi: 10.1098/rsif.2011.0182.

[12] K. A. Boyer, R. T. Johnson, J. J. Banks, C. Jewell, and J. F. Hafer, "Systematic review and meta-analysis of gait mechanics in young and older adults," *Exp Gerontol,* vol. 95, pp. 63-70, Sep 2017, doi: 10.1016/j.exger.2017.05.005.

[13] K. A. Conway and J. R. Franz, "Increasing the propulsive demands of walking to their maximum elucidates functionally limiting impairments in older adult gait," *Journal of aging and physical activity,* vol. 28, no. 1, pp. 1-8, 2020.

[14] P. DeVita and T. Hortobaryi, "Age causes a redistribution of joint torques and powers during gait," *Journal of Applied Physiology,* vol. 88, pp. 1804-1811, 2000.

[15] R. E. Pimentel, N. L. Pieper, W. H. Clark, and J. R. Franz, "Muscle Metabolic Energy Costs While Modifying Propulsive Force Generation During Walking," *bioRxiv,* 2020, doi: 10.1101/2020.07.31.230698.

[16] T. Delabastita, E. Hollville, A. Catteau, P. Cortvriendt, F. De Groote, and B. Vanwanseele, "Distal-to-proximal joint mechanics redistribution is a main contributor to reduced walking economy in older adults," *Scand J Med Sci Sports,* vol. 31, no. 5, pp. 1036-1047, May 2021, doi: 10.1111/sms.13929.

[17] G. S. Sawicki, O. N. Beck, I. Kang, and A. J. Young, "The exoskeleton expansion: improving walking and running economy," *J Neuroeng Rehabil,* vol. 17, no. 1, p. 25, Feb 19 2020, doi: 10.1186/s12984-020-00663-9.

[18] P. Slade, M. J. Kochenderfer, S. L. Delp, and S. H. Collins, "Personalizing exoskeleton assistance while walking in the real world," *Nature,* vol. 610, no. 7931, pp. 277-282, 2022, doi: 10.1038/s41586-022-05191-1.

[19] P. W. Franks, G. M. Bryan, R. M. Martin, R. Reyes, A. C. Lakmazaheri, and S. H. Collins, "Comparing optimized exoskeleton assistance of the hip, knee, and ankle in single and multi-joint configurations," *Wearable Technologies,* vol. 2, p. e16, 2021, doi: https://doi.org/10.1017/wtc.2021.14.

[20] B. A. Shafer, S. A. Philius, R. W. Nuckols, J. McCall, A. J. Young, and G. S. Sawicki, "Neuromechanics and Energetics of Walking With an Ankle Exoskeleton Using Neuromuscular-Model Based Control: A Parameter Study," *Front Bioeng Biotechnol,* vol. 9, p. 615358, 2021, doi: 10.3389/fbioe.2021.615358.

[21] J. A. Norris, K. P. Granata, M. R. Mitros, E. M. Byrne, and A. P. Marsh, "Effect of augmented plantarflexion power on preferred walking speed and economy in young and older adults," *Gait Posture,* vol. 25, no. 4, pp. 620-7, Apr 2007, doi: 10.1016/j.gaitpost.2006.07.002.

[22] R. C. Browning, J. R. Modica, R. Kram, and A. Goswami, "The effects of adding mass to the legs on the energetics and biomechanics of walking," *Med Sci Sports Exerc,* vol. 39, no. 3, pp. 515-25, Mar 2007, doi: 10.1249/mss.0b013e31802b3562.

[23] F. A. Panizzolo, S. Cimino, E. Pettenello, A. Belfiore, N. Petrone, and G. Marcolin, "Effect of a passive hip exoskeleton on walking distance in neurological patients," *Assist Technol,* Jan 22 2021, doi: 10.1080/10400435.2021.1880494.

[24] D. S. Peterson and P. E. Martin, "Effects of age and walking speed on coactivation and cost of walking in healthy adults," *Gait Posture,* vol. 31, no. 3, pp. 355-9, Mar 2010, doi: 10.1016/j.gaitpost.2009.12.005.

[25] D. Malatesta *et al.*, "Energy cost of walking and gait instability in healthy 65- and 80-yr-olds," *J Appl Physiol,* vol. 95, pp. 2248-2256, 2003.

[26] D. Malatesta, D. Simar, H. Ben Saad, C. Prefaut, and C. Caillaud, "Effect of an overground walking training on gait performance in healthy 65- to 80-year-olds," *Exp Gerontol,* vol. 45, no. 6, pp. 427-34, Jun 2010, doi: 10.1016/j.exger.2010.03.009.

[27] J. D. Ortega, L. A. Fehlman, and C. T. Farley, "Effects of aging and arm swing on the metabolic cost of stability in human walking," *J Biomech,* vol. 41, no. 16, pp. 3303-8, Dec 5 2008, doi: 10.1016/j.jbiomech.2008.06.039.

[28] J. D. Ortega and C. T. Farley, "Individual limb work does not explain the greater metabolic cost of walking in elderly adults," *J Appl Physiol,* vol. 102, no. 6, pp. 2266-73, Jun 2007, doi: 10.1152/japplphysiol.00583.2006.

[29] S. Song and H. Geyer, "Predictive neuromechanical simulations indicate why walking performance declines with ageing," *J Physiol,* vol. 596, no. 7, pp. 1199-1210, Apr 1 2018, doi: 10.1113/JP275166.

[30] V. Monaco and S. Micera, "Age-related neuromuscular adaptation does not affect the mechanical efficiency of lower limbs during walking," *Gait Posture,* vol. 36, no. 3, pp. 350-5, Jul 2012, doi: 10.1016/j.gaitpost.2012.03.031.

[31] O. S. Mian, J. M. Thom, L. P. Ardigo, M. V. Narici, and A. E. Minetti, "Metabolic cost, mechanical work, and efficiency during walking in young and older men," *Acta Physiol (Oxf),* vol. 186, no. 2, pp. 127-39, Feb 2006, doi: 10.1111/j.1748-1716.2006.01522.x.

[32] M. G. Browne and J. R. Franz, "More push from your push-off: Joint-level modifications to modulate propulsive forces in old age," *PLoS One,* vol. 13, no. 8, p. e0201407, 2018, doi: 10.1371/journal.pone.0201407.

[33] T. Krasovsky, A. Lamontagne, A. G. Feldman, and M. F. Levin, "Effects of walking speed on gait stability and interlimb coordination in younger and older

adults," *Gait Posture,* vol. 39, no. 1, pp. 378-85, 2014, doi: 10.1016/j.gaitpost.2013.08.011.

[34] S. Song, H. Choi, and S. H. Collins, "Using force data to self-pace an instrumented treadmill and measure self-selected walking speed," *J Neuroeng Rehabil,* vol. 17, no. 1, p. 68, Jun 3 2020, doi: 10.1186/s12984-020-00683-5.

[35] J. M. VanSwearingen and S. A. Studenski, "Aging, motor skill, and the energy cost of walking: implications for the prevention and treatment of mobility decline in older persons," *J Gerontol A Biol Sci Med Sci,* vol. 69, no. 11, pp. 1429-36, Nov 2014, doi: 10.1093/gerona/glu153.

[36] H. J. Ralston, "Energy-speed relation and optimal speed during level walking," *Internationale Zeitschrift für Angewandte Physiologie Einschliesslich Arbeitsphysiologie,* vol. 17, no. 4, pp. 277-283, 1958.

[37] K. A. McDonald, J. P. Cusumano, A. Hieronymi, and J. Rubenson, "Humans trade off whole-body energy cost to avoid overburdening muscles while walking," *Proc Biol Sci,* vol. 289, no. 1985, p. 20221189, Oct 26 2022, doi: 10.1098/rspb.2022.1189.

[38] S. Song and S. H. Collins, "Optimizing Exoskeleton Assistance for Faster Self-Selected Walking," *IEEE transactions on neural systems and rehabilitation engineering : a publication of the IEEE Engineering in Medicine and Biology Society,* vol. 29, pp. 786-795, 2021, doi: 10.1109/TNSRE.2021.3074154.

[39] Y. Ding, M. Kim, S. Kuindersma, and C. J. Walsh, "Human-in-the-loop optimization of hip assistance with a soft exosuit during walking," *Science Robotics,* vol. 3, no. 15, pp. 1-9, 2018.

[40] M. Kim *et al.*, "Human-in-the-loop Bayesian optimization of wearable device parameters," *PLoS ONE,* vol. 12, no. 9, pp. 6-8, 2017, doi: 10.1371/journal.pone.0184054.

[41] J. Zhang *et al.*, "Human-in-the-loop optimization of exoskeleton assistance during walking," *Science,* vol. 356, pp. 1280-1283, 2017, doi: 10.1126/science.aal5054.

[42] M. Kim *et al.*, "Bayesian optimization of soft exosuits using a metabolic estimator stopping process," *Proceedings - IEEE International Conference on Robotics and Automation,* pp. 9173-9179, 2019.

[43] K. L. Poggensee and S. H. Collins, "How adaptation, training, and customization contribute to benefits from exoskeleton assistance," *Sci Robot,* vol. 6, no. 58, p. eabf1078, Sep 29 2021, doi: 10.1126/scirobotics.abf1078.

[44] B. A. Shafer, J. C. Powell, A. J. Young, and G. S. Sawicki, "Emulator-based Optimization of a Semi-Active Hip Exoskeleton Concept: Sweeping Impedance

Across Walking Speeds," *IEEE Transactions on Biomedical Engineering,* 2022, doi: 10.1109/TBME.2022.3188482.

[45] H. G. Kang and J. B. Dingwell, "Dynamics and stability of muscle activations during walking in healthy young and older adults," *J Biomech,* vol. 42, no. 14, pp. 2231-7, Oct 16 2009, doi: 10.1016/j.jbiomech.2009.06.038.

[46] T. M. Owings and M. D. Grabiner, "Step width variability, but not step length variability or step time variability, discriminates gait of healthy young and older adults during treadmill locomotion," *J Biomech,* vol. 37, no. 6, pp. 935-8, Jun 2004, doi: 10.1016/j.jbiomech.2003.11.012.

[47] B. A. Eldadah, "Fatigue and fatigability in older adults," *PM R,* vol. 2, no. 5, pp. 406-13, May 2010, doi: 10.1016/j.pmrj.2010.03.022.

[48] W. Felt, J. C. Selinger, J. M. Donelan, and C. D. Remy, ""Body-In-The-Loop": Optimizing Device Parameters Using Measures of Instantaneous Energetic Cost," *PLoS One,* vol. 10, no. 8, p. e0135342, 2015, doi: 10.1371/journal.pone.0135342.

[49] D. J. Farris and G. S. Sawicki, "The mechanics and energetics of human walking and running," *Journal of the Royal Society Interface,* vol. 9, pp. 110-118, 2012, doi: 10.1098/rsif.2011.0182.

[50] G. S. Sawicki and D. P. Ferris, "Mechanics and energetics of level walking with powered ankle exoskeletons," *The Journal of experimental biology,* vol. 211, no. Pt 9, pp. 1402-13, May 2008, doi: 10.1242/jeb.009241.

[51] R. W. Jackson and S. H. Collins, "An experimental comparison of the relative benefits of work and torque assistance in ankle exoskeletons," *Journal of Applied Physiology,* vol. 119, pp. 541-557, 2015, doi: 10.1152/japplphysiol.01133.2014.

[52] P. Malcolm, W. Derave, S. Galle, and D. De Clercq, "A Simple Exoskeleton That Assists Plantarflexion Can Reduce the Metabolic Cost of Human Walking," *PLoS ONE,* vol. 8, pp. 1-7, 2013, doi: 10.1371/journal.pone.0056137.

[53] S. Galle, P. Malcolm, S. H. Collins, and D. De Clercq, "Reducing the metabolic cost of walking with an ankle exoskeleton: interaction between actuation timing and power," *J Neuroeng Rehabil,* vol. 14, no. 1, p. 35, Apr 27 2017, doi: 10.1186/s12984-017-0235-0.

[54] L. M. Mooney, E. J. Rouse, and H. M. Herr, "Autonomous exoskeleton reduces metabolic cost of human walking," *J Neuroeng Rehabil,* vol. 11, p. 151, Nov 3 2014, doi: 10.1186/1743-0003-11-151.

[55] M. Grimmer *et al.*, "Comparison of the human-exosuit interaction using ankle moment and ankle positive power inspired walking assistance," *J Biomech,* vol. 83, pp. 76-84, Jan 23 2019, doi: 10.1016/j.jbiomech.2018.11.023.

[56] S. M. Cain, K. E. Gordon, and D. P. Ferris, "Locomotor adaptation to a powered ankle-foot orthosis depends on control method," *J Neuroeng Rehabil,* vol. 4, p. 48, Dec 21 2007, doi: 10.1186/1743-0003-4-48.

[57] J. R. Koller, C. David Remy, and D. P. Ferris, "Comparing neural control and mechanically intrinsic control of powered ankle exoskeletons," *IEEE ... International Conference on Rehabilitation Robotics : [proceedings],* vol. 2017, pp. 294-299, Jul 2017, doi: 10.1109/ICORR.2017.8009262.

[58] W. Kirby, "Design, Characterization, and Implementation of Lower-Limb Exoskeletons for Performance Augmentation During Walking and Running," 2018. [Online]. Available: https://kilthub.cmu.edu/articles/Design_Characterization_and_Implementation_of_Lower-Limb_Exoskeletons_for_Performance_Augmentation_During_Walking_and_Running/7751855

[59] R. Jiménez-Fabián and O. Verlinden, "Review of control algorithms for robotic ankle systems in lower-limb orthoses, prostheses, and exoskeletons," *Medical Engineering & Physics,* vol. 34, no. 4, pp. 397-408, 2012/05/01/ 2012, doi: https://doi.org/10.1016/j.medengphy.2011.11.018.

[60] J. Zhang, C. C. Cheah, and S. H. Collins, "Experimental comparison of torque control methods on an ankle exoskeleton during human walking," in *2015 IEEE International Conference on Robotics and Automation (ICRA)*, 26-30 May 2015 2015, pp. 5584-5589, doi: 10.1109/ICRA.2015.7139980.

[61] J. Zhang, C. C. Cheah, and S. H. Collins, "Chapter 5 - Torque Control in Legged Locomotion," in *Bioinspired Legged Locomotion*, M. A. Sharbafi and A. Seyfarth Eds.: Butterworth-Heinemann, 2017, pp. 347-400.

[62] R. W. Nuckols and G. S. Sawicki, "Impact of elastic ankle exoskeleton stiffness on neuromechanics and energetics of human walking across multiple speeds," *J Neuroeng Rehabil,* vol. 17, no. 1, p. 75, Jun 15 2020, doi: 10.1186/s12984-020-00703-4.

[63] D. P. Ferris, J. M. Czerniecki, and B. Hannaford, "An ankle-foot orthosis powered by artificial pneumatic muscles," *Journal of Applied Biomechanics,* vol. 21, pp. 189-197, 2005, doi: 10.1123/jab.21.2.189.

[64] D. P. Ferris, K. E. Gordon, G. S. Sawicki, and A. Peethambaran, "An improved powered ankle-foot orthosis using proportional myoelectric control," *Gait Posture,* vol. 23, no. 4, pp. 425-8, Jun 2006, doi: 10.1016/j.gaitpost.2005.05.004.

[65] C. Fleischer, A. Wege, K. Kondak, and G. Hommel, "Application of EMG signals for controlling exoskeleton robots," *Biomedizinische Technik. Biomedical engineering,* vol. 51, no. 5-6, pp. 314-9, Dec 2006, doi: 10.1515/BMT.2006.063.

[66] R. W. Jackson and S. H. Collins, "Heuristic-Based Ankle Exoskeleton Control for Co-Adaptive Assistance of Human Locomotion," *IEEE transactions on neural systems and rehabilitation engineering : a publication of the IEEE Engineering in Medicine and Biology Society,* vol. 27, no. 10, pp. 2059-2069, Oct 2019, doi: 10.1109/TNSRE.2019.2936383.

[67] J. R. Koller, D. A. Jacobs, D. P. Ferris, and C. D. Remy, "Learning to walk with an adaptive gain proportional myoelectric controller for a robotic ankle exoskeleton," *J Neuroeng Rehabil,* vol. 12, p. 97, Nov 4 2015, doi: 10.1186/s12984-015-0086-5.

[68] M. S. Orendurff, J. A. Schoen, G. C. Bernatz, A. D. Segal, and G. K. Klute, "How humans walk: bout duration, steps per bout, and rest duration," *Journal of rehabilitation research and development,* vol. 45, no. 7, pp. 1077-89, 2008, doi: 10.1682/jrrd.2007.11.0197.

[69] F. E. Zajac, "Muscle and tendon: properties, models, scaling, and application to biomechanics and motor control," *Critical reviews in biomedical engineering,* vol. 17, no. 4, pp. 359-411, 1989. [Online]. Available: http://www.ncbi.nlm.nih.gov/pubmed/2676342.

[70] H. Geyer and H. Herr, "A Muscle-reflex model that encodes principles of legged mechanics produces human walking dynamics and muscle activities," *IEEE Transactions on Neural Systems and Rehabilitation Engineering,* vol. 18, pp. 263-273, 2010, doi: 10.1109/TNSRE.2010.2047592.

[71] M. F. Eilenberg, H. Geyer, and H. Herr, "Control of a Powered Ankle-Foot Prosthesis Based on a Neuromuscular Model," *IEEE Transactions on Neural Systems and Rehabilitation Engineering,* vol. 18, pp. 164-173, 2010.

[72] H. M. Herr and A. M. Grabowski, "Bionic ankle-foot prosthesis normalizes walking gait for persons with leg amputation," *Proc Biol Sci,* vol. 279, no. 1728, pp. 457-64, Feb 7 2012, doi: 10.1098/rspb.2011.1194.

[73] J. Markowitz, P. Krishnaswamy, M. F. Eilenberg, K. Endo, C. B. Chris, and H. Herr, "Speed adaptation in a powered transtibial prosthesis controlled with a neuromuscular model," *Philosophical Transactions of the Royal Society B: Biological Sciences,* vol. 366, pp. 1621-1631, 2011, doi: 10.1098/rstb.2010.0347.

[74] A. R. Wu *et al.*, "An Adaptive Neuromuscular Controller for Assistive Lower-Limb Exoskeletons: A Preliminary Study on Subjects with Spinal Cord Injury," *Frontiers in neurorobotics,* vol. 11, p. 30, 2017, doi: 10.3389/fnbot.2017.00030.

[75] G. Durandau *et al.*, "Voluntary control of wearable robotic exoskeletons by patients with paresis via neuromechanical modeling," *J Neuroeng Rehabil,* vol. 16, no. 1, p. 91, Jul 17 2019, doi: 10.1186/s12984-019-0559-z.

[76] F. Tamburella *et al.*, "Neuromuscular Controller Embedded in a Powered Ankle Exoskeleton: Effects on Gait, Clinical Features and Subjective Perspective of

Incomplete Spinal Cord Injured Subjects," *IEEE transactions on neural systems and rehabilitation engineering : a publication of the IEEE Engineering in Medicine and Biology Society,* vol. 28, no. 5, pp. 1157-1167, May 2020, doi: 10.1109/TNSRE.2020.2984790.

[77] K. A. Witte, "Design, characterization, and implementation of lower-limb exoskeletons for performance augmentation during walking and running," Ph.D., Mechanical Engineering, Carnegie Mellon University, 2018.

[78] G. S. Sawicki and N. S. Khan, "A Simple Model to Estimate Plantarflexor Muscle-Tendon Mechanics and Energetics During Walking With Elastic Ankle Exoskeletons," *IEEE Trans Biomed Eng,* vol. 63, no. 5, pp. 914-923, May 2016, doi: 10.1109/TBME.2015.2491224.

[79] S. Galle, P. Malcolm, W. Derave, and D. De Clercq, "Adaptation to walking with an exoskeleton that assists ankle extension," *Gait Posture,* vol. 38, no. 3, pp. 495-9, Jul 2013, doi: 10.1016/j.gaitpost.2013.01.029.

[80] J. M. Brockway, "Derivation of formulae used to calculate energy expenditure in man," *Human Nutrition: Clinical Nutrition,* vol. 41, pp. 463-471, 1987.

[81] S. H. Collins, M. Bruce Wiggin, and G. S. Sawicki, "Reducing the energy cost of human walking using an unpowered exoskeleton," *Nature,* vol. 522, pp. 212-215, 2015, doi: 10.1038/nature14288.

[82] O. N. Beck, L. K. Punith, R. W. Nuckols, and G. S. Sawicki, "Exoskeletons Improve Locomotion Economy by Reducing Active Muscle Volume," *Exercise and sport sciences reviews,* vol. 47, no. 4, pp. 237-245, Oct 2019, doi: 10.1249/JES.0000000000000204.

[83] K. Seo, J. Lee, Y. Lee, T. Ha, and Y. Shim, "Fully Autonomous Hip Exoskeleton Saves Metabolic Cost of Walking," *IEEE International Conference on Robotics and Automation,* 2016, doi: 10.1109/ICRA.2016.7487663.

[84] L. M. Mooney and H. M. Herr, "Biomechanical walking mechanisms underlying the metabolic reduction caused by an autonomous exoskeleton," *J Neuroeng Rehabil,* vol. 13, p. 4, Jan 28 2016, doi: 10.1186/s12984-016-0111-3.

[85] R. W. Nuckols, T. J. M. Dick, O. N. Beck, and G. S. Sawicki, "Ultrasound imaging links soleus muscle neuromechanics and energetics during human walking with elastic ankle exoskeletons," *Sci Rep,* vol. 10, no. 1, p. 3604, Feb 27 2020, doi: 10.1038/s41598-020-60360-4.

[86] R. Kram and C. R. Taylor, "Energetics of running: a new perspective," *Nature,* vol. 346, pp. 265-267, 1990.

[87] T. M. Griffin, T. J. Roberts, and R. Kram, "Metabolic cost of generating muscular force in human

walking: insights from load-carrying and speed experiments," *Journal of Applied Physiology,* vol. 95, pp. 172-183, 2003, doi: https://doi.org/10.1152/japplphysiol.00944.2002.

[88] K. E. Gordon, C. R. Kinnaird, and D. P. Ferris, "Locomotor adaptation to a soleus EMG-controlled antagonistic exoskeleton," *J Neurophysiol,* vol. 109, no. 7, pp. 1804-14, Apr 2013, doi: 10.1152/jn.01128.2011.

[89] J. C. Selinger, S. M. O'Connor, J. D. Wong, and J. M. Donelan, "Humans Can Continuously Optimize Energetic Cost during Walking," *Curr Biol,* vol. 25, no. 18, pp. 2452-6, Sep 21 2015, doi: 10.1016/j.cub.2015.08.016.

[90] J. C. Selinger, J. D. Wong, S. N. Simha, and J. M. Donelan, "How humans initiate energy optimization and converge on their optimal gaits," *The Journal of experimental biology,* vol. 222, no. Pt 19, Oct 8 2019, doi: 10.1242/jeb.198234.

[91] J. D. Wong, J. C. Selinger, and J. M. Donelan, "Is natural variability in gait sufficient to initiate spontaneous energy optimization in human walking?," *J Neurophysiol,* vol. 121, no. 5, pp. 1848-1855, May 1 2019, doi: 10.1152/jn.00417.2018.

[92] N. Hogan, "Controlling Impedance at the Man/Machine Interface," *IEEE International Conference on Robotics and Automation,* 1989.

[93] K. Seo, J. Lee, and Y. J. Park, "Autonomous hip exoskeleton saves metabolic cost of walking uphill," *IEEE ... International Conference on Rehabilitation Robotics : [proceedings],* vol. 2017, pp. 246-251, Jul 2017, doi: 10.1109/ICORR.2017.8009254.

[94] A. J. Young, J. Foss, H. Gannon, and D. P. Ferris, "Influence of Power Delivery Timing on the Energetics and Biomechanics of Humans Wearing a Hip Exoskeleton," *Front Bioeng Biotechnol,* vol. 5, p. 4, 2017, doi: 10.3389/fbioe.2017.00004.

[95] J. Zhang *et al.*, "Human-in-the-loop optimization of exoskeleton assistance during walking," *Science,* vol. 356, no. 6344, pp. 1280-1284, Jun 23 2017, doi: 10.1126/science.aal5054.

[96] J. Kim *et al.*, "Reducing the metabolic rate of walking and running with a versatile, portable exosuit," *Science,* vol. 365, no. 6454, pp. 668-672, Aug 16 2019, doi: 10.1126/science.aav7536.

[97] G. Lee *et al.*, "Reducing the metabolic cost of running with a tethered soft exosuit," *Sci Robot,* vol. 2, no. 6, May 31 2017, doi: 10.1126/scirobotics.aan6708.

[98] G. M. Bryan *et al.*, "Optimized hip-knee-ankle exoskeleton assistance at a range of walking speeds," *J Neuroeng Rehabil,* vol. 18, no. 1, p. 152, Oct 18 2021, doi: 10.1186/s12984-021-00943-y.

[99] R. W. Nuckols, K. Z. Takahashi, D. J. Farris, S. Mizrachi, R. Riemer, and G. S. Sawicki, "Mechanics of walking and running up and downhill: A joint-level perspective to guide design of lower-limb exoskeletons," *PLoS One,* vol. 15, no. 8, p. e0231996, 2020, doi: 10.1371/journal.pone.0231996.

[100] R. R. Neptune, K. Sasaki, and S. A. Kautz, "The effect of walking speed on muscle function and mechanical energetics," *Gait Posture,* vol. 28, no. 1, pp. 135-43, Jul 2008, doi: 10.1016/j.gaitpost.2007.11.004.

[101] J. M. Donelan, R. Kram, and A. D. Kuo, "Mechanical work for step-to-step transitions is a major determinant of the metabolic cost of human walking," *The Journal of experimental biology,* vol. 205, no. Pt 23, pp. 3717-27, Dec 2002. [Online]. Available: https://www.ncbi.nlm.nih.gov/pubmed/12409498.

[102] K. E. Zelik, K. Z. Takahashi, and G. S. Sawicki, "Six degree-of-freedom analysis of hip, knee, ankle and foot provides updated understanding of biomechanical work during human walking," *The Journal of experimental biology,* vol. 218, no. Pt 6, pp. 876-86, Mar 2015, doi: 10.1242/jeb.115451.

[103] K. Shamaei, G. S. Sawicki, and A. M. Dollar, "Estimation of quasi-stiffness of the human hip in the stance phase of walking," *PLoS One,* vol. 8, no. 12, p. e81841, 2013, doi: 10.1371/journal.pone.0081841.

[104] K. Shamaei, G. S. Sawicki, and A. M. Dollar, "Estimation of quasi-stiffness and propulsive work of the human ankle in the stance phase of walking," *PLoS One,* vol. 8, no. 3, p. e59935, 2013, doi: 10.1371/journal.pone.0059935.

[105] K. Shamaei, G. S. Sawicki, and A. M. Dollar, "Estimation of quasi-stiffness of the human knee in the stance phase of walking," *PLoS One,* vol. 8, no. 3, p. e59993, 2013, doi: 10.1371/journal.pone.0059993.

[106] D. J. Farris and B. J. Raiteri, "Modulation of leg joint function to produce emulated acceleration during walking and running in humans," *R Soc Open Sci,* vol. 4, no. 3, p. 160901, Mar 2017, doi: 10.1098/rsos.160901.

[107] D. J. Farris and B. J. Raiteri, "Elastic ankle muscle-tendon interactions are adjusted to produce acceleration during walking in humans," *The Journal of experimental biology,* vol. 220, no. Pt 22, pp. 4252-4260, Nov 15 2017, doi: 10.1242/jeb.159749.

[108] B. R. Umberger and J. Rubenson, "Understanding muscle energetics in locomotion: new modeling and experimental approaches," *Exercise and sport sciences reviews,* vol. 39, no. 2, pp. 59-67, Apr 2011, doi: 10.1097/JES.0b013e31820d7bc5.

[109] G. S. Sawicki, C. L. Lewis, and D. P. Ferris, "It pays to have a spring in your step," *Exercise and sport sciences reviews,* vol. 37, no. 3, pp. 130-8, Jul 2009, doi: 10.1097/JES.0b013e31819c2df6.

[110] F. A. Panizzolo, S. Cimino, E. Pettenello, A. Belfiore, N. Petrone, and G. Marcolin, "Effect of a passive hip exoskeleton on walking distance in neurological patients," *Assist Technol,* pp. 1-6, Mar 5 2021, doi: 10.1080/10400435.2021.1880494.

[111] F. A. Panizzolo, C. Bolgiani, L. Di Liddo, E. Annese, and G. Marcolin, "Reducing the energy cost of walking in older adults using a passive hip flexion device," *J Neuroeng Rehabil,* vol. 16, no. 1, p. 117, Oct 15 2019, doi: 10.1186/s12984-019-0599-4.

[112] F. A. Panizzolo *et al.*, "Metabolic cost adaptations during training with a soft exosuit assisting the hip joint," *Sci Rep,* vol. 9, no. 1, p. 9779, Jul 5 2019, doi: 10.1038/s41598-019-45914-5.

[113] K. Shamaei, A. A. Adams, M. Cenciarini, K. N. Gregorczyk, and A. M. Dollar, "Preliminary Investigation of Effects of a Quasi-Passive Knee Exoskeleton on Gait Energetics," *2014 36th Annual International Conference of the IEEE Engineering in Medicine and Biology Society,* pp. 3061-3064, 2014.

[114] K. Shamaei, M. Cenciarini, A. A. Adams, K. N. Gregorczyk, J. M. Schiffman, and A. M. Dollar, "Design and evaluation of a quasi-passive knee exoskeleton for investigation of motor adaptation in lower extremity joints," *IEEE Trans Biomed Eng,* vol. 61, no. 6, pp. 1809-21, Jun 2014, doi: 10.1109/TBME.2014.2307698.

[115] A. J. Young, H. Gannon, and D. P. Ferris, "A Biomechanical Comparison of Proportional Electromyography Control to Biological Torque Control Using a Powered Hip Exoskeleton," *Front Bioeng Biotechnol,* vol. 5, p. 37, 2017, doi: 10.3389/fbioe.2017.00037.

[116] J. Lee, K. Seo, B. Lim, J. Jang, K. Kim, and H. Choi, "Effects of assistance timing on metabolic cost, assistance power, and gait parameters for a hip-type exoskeleton," (in English), *Int C Rehab Robot,* pp. 498-504, 2017. [Online]. Available: <Go to ISI>://WOS:000426850800086.

[117] B. Lim *et al.*, "Delayed Output Feedback Control for Gait Assistance With a Robotic Hip Exoskeleton," (in English), *Ieee T Robot,* vol. 35, no. 4, pp. 1055-1062, Aug 2019, doi: 10.1109/Tro.2019.2913318.

[118] M. K. Shepherd and E. J. Rouse, "The VSPA Foot: A Quasi-Passive Ankle-Foot Prosthesis With Continuously Variable Stiffness," *IEEE transactions on neural systems and rehabilitation engineering : a publication of the IEEE Engineering in Medicine and Biology Society,* vol. 25, no. 12, pp. 2375-2386, Dec 2017, doi: 10.1109/TNSRE.2017.2750113.

[119] E. M. Glanzer and P. G. Adamczyk, "Design and Validation of a Semi-Active Variable Stiffness Foot Prosthesis," *IEEE transactions on neural systems and rehabilitation engineering : a publication of the IEEE Engineering in Medicine and Biology Society,* vol. 26, no. 12, pp. 2351-2359, Dec 2018, doi: 10.1109/TNSRE.2018.2877962.

[120] J. K. Leestma, K. H. Fehr, and P. G. Adamczyk, "Adapting Semi-Active Prostheses to Real-World Movements: Sensing and Controlling the Dynamic Mean Ankle Moment Arm with a Variable-Stiffness Foot on Ramps and Stairs," *Sensors (Basel),* vol. 21, no. 18, Sep 8 2021, doi: 10.3390/s21186009.

[121] H. L. Bartlett, S. T. King, M. Goldfarb, and B. E. Lawson, "A Semi-Powered Ankle Prosthesis and Unified Controller for Level and Sloped Walking," (in English), *Ieee Transactions on Neural Systems and Rehabilitation Engineering,* vol. 29, pp. 320-329, 2021, doi: 10.1109/Tnsre.2021.3049194.

[122] D. J. Braun, V. Chalvet, T. H. Chong, S. S. Apte, and N. Hogan, "Variable Stiffness Spring Actuators for Low-Energy-Cost Human Augmentation," (in English), *Ieee T Robot,* vol. 35, no. 6, pp. 1435-1449, Dec 2019, doi: 10.1109/Tro.2019.2929686.

[123] D. J. Braun, V. Chalvet, and A. Dahiya, "Positive-Negative Stiffness Actuators," (in English), *Ieee T Robot,* vol. 35, no. 1, pp. 162-173, Feb 2019, doi: 10.1109/Tro.2018.2872284.

[124] V. Chalvet and D. J. Braun, "Algorithmic Design of Low-Power Variable-Stiffness Mechanisms," (in English), *Ieee T Robot,* vol. 33, no. 6, pp. 1508-1515, Dec 2017, doi: 10.1109/Tro.2017.2719049.

[125] V. Chalvet and D. J. Braun, "Criterion for the Design of Low-Power Variable Stiffness Mechanisms," (in English), *Ieee T Robot,* vol. 33, no. 4, pp. 1002-1010, Aug 2017, doi: 10.1109/Tro.2017.2689068.

[126] A. Sutrisno and D. J. Braun, "Enhancing Mobility With Quasi-Passive Variable Stiffness Exoskeletons," *IEEE transactions on neural systems and rehabilitation engineering : a publication of the IEEE Engineering in Medicine and Biology Society,* vol. 27, no. 3, pp. 487-496, Mar 2019, doi: 10.1109/TNSRE.2019.2899753.

[127] C. G. Welker, A. S. Voloshina, V. L. Chiu, and S. H. Collins, "Shortcomings of human-in-the-loop optimization of an ankle-foot prosthesis emulator: a case series," *R Soc Open Sci,* vol. 8, no. 5, p. 202020, May 5 2021, doi: 10.1098/rsos.202020.

[128] G. M. Bryan, P. W. Franks, S. C. Klein, R. J. Peuchen, and S. H. Collins, "A hip–knee–ankle exoskeleton emulator for studying gait assistance," *The International Journal of Robotics Research,* vol. 40, no. 4-5, pp. 722-746, 2020, doi: 10.1177/0278364920961452.

[129] B. Whittington, A. Silder, B. Heiderscheit, and D. G. Thelen, "The contribution of passive-elastic mechanisms to lower extremity joint kinetics during human walking," *Gait Posture,* vol. 27, no. 4, pp. 628-34, May 2008, doi: 10.1016/j.gaitpost.2007.08.005.

[130] J. M. Brockway, "Derivation of Formulas Used to Calculate Energy-Expenditure in Man," (in English), *Hum Nutr-Clin Nutr,* vol. 41c, no. 6, pp. 463-471, Nov 1987. [Online]. Available: <Go to ISI>://WOS:A1987L345600006.

[131] J. C. Selinger and J. M. Donelan, "Estimating instantaneous energetic cost during non-steady-state gait," *J Appl Physiol (1985),* vol. 117, no. 11, pp. 1406-15, Dec 1 2014, doi: 10.1152/japplphysiol.00445.2014.

[132] P. Konrad, *ABC of EMG – A Practical Introduction to Kinesiological Electromyography*. Scottsdale, Arizona: Noraxon U.S.A. Inc., 2005, p. 61.

[133] J. Camargo, A. Ramanathan, W. Flanagan, and A. Young, "A comprehensive, open-source dataset of lower limb biomechanics in multiple conditions of stairs, ramps, and level-ground ambulation and transitions," *J Biomech,* vol. 119, p. 110320, Apr 15 2021, doi: 10.1016/j.jbiomech.2021.110320.

[134] G. M. Bryan *et al.*, "Optimized hip-knee-ankle exoskeleton assistance reduces the metabolic cost of walking with worn loads," *J Neuroeng Rehabil,* vol. 18, no. 1, p. 161, Nov 7 2021, doi: 10.1186/s12984-021-00955-8.

[135] M. Shepertycky, S. Burton, A. Dickson, Y. F. Liu, and Q. Li, "Removing energy with an exoskeleton reduces the metabolic cost of walking," *Science,* vol. 372, no. 6545, pp. 957-960, May 28 2021, doi: 10.1126/science.aba9947.

[136] K. A. Ingraham, D. P. Ferris, and C. D. Remy, "Evaluating physiological signal salience for estimating metabolic energy cost from wearable sensors," *J Appl Physiol (1985),* vol. 126, no. 3, pp. 717-729, Mar 1 2019, doi: 10.1152/japplphysiol.00714.2018.

[137] P. Slade, R. Troutman, M. J. Kochenderfer, S. H. Collins, and S. L. Delp, "Rapid energy expenditure estimation for ankle assisted and inclined loaded walking," *J Neuroeng Rehabil,* vol. 16, no. 1, p. 67, Jun 6 2019, doi: 10.1186/s12984-019-0535-7.

[138] D. Lee, E. C. Kwak, B. J. McLain, I. Kang, and A. J. Young, "Effects of Assistance During Early Stance Phase Using a Robotic Knee Orthosis on Energetics, Muscle Activity, and Joint Mechanics During Incline and Decline Walking," *IEEE transactions on neural systems and rehabilitation engineering : a publication of the IEEE Engineering in Medicine and Biology Society,* vol. 28, no. 4, pp. 914-923, Apr 2020, doi: 10.1109/TNSRE.2020.2972323.

[139] T. Lenzi, M. C. Carrozza, and S. K. Agrawal, "Powered hip exoskeletons can reduce the user's hip and ankle muscle activations during walking," *IEEE transactions on neural systems and rehabilitation engineering : a publication of the IEEE Engineering in Medicine and Biology Society,* vol. 21, no. 6, pp. 938-48, Nov 2013, doi: 10.1109/TNSRE.2013.2248749.

[140] K. E. Gordon and D. P. Ferris, "Learning to walk with a robotic ankle exoskeleton," *J Biomech,* vol. 40, no. 12, pp. 2636-44, 2007, doi: 10.1016/j.jbiomech.2006.12.006.

[141] J. R. Koller, D. H. Gates, D. P. Ferris, and C. D. Remy, "Confidence in the curve: Establishing instantaneous cost mapping techniques using bilateral ankle exoskeletons," *J Appl Physiol (1985),* vol. 122, no. 2, pp. 242-252, Feb 1 2017, doi: 10.1152/japplphysiol.00710.2016.

[142] C. S. Florence, G. Bergen, A. Atherly, E. Burns, J. Stevens, and C. Drake, "Medical Costs of Fatal and Nonfatal Falls in Older Adults," *J Am Geriatr Soc,* vol. 66, no. 4, pp. 693-698, Apr 2018, doi: 10.1111/jgs.15304.

[143] T. Thum, S. Von Haehling, and S. D. Anker, "Limitations of gait speed as an independent predictor of mortality and morbidity in cardiac patients," *Journal of the American College of Cardiology,* vol. 58, no. 7, pp. 776-776, 2011.

[144] L. Hou *et al.*, "Effect of Protein Supplementation Combined with Resistance Training on Muscle Mass, Strength and Function in the Elderly: A Systematic Review and Meta-Analysis," *J Nutr Health Aging,* vol. 23, no. 5, pp. 451-458, 2019, doi: 10.1007/s12603-019-1181-2.

[145] A. Kapsalyamov, P. K. Jamwal, S. Hussain, and M. H. Ghayesh, "State of the Art Lower Limb Robotic Exoskeletons for Elderly Assistance," *IEEE Access,* vol. 7, pp. 95075-95086, 2019, doi: 10.1109/access.2019.2928010.

[146] S. Galle, W. Derave, F. Bossuyt, P. Calders, P. Malcolm, and D. De Clercq, "Exoskeleton plantarflexion assistance for elderly," *Gait Posture,* vol. 52, pp. 183-188, Feb 2017, doi: 10.1016/j.gaitpost.2016.11.040.

[147] H. J. Lee *et al.*, "A Wearable Hip Assist Robot Can Improve Gait Function and Cardiopulmonary Metabolic Efficiency in Elderly Adults," *IEEE transactions on neural systems and rehabilitation engineering : a publication of the IEEE Engineering in Medicine and Biology Society,* vol. 25, no. 9, pp. 1549-1557, Sep 2017, doi: 10.1109/TNSRE.2017.2664801.

[148] H. Mehmet, S. R. Robinson, and A. W. H. Yang, "Assessment of Gait Speed in Older Adults," *J Geriatr Phys Ther,* vol. 43, no. 1, pp. 42-52, Jan/Mar 2020, doi: 10.1519/JPT.0000000000000224.

[149] S. Galle, P. Malcolm, W. Derave, and D. De Clercq, "Adaptation to walking with an exoskeleton that assists ankle extension," *Gait and Posture,* vol. 38, no. 3, pp. 495-499, 2013, doi: 10.1016/j.gaitpost.2013.01.029.

[150] E. E. Thomas, G. De Vito, and A. Macaluso, "Speed training with body weight unloading improves walking energy cost and maximal speed in 75- to 85-year-old healthy women," *J Appl Physiol (1985),* vol. 103, no. 5, pp. 1598-603, Nov 2007, doi: 10.1152/japplphysiol.00399.2007.

[151] J. D. Wong, S. M. O'Connor, J. C. Selinger, and J. M. Donelan, "Contribution of blood oxygen and carbon dioxide sensing to the energetic optimization of human walking," *J Neurophysiol,* vol. 118, no. 2, pp. 1425-1433, Aug 1 2017, doi: 10.1152/jn.00195.2017.

[152] I. Kang, D. Molinaro, S. Duggal, Y. Chen, P. Kunapuli, and A. Young, "Real-time gait phase estimation for robotic hip exoskeleton control during multimodal locomotion," *IEEE Robotics and Automation Letters,* pp. 1-1, 2021, doi: 10.1109/lra.2021.3062562.

[153] M. K. Shepherd, D. D. Molinaro, G. S. Sawicki, and A. J. Young, "Deep Learning Enables Exoboot Control to Augment Variable-Speed Walking," *IEEE Robotics and Automation Letters,* vol. 7, no. 2, pp. 3571-3577, 2022, doi: 10.1109/lra.2022.3147565.

[154] D. R. Carrier, C. Anders, and N. Schilling, "The musculoskeletal system of humans is not tuned to maximize the economy of locomotion," *Proceedings of the National Academy of Sciences,* vol. 108, no. 46, pp. 18631-18636, 2011, doi: 10.1073/pnas.1105277108.

[155] K. A. McDonald, J. P. Cusumano, P. Peeling, and J. Rubenson, "Multi-objective control in human walking: insight gained through simultaneous degradation of energetic and motor regulation systems," *J R Soc Interface,* vol. 16, no. 158, p. 20190227, Sep 27 2019, doi: 10.1098/rsif.2019.0227.